

**LIQUID - PHASE SYNTHESIS OF HIGHLY
CRYSTALLINE FUNCTIONAL FINE PARTICLES AND
THEIR APPLICATION TO OPTICAL MATERIALS**

A Thesis Submitted to
The Department of Chemical Engineering
Graduate School of Engineering
Hiroshima University

by

TAKASHI OGI

In partial Fulfillment of The Requirements
For The Degree of
Doctor of Engineering

Hiroshima University

February 2008

Approved by

Professor Kikuo Okuyama

Adviser

Abstract

Fine particles science and technology, including the preparation, characterization and technological applications have been attracted much attention in a wide range of fields. Many processes have been developed to synthesize functional fine particles, including liquid, solid and gas phase processes, etc. A liquid process, including sol-gel and spray pyrolysis is selected as the main methods for investigation in this thesis.

The objective of this thesis is to investigate the synthesis of high crystalline functional fine particles using the liquid phase processes, including sol-gel and spray method systematically. The applications to nitride/oxide phosphor materials, transparent conductivity oxide materials, and oxide porous materials were investigated. Especially in this thesis, gallium nitride (GaN) nanoparticles synthesis by gas solid reaction of oxide nanoparticles derived from sol-gel or spray method; new oxynitride phosphor composed of BCNO atoms by liquid phase process; $\text{BaMgAl}_{10}\text{O}_{17}:\text{Eu}^{2+}$ (BAM:Eu²⁺) particles synthesis by flame spray pyrolysis were reported. The major conclusions in this thesis are listed as follows.

In **Chapter 1**, the background, previous research, and the main objectives of the thesis are introduced.

In **Chapter 2**, highly crystalline GaN nanoparticles were prepared from Ga_2O_3 nanoparticles. The addition of a proportional amount of ammonia to the solution is a key factor in the production of Ga_2O_3 nanoparticles. Nitridation of Ga_2O_3 nanoparticles

under a flow of ammonia resulted in highly crystalline nano-sized GaN particles less than 40 nm in size. Furthermore, according to powder X-ray diffraction, nano-sized Ga₂O₃ particles were more easily converted into GaN than large-sized Ga₂O₃ particles.

In **Chapter 3**, GaN nanoparticles were synthesized from gallium nitrate and ammonia solution. This method has a number of advantages over the method shown in chapter 2 in that it is a straightforward process with a high production rate. The method permits GaN nanoparticles, approximately 20 - 50 nm in mean diameter, to be produced. It was found that the GaN nanoparticles had an intense photoluminescence (PL) at 364 nm when UV excitation at 254 nm was used.

In **Chapter 4**, in order to produce highly crystalline GaN nanoparticles with a narrow size distribution, Ga₂O₃ nanoparticles obtained from salt-assisted spray pyrolysis were used as a starting material for nitridation. Addition of a proportional amount of flux salt (LiCl) to the solution is a key factor in the production of Ga₂O₃ nanoparticles with a narrow size distribution. Nitridation of Ga₂O₃ nanoparticles under a flow of ammonia resulted in highly crystalline GaN nanoparticles with a mean size, d_p , of 23.4 nm and geometric standard deviation, σ_g , of 1.68. This study revealed that Ga₂O₃ particles prepared at low temperatures were more easily converted into GaN particles than those prepared at high temperatures.

In **Chapter 5**, we report a novel type of full-color-emitting phosphor, composed of BCNO atoms using liquid process at low temperatures (below 900°C) under atmospheric pressure in a one-step. BCNO phosphor particles with a tunable

emitted-light wavelength from 380 nm to 571 nm were prepared using a facile liquid process. The experimental results obtained in the present study revealed that control of the carbon content by optimizing the operating temperature and reaction time was important for the production of BCNO phosphor particles with tunable emitted-light wavelengths over the entire visible light spectrum. The BCNO phosphor has high external quantum efficiency.

In **Chapter 6**, a flame spray pyrolysis method was designed and used to directly prepare BAM: Eu²⁺ blue phosphors. Characteristics such as photoluminescence, crystallinity and particle morphology were investigated for products prepared under various conditions and they were compared with those of the commercial product. With post annealing, the PL emission intensity was increased to four times that of the as-prepared phosphors.

A summary and some comments in this thesis for further investigation are listed in **Chapter 7**.

Contents

Abstract.....	i
Contents.....	iv
1. Introduction.....	1
1.1 Background.....	1
1.1.1 White Light emitting Diodes (White LEDs).....	2
1.1.2 Field emission displays (FEDs).....	3
1.1.3 High refractivity index nanocomposite.....	4
1.1.4 Transparent conductive films.....	5
1.2 Review of functional fine particles for optical materials.....	7
1.2.1 Nitride Phosphor (gallium nitride; GaN).....	7
1.2.2 Oxynitride phosphors (boron carbide oxynitride; BCNO).....	10
1.2.3 Oxide phosphors (barium magnesium aluminate; BAM).....	12
1.2.4 Transparent conducting Oxide (Indium Tin Oxide; ITO).....	13
1.3 Synthesis methods for fine particle preparation.....	15
1.3.1 Gas phase process.....	15
1.3.2 Solid phase process.....	16
1.3.2 Liquid phase process.....	17
1.4 Objective.....	28
Reference.....	33
2. Fabrication and photoluminescence of highly crystalline GaN and GaN:Mg nanoparticles.....	39
2.1 Introduction.....	39
2.2 Experimental procedure.....	41
2.3 Results and discussion.....	44
2.4 Summery.....	55
References.....	55
3. Simple synthesis of GaN nanoparticles from gallium nitrate and ammonia aqueous solution under a flow of ammonia gas.....	57
3.1 Introduction.....	58
3.2 Experimental procedure.....	57
3.3 Results and discussion.....	59

3.4	Summery	64
	References	65
4.	Synthesis of nanocrystalline GaN from Ga ₂ O ₃ nanoparticles derived from salt-assisted spray pyrolysis	66
4.1	Introduction	66
4.2	Experimental procedure	68
4.3	Results and discussion	71
4.4	Summery	83
	References	83
5.	Facile synthesis of new full-color-emitting BCNO phosphors with high quantum efficiency	86
5.1	Introduction	86
5.2	Experimental procedure	88
5.3	Results and discussion	89
5.4	Summery	98
	References	98
6.	Direct synthesis of barium magnesium aluminate blue phosphor particles via a flame route	100
6.1	Introduction	100
6.2	Experimental procedure	101
6.3	Results and discussion	104
6.4	Summery	110
	References	110
7.	Summary	112
	Appendix I: List of Figures	115
	Appendix II: List of Tables	119
	Acknowledgements	120

Chapter 1

Introduction

1.1 Background

Fine particles science and technology, including the preparation, characterization and technological applications have been attracted much attention in a wide range of fields. In particular, nanoparticles, smaller than 100 nm, have many properties which differ from the corresponding bulk material, making them attractive for many new electronic, optical or magnetic applications. Furthermore, the synthesis and characterization of assembling of fine particles and the fabrication of novel ceramics with unique microstructure and complex material combination in a variety of morphologies and dimensions have been reported by many researchers. They can be used for these functional applications in the formation of films, nanocomposites or nanophase materials.

In this thesis, the main applications of optical materials will be dealt with including some discussions of the underlying phenomena. These applications include phosphor materials, transparent conductive materials and so on. Some applications of functional fine particles for optical materials, white light emitting diodes (LEDs), field emitting displays (FEDs), high refractivity materials, and transparent conducting thin films are introduced as follows.

1.1.1 White Light Emitting Diodes (LEDs)

The field of solid-state lighting based on gallium nitride (GaN) semiconductors has seen remarkable breakthroughs in efficiency. Essentially, it is expected that white light emitting diodes (LEDs) can offer advantages of high brightness, reliability, low power consumption, and a long life time compared to conventional light bulbs and fluorescent lamps. The schematic diagram of white LED system is shown in Fig. 1.1. The conventional way involves combining a blue LED with a yellow-emitting $\text{Y}_3\text{Al}_5\text{O}_{12}:\text{Ce}^{3+}$ phosphor. This method is relatively easy to perform and the device has been commercialized. Sublimation (Sakai et al., 2004) and high-pressure solution methods (Porowski et al., 1996) are considered for crystal growth of GaN. The methods require the availability of well-characterized GaN powder source with high purity and signal phase. In addition, GaN powders themselves could be used as high quality phosphors.

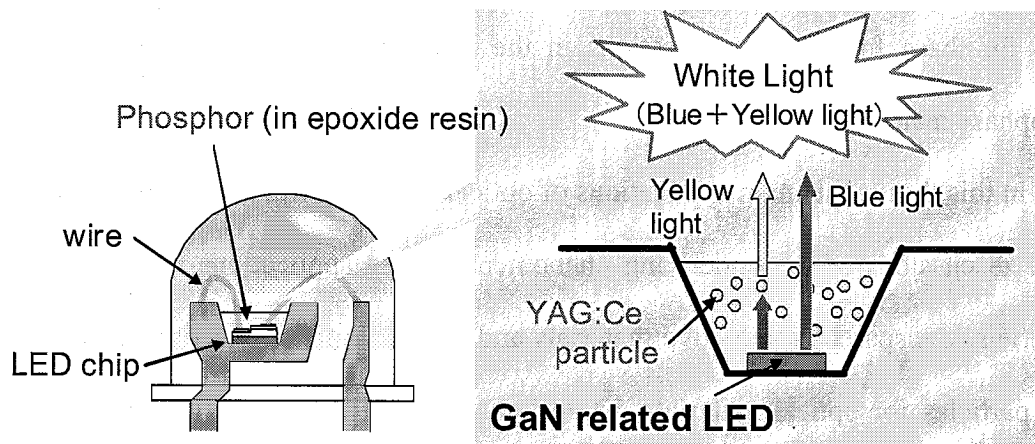


Fig1.1 Schematic diagram of white LEDs system

1.1.2 Field Emission Displays (FEDs)

Field emission displays (FEDs) are one of the most promising flat panel displays since its technology provides the potential of low power consumption as, in principle, the emission current flows only to light emitting part in proportion to the light intensity (Itoh et al., 2004). FEDs have a number of excellent features such as thin panel thickness ($\sim 2\text{mm}$), self emissive, distortion free image, wide viewing angle (about 170°), quick response (μs order), free from terrestrial magnetic effect and changes in ambient magnetism, quick start of operation, less dead space of image, etc. The schematic diagram of FEDs system is shown in Fig. 1.1b. In FEDs device, the elemental functions are principally similar with that of in cathode ray tubes (CRTs). FEDs use vacuum tubes with conventional red, green and blue (RGB) phosphor. The FEDs device can be considered as a flat cathode ray tube where the visible light is generated when electrons accelerated by moderate voltage excite the phosphor. Each pixel in FEDs acts as a microscopic CRT and produces its own light. Thus the FEDs have millions of individual CRT-accelerated electron crossing a vacuum gap impinging upon a phosphor-coated screen to emit light.

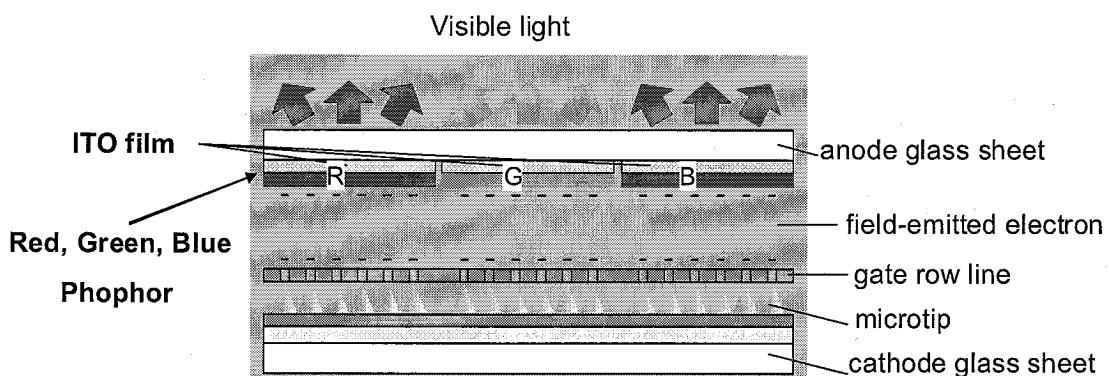


Fig1.2 Schematic diagram of FEDs system

1.1.3 High Refractivity Index Nanocomposites

Organic–inorganic hybrid materials have attracted considerable attention in recent years due to their novel physical and chemical properties. Incorporating nanoparticles into the polymer matrix becomes the most common method in producing these hybrid materials. The nanocomposite can have specialized properties that cannot be found in their respective single phase. Hybrid materials with enhanced electrical, mechanical and optical properties have been reported (Kanatzidis et al., 1990; Schmidt et al., 1996, Cartenuto et al., 1996). High refractive index nanocomposites have attracted considerable interests in light emitting diodes (LEDs) encapsulation (Ju et al., 2006; Steigerwald et al., 1993). If an encapsulating resin with an refractive index of 1.80 or more can be prepared, the light extraction efficiency will be greatly enhanced due to internal reflection phenomena occurring at the interface between the light emitting semiconductor layer and the resin. Inorganic nanoparticles can be embedded in polymer matrix to form high refractive index nanocomposite. For example, incorporating PbS nanoparticles into gelatin or poly (ethyleneoxide) has been reported (Zimmermann et al., 1993; Kyprianidou-Leodidou et al., 1994). Their studies proved that the PbS particles loading affects significantly the overall refractive index of the nanocomposite. Refractive index of 1.60–1.76 prepared from a solvent based polyarylether(sulfone) containing $\text{SiO}_2\text{-TiO}_2\text{-ZrO}_2$ has also been reported (Wang et al., 1992). Titania nanoparticles/polymer hybrid materials have been widely studied for their novel optical properties. The dispersion property of the TiO_2 nanoparticles in the polymer matrix becomes one critical issue in the successful preparation of these transparent hybrid nanocomposites.

1.1.4 Transparent Conductive Films

Transparent conductive films have been widely used as the transparent electrode for flat-panel displays and solar cells. Transparent electrodes based on doped oxide semiconductors make use of a wide-bandgap host material – normally of In_2O_3 , SnO_2 or ZnO - which is doped either by substitution of some of atoms or by oxygen vacancies. At the moment, the most visible alternatives are $\text{In}_2\text{O}_3:\text{Sn}$, $\text{SnO}_2:\text{Sb}$, and $\text{ZnO}:\text{Al}$. Thin-film and surface modification technologies cover a wide range, from high-functionality films for automotive and architectural applications such as photocatalytic glass, heat shielding glass and water-repellent glass, to transparent conducting films and reflection-control films used in liquid crystal displays, and micro-roughness control for solar control glass surfaces. Various types of coating technologies are necessary to realize these usages, such as online CVD, sol-gel coating, vacuum deposition and sputtering. Further technology is required to evaluate cleaning and pre-coating substrate treatment technology. Technologies in the thin-film and surface modification field are maximally exploited to meet the need to make glass into more sophisticated devices.

However, in the case of white LEDs, there are several problems, such as white emitting color changing with input power, low color rendering index due to two-color mixing, and low color reproducibility due to strong dependence of white color purity on the quantity of phosphors. Thus development of single λ -phased full color emitting phosphors for invisible UV ($<380\text{ nm}$) λ -pumped white LEDs is required to enhance the luminous efficiency.

Most of phosphor particles applying for FEDs were prepared by solid phase synthesis. However, the solid state method requires high energy consumption and many

preparation steps in order to obtain highly crystalline phosphor particles. Furthermore, this method often results in inhomogeneous product with large size and hence leads to localized concentration quenching. Therefore, it is important to synthesis highly crystalline phosphor particles with good properies using a one step low energy process.

GaN and ITO thin film were usually fabricated by chemical vapor deposition (CVD) and sputtering process. However, as an alternative process, film fabrication process using well-ordered closely packed nanoparticles has been widely studied nowadays because of their unique electronic, optical and magnetic properties. In this process, nanoparticles are usually prepared by liquid phase method, since this method has the advantages, such as low cost and high production rate, compared with gas phase method.

Therefore, to apply functional fine particles for above optical materials, particles with good characteristics such as high crystallinity, non-aggregation, sphericity, a clean surface, and a narrow size distribution, are required. Especially, in the case of phosphor materials and transparent conductive materials, it is important to prepare highly crystalline particles since the effect of particle crystallinity on characteristic is strong. Furthermore, finding a method that is capable of producing these functional fine particles at high production rates is critical for mass production of the next generation of electronic devices. Some functional fine particles, which will be investigated in this work, e.g., gallium nitride, boron carbide oxynitride, barium magnesium aluminate, and indium tin oxide are introduced as follows.

1.2 Review of Functional Fine Particles for Optical Materials

1.2.1 Nitride Phosphors (Gallium Nitride; GaN)

Gallium nitride is a commercially important material since Nakamura et al. proved its usefulness for light-emitting devices such as LEDs and LASERS (Nakamura et al., 1998). Since GaN is an efficient light-emitting semiconductor, it would be natural to expect a wider variety of future applications including those involving nanoparticles. Nanoparticles and nanostructured materials comprised of metals and semiconductors that exhibit size –dependent optical, magnetic, electronic devices that will utilize advanced materials in their design. Fluorescent markers and electroluminescent, displays, and photocatalysis are major future applications of GaN nanoparticles. In particular, combination of GaN-based blue LEDs and YAG:Ce powder has potential for use in the development of luminescence conversion LEDs that will emit white light. In addition to the above applications, GaN and indium gallium nitride (InGaN) have another potential application, as a phosphor. It is well-known that GaN and InGaN have a high conductivity of electricity. In the case of phosphors excited by electron beam, it is crucial for the material to have a certain level of conductivity. Materials with poor conductivity are easily charged up by the electron beam and it prevents from emitting light efficiently. In this case, doping with magnesium or zinc could be preferably utilized. Thus, phosphors are another expected future application of GaN nanoparticles. Producing of GaN nanoparticle has been reported by many researches, including by techniques such as chemical vapor synthesis (CVS), plasma synthesis, solvothermal synthesis, ammonothermal synthesis, pyrolysis method. GaN phosphors materials prepared by various methods are reviewed in Table 1.1. However, these methods have several demerits. First, in the case of solvothermal synthesis and ammonothermal

synthesis, low crystal quality, due to the low reaction temperature and a relatively long reaction time is needed. Additionally, reaction vessel which is resistant to very high pressure is often required. On the other hand, in the case of gas phase synthesis such as CVS, plasma synthesis, expensive raw materials are needed and the production rate of GaN nanoparticles prepared is relatively low.

Table 1.1 GaN phosphors materials prepared by various methods

Methods	Group	precursor	condition	Particles size
gas-solid reaction	Xiao et al.	Ga ₂ O ₃ powder under a NH ₃ gas	900°C for 35min	micrometer size
gas-solid reaction	Yang et al.	Ga(NO ₃) ₃ and teramethoxyorthosilicate(TMOS)	900°C for 15h	5 nm
gas-solid reaction	Yang et al.	cyclotrigallazane in a copolymer matrix	180°C for 20h	40nm
combution	Qiu et al.	Ga-urea compound with gaseous NH ₃	600°C for 24h	24nm
solvothermal method,	Xiao et al.	GaCl ₃ and Li ₃ N in benzen	280°C for 10 min	30nm
ammonothermal method	Jegier et al.	cyclotrigallazane NH ₃ gas	150 h	3 nm
pyrolysis method	Micic et al.	gallium imide, NH ₃ gas	360°C for 24 h	2.3-4.5 nm
detonation method	Frank et al.	nitrogen-containing gallium compounds	216°C	200 nm
chemical vapor synthesis	Hara et al.	vaporized gallium and NH ₃ gas	1100°C	0.3-2.0 μm
	Hara et al.	GaCl and NH ₃ gas	1000°C	1.2-1.8 μm
	Azuma et al.	trimethylgallium and NH ₃ gas	1100°C	6.4 nm
RF plasma synthesis	Takai et al.	vaporized gallium metal and ionized N ₂	130-2700 Pa	~hundred nm
microwave plasma synthesis	Azuma et al.	trimethylgallium, NH ₃ , and N ₂ gas	4h	nanometer size

1.2.2 Oxynitride Phosphors (Boron Carbide Oxynitride; BCNO)

Oxynitride compounds have attracted much attention as host lattices for phosphors, due to their excellent properties, such as nontoxicity, outstanding thermal and chemical stability, a broad range of excitation and emission wavelengths, and high luminescence efficiency when activated by rare-earth ions, etc (Hirosaki et al., 2000). Recently we developed for the first time a new oxynitride phosphor, which is composed of BCNO atoms, produced by a one-step liquid phase process at low temperature (below 900°C) under ambient atmospheric conditions. The properties of this material are similar to those of boron/carbon/nitrogen (B/C/N) materials as will be described below. The idea of synthesizing B/C/N materials based on the graphite network originated from the structural similarity but quite different physical properties of graphite, which is a semimetal and an excellent host material, and hexagonal boron nitride (h-BN), which is an insulator having limited intercalation properties (Kawaguchi et al., 1997). Especially B/C/N materials are expected to behave as light-emitting semiconductors, whose band gaps are thought to be intermediate between semimetallic graphite and insulating hexagonal-BN (h-BN) and can be determined by the atomic composition and atomic arrangement. B/C/N phosphors materials prepared by various methods are reviewed in Table 1.2. Since 1991, the study of photoluminescence (PL) from the B/C/N compounds has been followed with interest (Kawaguchi et al., 1991). Photoluminescence and cathodoluminescence have been observed for the BN(C,H) films prepared by the chemical vapor deposition (CVD). The luminescence was observed in a wide range (300-500 nm) with a peak at 375 nm (3.3 eV), which was effectively excited by light near 310 nm (4.0 eV). A white-blue color could be seen with the naked eye. The visible-light PL from the layered BC₂N compounds at 4.2 K was

characterized in 1996 (Watanabe et al., 1996). The photoluminescence (PL) properties of the BC₂N were measured by using an argon laser beam as the excitation source. The PL peak energy was found to be 600 nm at room temperature and 580 nm at 4.2 K. The external quantum efficiency was more than 0.5% and more than 1% at room temperature and 4.2 K, respectively. The room temperature PL from the turbostratic BCN films synthesized by bias-assisted hot filament chemical vapor deposition was also studied (Bai et al., 2000a, Bai et al., 2000b). Room temperature PL experiments were taken by using a He–Cd laser as the excitation source with an wavelength $\lambda_{exc} = 325$ nm. With a change of the inlet B₂H₆ concentrations in the reactive gas mixture, the peak centers shift in the range of 470–390 nm. New type of porous boron carbonitride nanotubular fibers with the overall BCN stoichiometry and homogeneous B,C, and N species distributions was fabricated via the CVD method (Yin et al., 2005). CL spectra clearly revealed intense ultraviolet emission centered at 319 nm, suggesting the characteristics of a semiconductor with a band gap of 3.89 eV.

Table 1.2 B/C/N phosphors materials prepared by various methods

Product	Type	Method	Group	Luminescence property
BN(C, H)	film	CVD	Kawaguchi et al.	343nm (@300nm)
BC ₂ N	film	CVD	Watanabe et al.	600nm
BCN	nanostructures	bias-assisted hot-filament CVD	Yu et al.	1240nm
BCN	nanotube	hot-filament CVD	Bai et al.	390-470nm (@325nm)
BCN	nanotube	bias-assisted hot filament CVD	Yu et al.	1240nm
BCN	nanofibers	plasma-enhanced hot filament CVD	Bai et al.	blue- and violet
BxCyNz	nanotube	CVD	Wu et al.	315-355nm (@267nm)
BCN	Porous nano fibers	CVD	Yin et al.	319nm
B ₃ CN ₃	fibres	pyrolysis process	Yang et al.	370 nm and 700 nm

1.2.3 Oxide Phosphors (Barium Magnesium Aluminate; BAM)

Phosphors in oxide system such as Y₂O₃, SrTiO₃, LaPO₄, ZnO, BaMgAl₁₀O₁₇, CaWO₄ and Y(Al, Ga)₅O₁₂ have many advantages rather than another system such as sulfide system. The stoichiometry of host lattice in oxide systems are easy to control since the stoichiometry can be achieved by firing in control atmosphere (Vecht et al., 1999). BAM:Eu³⁺ is a blue phosphor having a crystal structure similar to hexagonal β-alumina. BAM:Eu³⁺ has been the most important blue phosphor for lighting applications since it denotes high emission efficiency and stability. This phosphor shows emission peaking at ~ 450 nm, originate from a 4f⁶5d to 4f⁷ transition of Eu²⁺ ions.

Since the 5d electron is involved in the excitation process, the emission spectrum is strongly influenced by the crystal field strength (Yen et al., 1998). The emission region at ~ 450 nm of BAM:Eu³⁺ is practical interest for three band lamp phosphor and high durability of BAM:Eu³⁺ under intense UV irradiation allow this phosphor to be used in very high loading fluorescent lamps. Recently, the BAM phosphor has been widely applied for low voltage driving device such as FEDs, CRT and PDPs. The complicated nature of BAM:Eu³⁺ composition related to its hexagonal β -alumina structure has been a big challenge in the field of fine phosphor preparation since its material preparation requires high temperature synthesis (1600-1800 °C) and milling or further treatment lowering luminescent intensity of its material. The preparation of BAM:Eu³⁺ below 1600°C often result another phase such as BaAl₂O₄ and Al₂O₃ which deleterious the luminescent strength. There are numerous studies that consider in the preparation of BAM:Eu³⁺ phosphor including solid state, combustion, conventional spray pyrolysis (CSP), salt assisted spray pyrolysis(SASP), sol gel and microwave irradiation. In the preparation methods of BAM, firing in reduction atmosphere is required for reduce Eu³⁺ ions to divalent oxidation state. The europium content can vary widely but generally the amount of Eu²⁺ ions ~ 10% substitution for Ba²⁺ ion (Toki et al., 1996).

1.2.4 Transparent Conducting Oxide (Indium Tin Oxide; ITO)

Indium Tin Oxide (ITO) has been extensively studied, because of its properties that include its low resistivity (<10⁻⁴ Ω•cm) and high transparency to visible light (Vossen, 1977). Both thick and thin films of ITO are used in optoelectronic, electroluminescent, electrochromic, and biological devices, photovoltaic cells, liquid crystals and flat panel displays, sensors, storage-type cathode ray tubes, and heat reflecting mirrors. Fluorine

or antimony doped tin oxide (FTO, ATO), and aluminium or gallium doped zinc oxide (AZO, GZO) are also used as transparent electrodes. All of the materials mentioned thus far exhibit n-type semiconductor properties. Conventional methods for the preparation of ITO films including vacuum and electron beam evaporation, RF and DC sputtering, pulsed laser ablation, and chemical vapor deposition are costly and require complex equipment and procedures. In general, ITO thin films produced by the above mentioned methods are polycrystalline with a grain size in the range of 10 to 100 nm, depending on the specific method used and the processing steps involved (Lee & Huang, 1994). The properties of ITO nanocrystalline films are strongly dependent on the production method. ITO film are usually amorphous and have a low conductivity at low substrate temperatures and a post annealing process at high temperature is subsequently required to modify the properties. El-Akkad et al. (2000) and Meng and d.s-Sant.s (1998) reported on the effect of substrate temperature on structural, electrical, and optical properties. They reported that the resistivity decreased above a substrate temperature up to 400°C. Kim et al. (2000) reported on the effect of film thickness on film properties using a pulsed laser deposition method. The optimum ITO thickness for maximum device efficiency was found to be 60- 100 nm. The resistivity and transmittance of ITO films prepared by these conventional methods, were, respectively, lower than $1.0 \times 10^{-3} \Omega \cdot \text{cm}$ and larger than 85%. Spray pyrolysis is also used in the film formation process, because of the higher deposition rate and the fact that it does not require a vacuum system (Lee, & Huang, 1994; Sawada et al., 2002). Particulate deposition techniques, employing nanoparticles capable of facile sintering, may open new avenues for making transparent conducting films (Wei et al., 2001; Tbmomaga & Morimoto, 2001). Recently, an ITO nanoparticle suspension prepared by wet chemical technology

constituting precursors for spin-coated layers has been reported. The conductivity ($10^{-2} \Omega \cdot \text{cm}$) of spin-coated film using this precursor is far off from that of the best films prepared by physical or chemical vapor deposition methods (Granqvist & Hultaker, 2002). Several routes for the synthesis of ITO particles, including coprecipitation (Gao et al., 1999), emulsion (Devi et al., 2002), sol-gel (Alam & Cameron, 2000), and hydrothermal (Yanagisawa et al., 2000; Udawatte & Yanagisawa, 2001) techniques have been reported. Wet chemical techniques are used commercially for the preparation of fine and homogeneous particles with a low cost and ease of production. The fatal properties of these techniques are strong agglomeration, a rather poor morphology, and a low crystallinity. The use of a surface modifier to prevent agglomeration results in the degradation of the electrical conductivity (Gao et al., 1999; Goebbert et al., 1999). In addition to this, several hours are required to produce homogeneous and highly crystalline particles (Gao et al., 1999; Udawatte & Yanagisawa, 2001).

1.3 Synthesis Methods for Particle Preparation

Many processes have been developed to synthesize functional fine particles that include gas phase process, solid phase process and liquid phase process, and so on.

1.3.1 Gas Phase Synthesis

In gas phase process, particles are built from molecules all the way up to the desired size. Typical gas-to-solid conversion includes physical vapor deposition (PVD) and chemical vapor deposition (CVD) (Okuyama et al., 1991). The primary advantages of the gas-to-particle conversion method are the small particle size (a few nanometers to micron), narrow size distribution and high purity of the product particles. However, as

disadvantages, the formation of hard agglomerates in the gas phase leads to difficulties in preparing high-quality bulk materials. It is also difficult to synthesize multi-component materials, because of the differences in chemical reaction rate, vapor pressure, nucleation and growth rate which occur during the gas-to-particle conversion may lead to non-uniform composition.

1.3.2 Solid Phase Synthesis

Functional fine particles such as phosphors mostly are usually prepared by conventional solid state method. The general concept of solid states method for phosphor particles preparation comprises of three main parts, i.e. raw materials refinement, synthesis and advances treatments for particles generation. Selecting and using good raw material is a significant point in producing high-quality phosphor particles. The relationship of various factors in the synthesis processes should take into account in deciding the appropriate choices of raw material. Purity of raw material is a very important factor since a small amount of impurity often drastically changing the phosphor characteristics. Generally, the refinement process of raw material has to follow complex steps. In the case of raw material preparation for zinc sulfide phosphor, iron-group ions have to be removed by means of alkali method or acid method, while separation of single rare-earth ion from the other is the most important in the rare-earth raw materials preparation. In synthesis process, there are two kind of reactions occurred between host matrix and activator, i.e. firstly, activator ions are introduced into an existing host material and the other is host material synthesis and activator incorporation process simultaneously during firing. High firing temperature is required to cause solid state reaction and to well crystallize of phosphor. In order to accelerate

the crystal growth of phosphor, a kind of low melting point flux is usually added to the mixture of raw materials before firing process. Additional of flux sometimes used to obtain the phosphor with desire size and morphology, however, the fired phosphor is usually obtained as a sintered cake. Phosphors in particles form are achieved after broken the sintered cake phosphor form by coarse crushing followed by particles classification, washing, surface treatment and sieving.

1.3.3 Liquid Phase Synthesis

Methods of preparing functional fine particles in the liquid phase could be classified into the techniques: precipitation methods (Addition of precipitating agent, Hydrolysis, Redox reaction, Decomposition of compound, Sol-gel), Special reaction field (Hydrothermal Supercritical fluid, Microemulsion), solvent evaporation methods (Spray pyrolysis, Spray drying).

1.3.3.1 Addition of precipitating agent

Techniques of the addition of precipitating agents are further classified as to the formation of metal hydroxides, coprecipitation, and homogeneous precipitation.

The metal hydroxide precipitates from an aqueous solution of metal salt by adjusting, certain pH values. When the simultaneous precipitation occurs at a certain PH value from the solution mixed with various metal salts, all metal hydroxides are precipitated, and the polycomponent oxide powder is prepared from the metal hydroxides mixture by thermal decomposition. This technique is called coprecipitation. However, the homogeneity of the metal hydroxides mixture is difficult because of the different conditions of the precipitation of each hydroxide. It is necessary to make

multicomponent powder where the precipitated conditions are nearly the same among the metal components, and each precipitation rate is fast. Moreover, it may be necessary to have operating conditions, such as the addition of a large amount of precipitating agent and vigorous agitation in the solution. In the special case of compound precipitation, there is a useful precursor compound with a desired composition such as $\text{BaTiO}(\text{C}_2\text{O}_4)_2$ or $\text{CaZrO}(\text{C}_2\text{O}_4)_2$. The homogeneous precipitation technique is a different operation from the above techniques of the addition of precipitating agents, where precipitating agents are produced by a chemical reaction instead of the addition in the solution. This technique is superior to precipitate metal hydroxide, because the concentration of the precipitating agent becomes more homogeneous in the solution. For example, urea, thioacetamide, or dimethyl oxalate can be used by hydrolysis as a precipitating agent, instead of ammonia, hydrogen sulfide, or oxalic acid.

1.3.3.2 Hydrolysis

In the category of hydrolysis, there is formation from the corresponding metal alkoxides in alcohol solution as well as from metal salt solution. The technique to produce particles by hydrolysis of metal alkoxides is called the alkoxide method. The particles prepared by this technique are normally amorphous metal oxide and hydrated. This technique has several advantages, such as the simple and rapid reaction around room temperature, the easy achievement of high purity of the product because it is free from inorganic ions of all kinds, and the strong possibility of the formation of a complex component product from the mixture of metal alkoxides. The metal hydroxide sol is easily generated by the hydrolysis from metal salt solution, especially with a small ionic radius metal such as Si^{4+} or Al^{3+} , or with a high ionic charged metal such as Fe^{3+} or Ti^{4+} .

⁺. Metal oxide particles are produced by thermal decomposition. When metal salts are highly purified, the particles with high purity will be produced very easily, and the average size and size distribution of particles could be controlled by an aging process. Matijevic developed many procedures of uniform metal (hydrous) oxide particles, and some are reviewed as the formation of iron oxide (Blesa and Matijevic, 1989).

1.3.3.3 Redox reaction

In the redox reaction technique (House, 1972), the fine metal particles, such as noble metals and sulfur, are produced by reducing or oxidizing the metal salt or the metal chelate complex solutions. Many kinds of complex or protective colloid agents are frequently employed to moderate the reaction speed and to stabilize the generated particles, so that highly monodispersed particles are obtained. Matijevic(1991) also reported that precipitation of fine powders of some noble metals and copper, using this technique, was combined with the following technique, called decomposition of compound. Some organic compounds such as EDTA, triethanol amine, thioacetamide, and urea can be used in the technique of decomposition of compound.

1.3.3.4 Hydrothermal method

The hydrothermal method is one method for producing metal (hydrous) oxide crystalline particles in aqueous solution under high temperature and high pressure. This method can be classified as hydrothermal oxidation, hydrothermal precipitation, hydrothermal synthesis, hydrothermal decomposition, hydrothermal crystallization, or hydrothermal reduction, according to the reaction mechanism. When an autoclave is used as a reaction vessel, it takes several hours or days to produce the metal oxide

particles, because of the slow dehydration rate. Recently, Adschiri et al. (1992) proposed a new process using supercritical water and showed the synthesis time of AlOOH particles was a few minutes.

1.3.3.5 Supercritical fluids

The methods of particle formation using supercritical fluids are the rapid expansion of the supercritical solution (RESS) method (Mohamed et al., 1989) and the gas antisolvent recrystallization method reported by Gallagher et al. (1989). As the operating temperature is relatively low when carbon dioxide supercritical fluid is used, these methods are now being applied to make the products for medical and food industries.

1.3.3.6 Microemulsions

The ultrafine particles, which sometimes have quantum size effects, can be produced by the reaction in water pools of water in (water-in-oil) microemulsions. The redox reactions can be used by mixing more than two kinds of microemulsion with the reactant in the water pool, or by adding gas or an aqueous solution into the microemulsion. Nagy et al. (1989) prepared uniform and very fine nickel boride and cobalt boride particles for catalysis, and also reviewed the formation of many metal particles. Fendler's review (1987) is focused on novel particle formation by the use of a surfactant assembly, such as reversed micelles, microemulsions, vesicles, and bilayer liquid membranes.

Among liquid phase processes, sol-gel process and spray process are considered to be better methods because they have many advantages as shown below:

1. The particles produced by a spray method are spherical with controllable size and more uniform composition than those produced by other techniques.
2. Multi-component (composite) materials are easily obtained by these methods. It is an advantage over the spray and sol gel process where it is difficult to condense several components simultaneously from vapor phase in the desired composition.
3. A highly purity product is produced.
4. The process are relatively simple and low cost.

1.3.3.7 Sol Gel Synthesis

Sol gel is a method for preparing metal oxide glasses and ceramic materials by hydrolyzing a chemical precursor that pass sequentially through a solution state and a gel state before being dehydrated to a glass or ceramics. Sol gel technology has expanded dramatically for prepared various special shapes obtained directly from the gel state such as films and coatings, monoliths, fibers, powders, grains, spheres, porous gels and membranes. Preparation of metal oxides by the sol gel route proceeds through the three basic steps, i.e. monomer formation (partial hydrolysis), sol formation (polycondensation) and gelation (cross-linking). These reactions occur simultaneously after the initial processing stage. In the sol-gel process, the precursors (starting compounds) for preparation of colloid consist of a metal or metalloid element surrounded by various ligands. Even economically not efficient, alkoxides are the most widely precursors used in sol-gel method since they react readily with water.

The modification of sol gel method, in this research, is shown in Fig. 1.3. The modification is the introducing an additional material to prevent large agglomeration

during heating process. The precursors sources used are combination of metal alkoxide with metal chloride (semihydroxide). In this step, the mixing of materials is made under boiling point of the solvent hence the material compositions are homogeneous mixed. After hydrolysis completely formed, high molecular weigh of polymers were introduced. The additional polymer was designed for covering the particles precursor during heating treatment therefore large agglomeration can be prevented. Exothermic reaction of polymer also assists the particles growth (Abdullah et al., 2005a, Panatarani et al., 2005, Abdullah et al., 2005b).

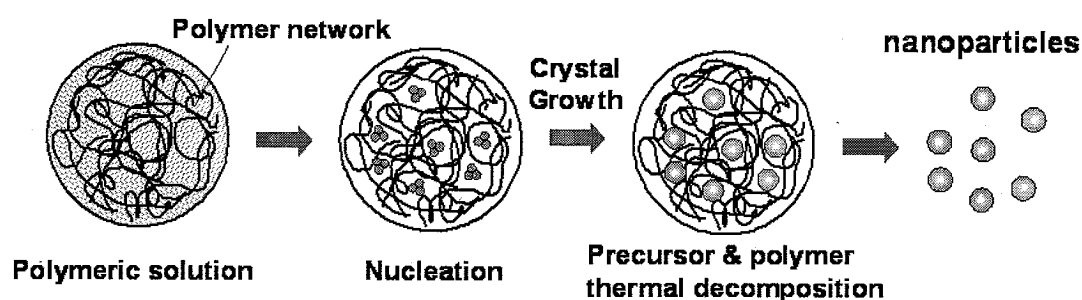


Fig. 1.3 Modification of sol gel process

1.3.3.8 Spray Pyrolysis

Conventional spray pyrolysis (CSP) is a method for producing particulate materials that combines both liquid and gas phase aerosol processes (Messing et al., 1993). Spray pyrolysis has a number of advantages such as particles produces are spherical, the distribution of particles size is uniform and controllable from submicron to micrometer, the purity of product is high and the process is continuous (Lenggoro et al 2000). In CSP, the precursor sources are mixed in solution at a molecular level. After atomization, all

component of particles formation are integrated inside the droplet. Because of each droplet has the same composition, thus the multicomponent and composite material easily to obtain. The physical and chemical characteristics of soluble chemical precursors strongly influence the characteristics of particles formed by CSP. CSP apparatus was consists of ultrasonic nebulizer, hot wall tubular reactor and electrostatic precipitator. The precursor solution are atomized and misted by means of an ultrasonic transducer. The misted droplet is carried by gas flow into hot wall tubular reactor then in-flight heated for several second in the reactor. The produced particles are collected by electrostatic precipitator. The concept of CSP is to produce one particle from one droplet. Atomizer for application in CSP for powder generation, require droplet of 1 to 10 μm in size at concentration greater than 10^7 droplets/ cm^3 (Kodas et al 1999). This has led to an emphasis on ultrasonic, electrostatic and other technology capable of producing droplets with sizes less than 10 μm at high concentration. For specific atomizer, the droplet characteristics depend on the solution density, viscosity and surface tension (Nalwa et al 2003). There are numbers of modification of CSP process, such as salt- assisted spray pyrolysis (SASP), low pressure spray pyrolysis (LPSP), and flame spray pyrolysis (FSP) (Okuyama et al., 2003).

Salt-assisted spray pyrolysis

Salt-assisted spray pyrolysis (SASP) is a modified method of CSP by introducing a salt into precursor solution before atomization (Xia et al 2001a, and Xia et al 2001b).The SASP method is proposed to focus on the strategy for separating the nanocrystallites by introducing some compounds that can distribute on the nanocrystallite surface to prevent them from agglomeration and they are easy to remove.

During the SASP process, when the particle temperature exceeds the melting point of the salts, the salts melt and act as high-temperature solvents. The material or its components can then dissolve, undergo reactions, and, upon exceeding the solubility limit, precipitate in the solvent. These processes can remarkably enhance mass transfer due to the liquid-state solvent, in contrast to the very small solid-state diffusion coefficients in the case of CSP process.

Low pressure spray pyrolysis

The low pressure spray pyrolysis method was first studied by Kang and Park (1995a). In this process, a two-step atomizer, typically known as (filter expansion aerosol generator, FEAG) was introduced into this process for producing droplets. The glass filter was made by calcination of ceramic particles with average pore size around several microns. The original aim of this process was focus on generating small droplets with large production rate rather than preparing nanoparticles. Various kinds of particles were then synthesized using LPSP by Kang et al. (1995a; 1995b; 1997; 1999a; 1999b; 2000).

In this thesis, $\text{In}_2\text{O}_3:\text{Sn}$ (Indium Tin Oxide; ITO) films were prepared from a sol solution with highly crystalline ITO nanoparticles (less than 20 nm in size with 10 at.% Sn) which had been prepared by LPSP in a single step. The ITO sol solution was prepared by dispersing LPSP-prepared ITO nanoparticles into ultra pure water. The nanoparticles ITO film was deposited on a glass substrate using a dip-coating method and then annealed in air at various temperatures. The optical transmittances of the ITO films were measured by UV-Vis spectrometry, and the films were found to have a high transparency to visible light (in the case of a film thickness of 250 nm annealed at

400⁰C, the transparency was in excess of 95% over the range $\lambda=450\text{--}800$ nm, with a maximum value near 100% at wavelengths above $\lambda=700$ nm). The optical transmittances of the films were influenced by the size of the ITO particle used, the film thickness and the annealing temperature. The ITO films showed a minimum resistivity of $9.5 \times 10^{-2} \Omega \cdot \text{cm}$, and their resistivity was affected by both the ITO particle size and the annealing temperature used. Details of this study method can be found on reference (Ogi. et al., 2006).

Flame spray pyrolysis

Flame spray pyrolysis has been used to produce various particles such as ceramic, metal and composite powders because it provides good control of particle size, particle crystal structure and this method also can produce highly pure particles continuously without further subsequent process, for example, drying, calcinations and milling in the wet chemical processes (Gurav et al., 1993). The sizes of flame-made particles range from a few to several hundred nanometers in diameter depending on process conditions. FSP has the major advantages that it can handle multi-component materials containing a large number of elements and that aqueous solution of precursors can be used (Kilian et al., 2001; Limaye et al., 2002; Madler et al., 2002; Tani et al., 2004 Vemury et al., 1995). Many Studies on the effect of additives , electrical charging, reactant gas mixing, burner types, different precursors in flame reactors have been conducted to investigate new characteristics of the product particles.

1.3.3.9 Spay Drying

Spray drying is the most widely used industrial process involving particle

formation and drying. It is highly suited for the continuous production of dry solids in either powder, granulate or agglomerate form from liquid feedstocks as solutions, emulsions and pumpable suspensions. Therefore, spray drying is an ideal process where the end-product must comply to precise quality standards regarding particle size distribution, residual moisture content, bulk density, and particle shape. Spray drying involves the atomization of a liquid feedstock into a spray of droplets and contacting the droplets with hot air in a drying chamber. The sprays are produced by ultrasonic nebulizer or nozzle atomizers. Evaporation of moisture from the droplets and formation of dry particles proceed under controlled temperature and airflow conditions. Powder is discharged continuously from the drying chamber. Operating conditions and dryer design are selected according to the drying characteristics of the product and powder specification.

Our group (Okuyama et al., 2003, Iskandar et al., 2001a, 2003a, 2003b) prepared functional nanostructured particles by spray drying. Iskandar et al, reported producing of silica powder containing ordered mesopores which were derived from sol by using an ultrasonic nebulizer that generated 4-5 μm droplets (Iskandar et al., 2001b, 2002). A colloidal mixture of silica nanoparticles and polystyrene latex nanoparticles was mixed and sprayed as droplets into a vertical reactor which contained two temperature zones. The solvent in the droplets was evaporated at the low temperature zone of the reactor to produce a powder composite consisting of silica and PS nanoparticles. The PS nanoparticles in the powder were evaporated in the high temperature zone of the reactor to produce a silica powder consisting of mesopores. The mesopores was observed to be arranged into a hexagonal packing, indicating the self organization process occurred spontaneously during the solvent evaporation. The entire process was completed in only

several seconds, which is the contrary to currently available methods that require several hours or up to several days to complete this self-organization process. Offer of porous particles is now very large, from the industrial market. From this background, in this thesis, preparation of porous silica and titania particles using a two-fluid nozzle as the droplet atomizer in spray drying process was investigated. Spray drying method with two fluid nozzle was used to produce composite particles consisting of silica or titania nanocolloids and template particles (polystyrene latex: PSL). After removing template particles from the composite particles by heating and washing with organic solvent respectively, porous SiO₂ and TiO₂ particles were prepared. The average size and standard deviation of particles prepared by spray drying method with two fluid nozzle were 1.31 μm and 1.59 respectively. By changing template particles size ranging from 100 - 400 nm, porous particles were synthesized when using the template particles with the size of 200 nm or smaller, while hollow particles were obtained using template particles of 300 nm or larger. In addition, polyethylene glycol (PEG) porous particles can be obtained using the same method. Details of this research can be found on reference (Ogi. et al., 2007).

1.4 Objectives

The objective of this thesis is to investigate the synthesis of high crystalline functional fine particles using the liquid phase processes, including sol-gel and spray method systematically. The applications for nitride/oxide phosphor materials, transparent conductivity oxide materials, and oxide porous materials were investigated. Especially in this thesis, synthesis of gallium nitride (GaN) nanoparticles, oxynitride B-C-N-O phosphors and $\text{BaMgAl}_{10}\text{O}_{17}:\text{Eu}^{2+}$ (BAM: Eu^{2+}) particles was reported.

The schematic diagram of organization and structure of this dissertation is shown below (Fig. 1.4).

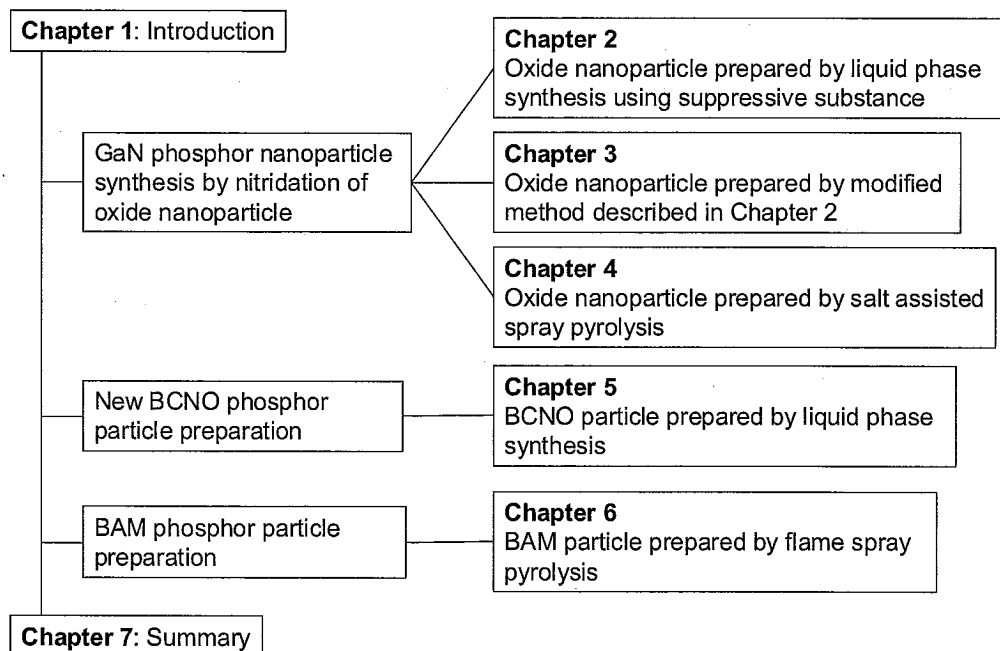


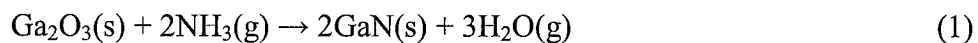
Fig. 1.4 Organization and structure of chapters of present thesis

Preparation of ordered porous particles using a spray drying method and fabrication and characterization of ITO film using its nanoparticles prepared by LPSP

were also reported as well (Ogi. et al., 2006, Ogi. et al., 2007).

In **Chapter 1**, the background, previous research, and the main objectives of the thesis are introduced.

In **Chapters 2 to 4**, the preparation of highly crystalline GaN nanoparticles using nitridation of Ga₂O₃ nanoparticles under a flow of ammonia was investigated. The nitridation reaction to form GaN is by reacting gallium oxide, Ga₂O₃ with ammonia as the following equation reaction (Jung et al., 2006):



The reaction between Ga₂O₃ particle and ammonia gas can be assumed heterogeneous shrinking-core model of unchanging size of spherical particles (Froment et al., 1979). The succession mechanism is shown in Fig. 1.5.

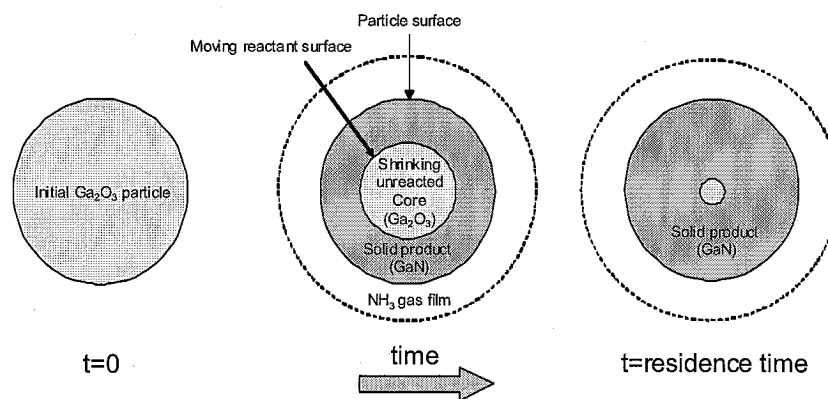


Fig. 1.5 Shrinkage core model illustration without changing particle size

Most of the reported methods for the preparation of GaN from Ga₂O₃ used micrometer/submicrometer sized Ga₂O₃ to produce submicrometer sized GaN. This usually results in a longer nitridation time, i.e. a longer time for the N atom to diffuse

into Ga_2O_3 particles for the reason above-mentioned. Consequently, if the time allocated is insufficient, incomplete transformation of Ga_2O_3 to GaN may occur. Therefore, instead of obtaining pure GaN particles, one merely obtains GaN-coated Ga_2O_3 particles. (Fig. 1.6a) It is a challenge to use nanometer sized Ga_2O_3 as the starting material for conversion, in order to reduce the nitridation time. The large surface area and small penetration depth provided by nanometer sized particles will allow a reduction in the nitridation time. (Fig. 1.6b) Therefore, the objective of chapters 2 to 4 is to produce highly crystalline nano-sized GaN particles derived from Ga_2O_3 nanoparticles by nitridation.

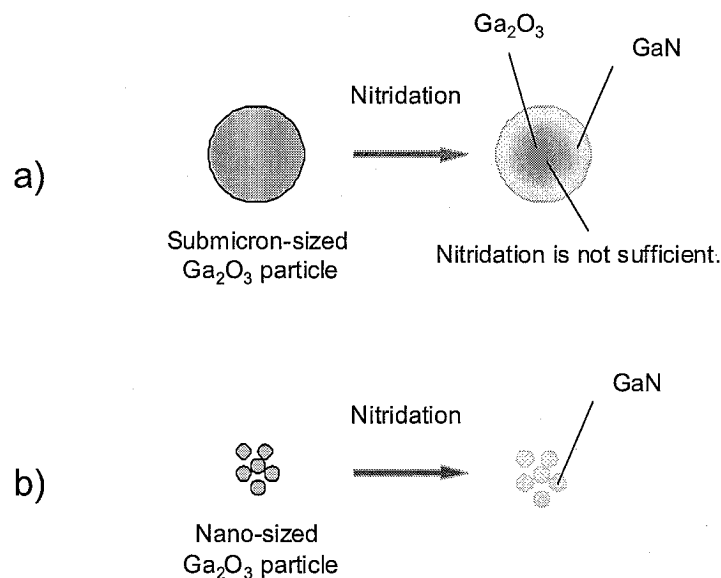


Fig. 1.6 Preparation methods of GaN nanoparticles in this thesis

In **Chapter 2**, the preparation of highly crystalline GaN nanoparticles using nitridation of Ga_2O_3 nanoparticles under a flow of ammonia was examined. Mixtures of gallium nitrate aqueous solution and ammonia solution were heated to between 600 and 800 °C. The effects of aqueous ammonia concentration and conversion temperature on

the morphology and crystallinity of GaN particles were investigated and optimum conditions for the production of well-dispersed nano-sized GaN particles are discussed. The mechanism of nanoparticles formation of GaN via this method is also discussed.

In **Chapter 3**, the producing of GaN nanoparticles from gallium nitrate and ammonia solution were examined. This method has a number of advantages over the method shown in chapter 2 in that it is a straightforward process with a high production rate. The effects of preparation conditions such as solution composition, operating temperature, and reaction time on the characteristics of GaN particles were investigated.

In **Chapter 4**, the synthesis of GaN nanoparticles from nano-sized Ga₂O₃ particles were prepared by salt-assisted spray pyrolysis (SASP) under a flow of ammonia gas was investigated. A mixture of metal nitrate and salt dissolved in an aqueous solution was sprayed into the tubular reactor by means of an ultrasonic atomizer. The effects of salt concentration and operating temperature on the morphology and crystallinity of Ga₂O₃ particles were investigated and optimum conditions for the producing of Ga₂O₃ nanoparticles with a narrow particles size distribution are discussed. The effects of the crystallinity of the Ga₂O₃ particles and of the nitridation time on transformation to GaN also were investigated. The effects of the crystallinity of the Ga₂O₃ particles and nitridation time on transformation to GaN were characterized using X-ray diffraction and scanning/transmission electron microscopy.

In **Chapter 5**, the preparation of a new full-color-emitting phosphor, composed of BCNO atoms using liquid process at low temperatures (below 900°C) under

atmospheric pressure in a one-step was reported. The BCNO phosphors were synthesized from the following precursors: boron acid (H_3BO_3), as the boron source; urea ($(\text{NH}_2)_2\text{CO}$), as the nitrogen source; and, polyethylene glycol, $(\text{H}(\text{EG})_n\text{OH})$, with $M_w = 20,000$ and $\text{EG} = \text{OCH}_2\text{CH}_2$, as the carbon source. Effects of operating temperature, reaction time, and PEG concentration on photoluminescence properties were investigated systematically.

In **Chapter 6**, the producing of $\text{BaMgAl}_{10}\text{O}_{17}:\text{Eu}^{2+}$ (BAM:Eu) phosphor particles using flame spray pyrolysis method was designed. Characteristics such as photoluminescence, crystallinity and particle morphology were investigated for products prepared under various conditions and they were compared with those of the commercial product.

Chapter 7 contains the general conclusion of all topics discussed in Chapters 2 to 7.

References

- Abdullah, M., F. Iskandar, S. Shibamoto, T. Ogi and K. Okuyama, *Acta Mater.*, **52**, 5151-5156 (2004)
- Abdullah, M., K. Okuyama, I. W. Lenggoro, and S. Taya, *J. Non-Cryst. Solids*, **351**(8-9), 697-704 (2005a)
- Abdullah, M., I. W. Lenggoro, B. Xia and K. Okuyama, *J. Ceram. Soc. Jpn. (Spec. Issue - Innovative Ceramics)*, **113**(1), 97-100 (2005b)
- Adschiri, T. K., Kanazawa, K., and Aesai, K., *J Am. Ceram. Soc.*, **75**, 2615 (1992)
- Akkad, El, F. Marafi, M., Punnoose, A., Prabu, G., *Physica Status Solidi (A) Applied Research* **177** (2), 445 (2000)
- Alam, M.J., Cameron, D.C., *Thin Solid Films* **377**, 455 (2000)
- Azuma, Y., Shimada, M., Okuyama, K., *Chem. Vapor Depos.* **10**(1), 11 (2004)
- Azuma, Y., Shimada, M., Okuyama, K., *J. Chem. Eng. Jap.* **38** (7), 516 (2005)
- Bai, X. D., Wang, E. G., Yu, J. and Yang, H., *Appl. Phys. Lett.*, **77**, 67. (2000a)
- Bai, X. D., Guo, J. D., Yu, J., Wang, E. G., Yuan, J., Wang, W., *Appl. Phys. Lett.*, **76**, 2624 (2000b)
- Cartenuto G., Y.S. Her, E. Matijevic, *Ind. Eng. Chem. Res.* **35**, 2929 (1996)
- Fendler, J. H., *Chem. Rev.*, **87**, 877, (1987)
- Fotou, G.P., Scott, S.J., Pratsinis, S.E., *Combust. Flame* **101** (4), 529 (1995)
- Frank, A. C., R. A. Fischer, *Adv. Mater.*, **10**(12), 961 (1998)
- Froment, G. F.; K. B., Bischoff, *Chemical reactor analysis and design*. John Wiley & Sons, Inc.: USA, (1979).
- Gao, Z, Y. Z. Gao, Y.H. Li, and L. Li, *Nanostruct. Mater.*, **11**, 611 (1999)
- Goebbert, C., Nonninger, R., Aegerter, M.A., Schmidt, H., *Thin Solid Films* **351** (1-2),

- 79 (1999)
- Granqvist, C.G, Hultaker, A., *Thin Solid Films* **411** (1), 1 (2001)
- Gurav, A., Kodas, T., Pluym, T., Xiong, Y., *Chem. Mat.* **5** (2), 214 (1993)
- Hara, K., Y. Matsuno, Y. Matsuo, *Jpn. J. Appl. Phys.*, **40**, 242 (2001)
- Hara, K., T. Matsumoto, E. Okuyama, *Jpn. J. Appl. Phys.*, **41**, 1351 (2002)
- Hirosaki, N., R. J. Xie, K. Kimoto, T. Sekiguchi, Y. Yamamoto, T. Suehiro, M. Mitomo, *Appl. Phys. Lett.*, **86**, 1-3 (2005)
- House, H. O., *W.A. Benjamin Inc., Redwood, CA.* (1972)
- Iskandar, F., I. W. Lenggoro, B. Xia and K. Okuyama, *Journal of Nanoparticle Research*, **3**, 263-270 (2001a)
- Iskandar, F., Mikrajuddin, Okuyama, K., *Nano Lett.*, **1** (5), 231 (2001b)
- Iskandar, F., Mikrajuddin, Okuyama, K., *Nano Lett.*, **2** (4), 389 (2002)
- Iskandar, F., L. Gradon and K. Okuyama, *Journal of Colloid and Interface Science*, **265**, 296-303 (2003a)
- Iskandar, F., H. W. Chang and K. Okuyama, *Advanced Powder Technology*, **14**, 349 (2003b)
- Itoh S., H. Toki, K. Tamura, F. Kataoka, *Jpn. J. Appl. Phys.* **38** 6387 (1999)
- Jegier, J. A., S. McKernan, W. L. Gladfelter, *Chem. Mater.*, **10**, 2041 (1998)
- Jegier, J. A., S. McKernan, A. P. Purdy, W. L. Gladfelter, *Chem. Mater.*, **12**(4), 1003, (2000)
- Ju, Y.G., G. Almuneau, T.H. Kim, B.W. Lee, *Jpn. J. Appl. Phys.* **45** (4A) 2546 (2006)]
- Jung, W., -S., *Mater. Lett.*, **60**, (24), 2954 (2006)
- Kanatzidis M.G., C. Wu, H.O. Marcy, D.C. DeGroot, C.R. Kannewurf, *Chem. Mater.* **2** 222 (1990)

- Kang, Y. C., S. B. Park, *J. Aerosol Sci.*, **26** (7), 1131 (1995a)
- Kang, Y. C., S. B. Park, Y. W. Kang, *Nanostruct. Mater.*, **5** (7-8), 791 (1995b)
- Kang, Y. C., S. B. Park, *J. Mater. Sci. Lett.*, **16**, 131 (1997)
- Kang, Y. C., Y. S. Chung, and S. B. Park, *J. Am. Ceram. Soc.*, **82** (2), 2056 (1999a)
- Kang, Y. C., and S. B. Park, *J. Mater. Sci. Lett.*, **18**, 779 (1999b)
- Kang, Y. C., and S. B. Park, *Mater. Res. Bull.*, **35**, 1143 (2000)
- Kawaguchi, M., K. Nozaki, Y. Kita, and M. Doi, *J. Mater. Sci.* **26**, 3926 (1991)
- Kawaguchi, M., *Adv. Mater.*, **9**, 615 (1997)
- Kilian, A., Morse, T.F., *Aerosol Sci. Technol.* **34** (2), 227 (2001)
- Kim, H., Horwitz, J.S., Kushto, G., Piqué, A., Kafafi, Z.H., Gilmore, C.M., Chrisey, D.B.
J. Appl. Phys. **88** (11), 6564 (2000)
- Kodas, T. T., M. H. Smith, *Aerosol Processing of Materials*, Wiley VCH, New York,
(1999)
- Kyprianidou-Leodidou, T., W. Caseri, U.W. Suter, *J. Phys. Chem.* **98**, 8992 (1994)
- Lee, C. H., C. S. Huang, *Mater. Sci. Eng.*, **B22**, 233 (1994)
- Lenggoro, I. W. T. Hata, F. Iskandar, M. M. Lunden and K. Okuyama, *J. Mater. Res.*, **15**
733 (2000)
- Levenspiel, O., *Chemical Reaction Engineering*. Third Edition ed.; John Wiley & Sons,
Inc.: New York, (1999)
- Limaye, A.U., Helble, J.J., *J. Am. Ceram. Soc.* **85** (5), 1127 (2002)
- Look, D. C., B. Claflin, Ya. I. Alivov, S. J. Park, *Phys. Stat. Sol. (a)* **201**, 2203 (2004)
- Matijevic, E. *Faraday Discuss.*, **92** :229 (1991)
- Mädler, L., Kammler, H.K., Mueller, R., Pratsinis, S.E., *J. Aerosol. Sci.*, **33** (2), 369
(2002)

- Meng, L.-J., Dos Santos, M.P., *Thin Solid Films* **322** (1-2), 56 (1998)
- Messing, G. L., S. C. Zhang, G. Jayanthi, *J. Am. Ceram. Soc.*, **76**, 2702 (1993)
- Nagy, J. B., Derouane, E. G., Gourgue, A., Lufimpadio, N., Ravet, I., and Verfaillie, J. P., *Surfactants in solution*, **10** K. L. Mittal, ed., Plenum Press, New York 1, (1989)
- Nakamura, S., *Science*, **281**, 956 (1998)
- Nalwa, H. S., L. S. Rohwer, *Handbook of Luminescence, Display Materials and Nanocomposite*, American Scientific Publisher, California, (2003)
- Ogi, T., Iskandar, F., Itoh, Y., Okuyama, K. *J. Nanoparticle Res.* **8** (3-4), 343 (2006)
- Ogi, T., Iskandar, F., Yabuki, A., Okuyama, K., *Kag. Kog. Ronbunshu* **33** (5), 468 (2007)
- Okuyama K., D.D. Hung, J.H. Seinfeld, N. Tani, Y. Kousaka, *Chem Eng. Sci.*, **46**, 1545 (1991)
- Okuyama K., M. Abdullah, I.W. Lenggoro, F. Iskandar, *Adv. Powder Technol.* **17**, 587-611 (2006)
- Okuyama K., I. W. Lenggoro, *Chem. Eng. Sci.* **58**, 537-547 (2003)
- Panatarani, C., I. W. Lenggoro, N. Itoh, H. Yoden, and K. Okuyama, *Mater. Sci. Eng. B.*, **122** (3), 188-195 (2005)
- Porowski S., *J. Cryst. Growth* **166**, 583 (1996)
- Qiu, Y., L. Gao, *Chem. Lett.*, **32**(8), 774 (2003)
- Sakai, S., S. Kurai, T. Abe, Y. Noi, *Jpn. App. Phys.*, **35**, L77 (1996)
- Sawada, Y., Kobayashi, C., Seki, S., Funakubo, H., *Immunol. Lett.* **81** (3), 171 (2002)
- Schmidt, H.K., *Macromol. Symp.* **101**, 333 (1996)
- Steigerwald, D., *IEEE J. Sel. Top. Quantum Electron.* **8** (2), 310 (2002)
- Sujatha Devi, P., Chatterjee, M., Ganguli, D., *Mater. Lett.* **55** (4), 205 (2002)
- Takai, O., J. Tomizawa, Y. Hisamatsu, *Ext. Abstr. (Proc. 7th ICVM 1982): The Iron and*

Steel Institute of Japan, 981 (1982)

- Tani, T., Takatori, K., Pratsinis, S.E., *J. Am. Ceram. Soc.* **87** (3), 365 (2004)
- Toki, H., Y. Sato, K. Tamura, F. Kataoka, S. Itoh, *IDW'96*, 519 (1996)
- Tomonaga, H., Morimoto, T., *Thin Solid Films* **392** (2), 243 (2001)
- Vecht, A., C. Gibbons, D. Davies, X. Jing, P. Marsh, T. Ireland, J. Silver, A. Newport and D. Barber, *J. Vac. Sci. Technol.* **B 17**, 750 (1999)
- Vemury, Srinivas, Pratsinis, Sotiris E. *J. Am. Ceram. Soc.* **78** (11), 2984 (1995)
- Vossen, J. L., *Phys. Thin Films*, **9**, 1 (1997)
- B. Wang, G.L. Wilkes, U.S. Patent No. 5109080, (1992).
- Watanabe, M. O., S. Itoh, T. Sasaki, and K. Mizushima, *Phys. Rev. Lett.* **77**, 187 (1996)
- Wei, Q., Zheng, H., Huang, Y., *Sol. Energy Mater. Sol. Cells* **68** (3-4), 383 (2001)
- Wu, J., Han, W.-Q., Walukiewicz, W., Ager III, J.W., Shan, W., Haller, E.E., Zettl, A., *Nano Lett.*, **4** (4), 647 (2004)
- Xia, B., I. W. Lenggoro, K. Okuyama, *Adv. Mater.*, **13** (20), 1579 (2001)
- Xia, B., I. W. Lenggoro, K. Okuyama, *J. Mater. Res.*, **15** (10), 2157 (2000)
- Xia, B., I. W. Lenggoro, K. Okuyama, *J. Mater. Sci.*, **36** (7), 1701 (2001a)
- Xia, B., I. W. Lenggoro, K. Okuyama, *J. Am. Ceram. Soc.*, **84** (7), 1425 (2001b)
- Xiao, H. -D., H. -L. Ma, C. -S. Xue, J. Ma, F. -J. Zong, X. -J. Zhang, F. Ji, W. -R. Hu *Mater. Chem. Phys.*, **88**(1), 180 (2004)
- Yanagisawa, K., Udawatte, C.P., Nasu, S., *J. Mater. Res.* **15** (6), 1404 (2000)
- Yang, Y., C. Tran, V. Leppert, S. H. Risbud, *Mater. Lett.*, **43**, 240 (2000)
- Yang, Y., V. J. Leppert, S. H. Risbud, B. Twamley, P. P. Power, H. W. H. Lee *Appl. Phys. Lett.*, **74**(16), 2262 (1999)
- Yen, W. M., , S. Shionoya , *Phosphor Handbook*, CRC, Boca Raton, (1998)

Yin, L., W. Y. Bando, D. Golberg, A. Gloter, M. S. Li, X. L. Yuan, T. Sekiguchi, *J. Am. Chem. Soc.* **127**, 16354 (2005)

Yu, J., J. Ahn, S. F. Yoon, Q. Zhang, Rusli, B. Gan, K. Chew, M. B. Yu, X. D. Bai and E. G. Wang, *Appl. Phys. Lett.*, **77** (13), 1949 (2000)

Yu, J., Bai, X.D., Ahn, J., Yoon, S.F., Wang, E.G., *Chem. Phys. Lett.*, **323**(5-6), 529 (2000)

Zimmermann, L., M. Weibel, W. Caseri, U. W. Suter, *J. Mater. Res.* **8**, 1742 (1993)

Chapter 2

Fabrication and photoluminescence of highly crystalline GaN and GaN:Mg nanoparticles

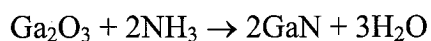
2.1 Introduction

GaN and its related compounds are the most promising wide band gap semiconductors for blue, violet and ultraviolet light emitting devices (Nakamura et al., 2000) and high temperature or high power electronic devices (Zolper et al., 1996). GaN-based light-emitting diodes (LEDs) have been shown to exhibit superior lifetimes and emitting output power compared to conventional LEDs (Zolper et al., 1996). Combination of GaN-based blue LEDs and cerium-doped yttrium aluminium garnet (YAG:Ce) powder has potential for use in the development of luminescence conversion LEDs (LUCOLEDs) that emit a white light (Schlotter et al., 1999).

Nanoparticles and nanostructured materials comprised of metals and semiconductors that exhibit size-dependent optical, magnetic, electronic and catalytic properties have recently been heralded as the next generation of electronic devices in the design of advanced materials. Synthesis of GaN nanoparticles has been reported by many authors, including techniques such as metal organic chemical vapor deposition

(MOCVD) (Azuma et al., 2004), in-situ synthesis of amorphous GaN nanoparticles in a polymer (Yang et al., 1999) pyrolysis at high temperatures (Janik et al., 2004, Coffey et al., 1997), and formation of colloidal GaN quantum dots (Mićić et al., 1999). However, the production rates of GaN nanoparticles prepared by the above methods are relatively low. Therefore, finding a method that is capable of producing nanoparticles at high production rates is very important for use in the mass production of devices.

One simple scheme for producing metal nitride powder with a high production rate is transformation of metal oxides into their nitrides under a flow of ammonia. Application of this method to the production of GaN particles has been reported by several authors, who flowed ammonia gas over a metal organic precursor (Kisailus et al., 2003) and gallium oxide at high temperatures (Cheng et al., 2000, Park et al., 2004, Jung et al., 2002, Cheng et al., 1999). When a metal organic precursor was used, a high temperature around 1200°C was needed to obtain GaN particles. However, when using gallium oxide as the precursor, the preparation temperature required was lower (i.e. below 1000°C). The chemical reaction for this transformation is below.



However, most of the reported methods for the preparation of GaN from Ga₂O₃ used micrometer/submicrometer sized Ga₂O₃ to produce submicrometer sized GaN. This usually results in a longer nitridation time, i.e. a longer time for the N atom to diffuse into Ga₂O₃ particles. Consequently, if the time allocated is not sufficient, incomplete transformation of Ga₂O₃ to GaN may occur. Therefore, instead of obtaining pure GaN particles, one merely obtains GaN-coated Ga₂O₃ particles. It is a challenge to

use nanometer sized Ga_2O_3 as the starting material for conversion, in order to reduce the nitridation time. The large surface area and small penetration depth provided by nanometer sized particles will allow a reduction in the nitridation time. In addition, using nanometer sized gallium oxide particles will allow production of nanometer sized GaN particles. Therefore, development of a method for the production of fine, homogeneous, highly crystalline nanoparticles at a high production rate is desirable for industrial application.

The objective of this chapter is to produce highly crystalline nano-sized GaN particles derived from Ga_2O_3 nanoparticles by nitridation, using a scalable method. Ga_2O_3 particles can be obtained by heating gallium nitrates. However, this approach results in agglomerated Ga_2O_3 particles (several micrometers in size). We found that addition of ammonia to the precursor resulted in well-dispersed nanometer sized oxide particles and reduced the particle size. Ammonia assisted in avoiding agglomeration of Ga_2O_3 particles. The method was then expanded to produce magnesium-doped GaN nanoparticles, to emit intense blue luminescence.

2.2 Experimental procedure

2.2.1. Precursor preparation

The procedure employed in this study for preparing the starting solution of Ga_2O_3 is shown as a flow diagram in Fig. 2.1. Gallium nitrate ($\text{Ga}(\text{NO}_3)_3 \cdot n\text{H}_2\text{O}$, Mitsuwa Chemicals Co., Ltd., Japan) was used as the gallium source. The number, n , of $\text{Ga}(\text{NO}_3)_3 \cdot n\text{H}_2\text{O}$ was determined to be 7.64 by ICP-AES analysis. $\text{Ga}(\text{NO}_3)_3$ was dissolved in ultra pure water and the total concentration of Ga was fixed at 0.5 mol/l.

Ammonia solutions (28 wt%, Kanto Kagaku, Japan), ranging from 0 to 6 mol/l, were mixed with the precursor solution at room temperature. The prepared solution was transparent except at high NH₃ concentrations.

2.2.2. Preparation of oxide nanoparticles

In the preparation of oxide nanoparticles, air, an oxidizing agent, was introduced into a tubular quartz tube reactor (0.038 m inner diameter, 0.8 m length) using a mass flow controller (MFC, FC-260 Tylan General) without preheating. The tubular reactor was heated in an electric furnace with three heating zones (0.05, 0.2, and 0.2 m in length). The mixed solution in the quartz boat was settled in a quartz tube heated at 800°C, unless otherwise stated.

2.2.3. Preparation of nitride nanoparticles

For the preparation of nitride particles from oxide nanoparticles, ammonia (NH₃) gas and Argon were used as the nitrogen source and carrier gas, respectively. First, the tubular reactor was heated at a fixed temperature of 700°C, 800°C or 900°C. The quartz boat was settled in the furnace and carrier gas and NH₃ were introduced into the reactor. The flow rates of NH₃ and Ar were kept at 500 sccm and 500 sccm, respectively, using MFCs. The reaction time was varied between 1 and 8 hours. After nitridation, the sample was cooled down to room temperature under an Ar atmosphere.

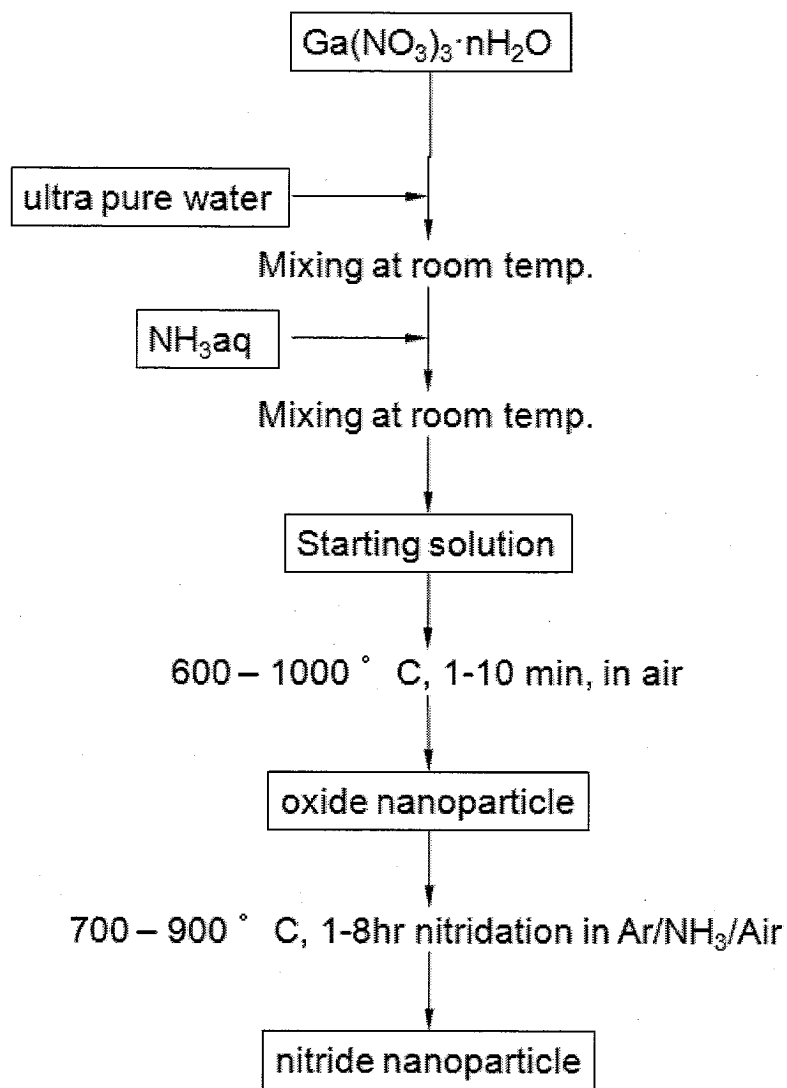


Fig. 2.1 Powder preparation procedure

2.2.4. Characterization

The resulting particles were collected under a nitrogen atmosphere and stored in a sample vessel with calcium oxide to avoid oxidation and absorption of water vapor. The surface morphology and crystal structure were observed by field emission scanning electron microscopy (FE-SEM; HITACHI S-5000) and high-resolution transmittance electron microscopy (HR-TEM; HITACHI HF-2000), respectively. The crystal phase was identified by powder X-ray diffraction (XRD; RIGAKU RINT-2200V) with $\text{CuK}\alpha$ radiation ($\lambda = 1.54058 \text{ \AA}$). The crystal size was estimated using the Scherrer formula. Elemental analysis of the resulting particles was performed by scanning Auger electron spectroscopy (AES PHI, SAM-670). For the AES sample, GaN powders were placed on a Si substrate under a nitrogen atmosphere. Photoluminescence (PL) spectra were recorded at room temperature using a spectrophotometer (SHIMADZU RF-5300PC) with a xenon lamp source. The chemical composition of gallium and nitrogen in the resulting powders was measured by inductively coupled plasma-atomic emission spectroscopy (ICP-AES; SII SPS-3000) and a nitrogen analyzer (HORIBA EMGA-620W/C), respectively. The nitrogen content of the GaN particles was measured by a thermal conductometric method after fusion in a current of inert gas.

2.3. Results and Discussion

SEM images of prepared Ga_2O_3 nanoparticles showing the effect of ammonia in the starting precursor on the size and dispersity of particles are given in Fig. 2.2 [$\text{NH}_3(\text{aq})/\text{Ga}(\text{NO}_3)_3 = (\text{a}) 0, (\text{b}) 0.1, (\text{c}) 1.0, (\text{d}) 10 \text{ mol/mol}$]. All samples were prepared at 800°C for 5 minutes. In the absence of ammonia, hard agglomerates of Ga_2O_3 particles were produced, as shown in Fig. 2.2(a). However, when ammonia was added,

the prepared Ga_2O_3 particles changed dramatically to being well-dispersed, and the particle size was reduced to a nanometer scale, as shown in Fig. 2.2(b-d). With a changing ammonia concentration, the particle sizes initially decrease with increasing ammonia concentration, and then increase after reaching a minimum value at $\text{NH}_3(\text{aq})/\text{Ga}(\text{NO}_3)_3 = 1$ (mol/mol). The prepared particle size was found to be around 40 nm in the case of an $\text{NH}_3(\text{aq})/\text{Ga}(\text{NO}_3)_3$ ratio of 0.1 (mol/mol) and decreased to around 20 nm with an $\text{NH}_3(\text{aq})/\text{Ga}(\text{NO}_3)_3$ ratio of 1 (mol/mol). Addition of ammonia at a high concentration ratio (e.g. 10 mol/mol) produced larger particles around 30 nm in size that formed soft agglomerates.

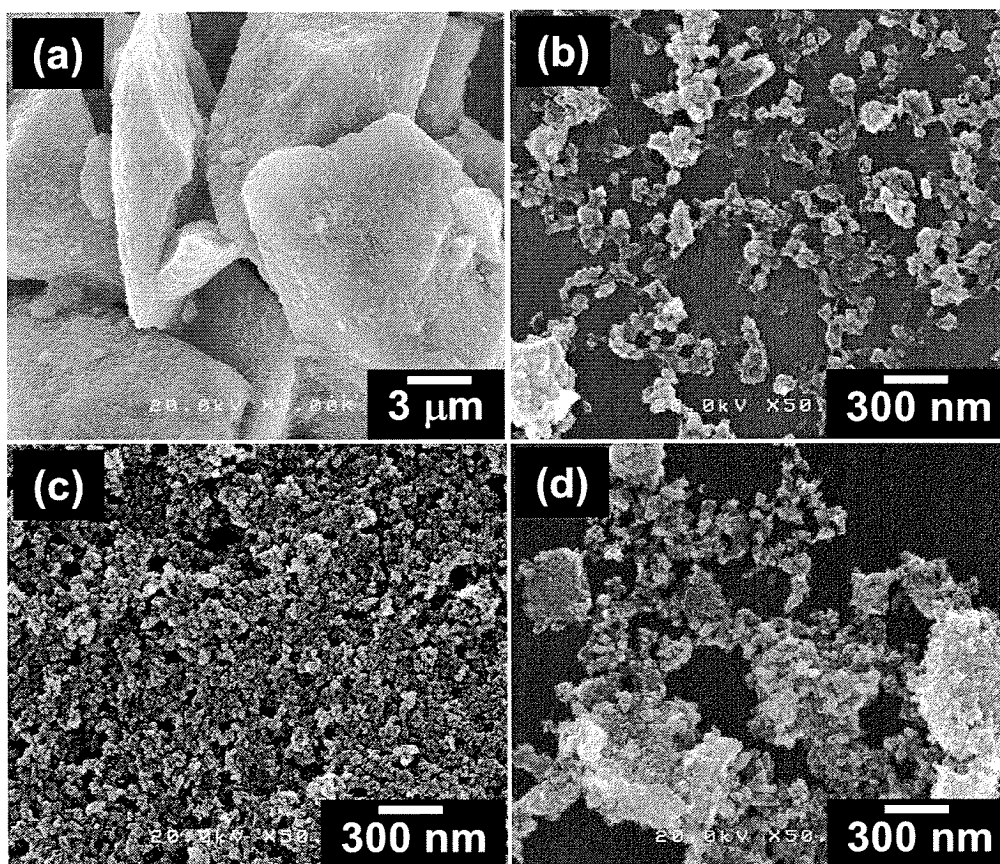
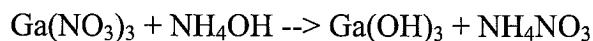


Fig.2.2 SEM images of Ga_2O_3 prepared at 800°C with various ratios of $\text{NH}_3(\text{aq})/\text{Ga}(\text{NO}_3)_3$:

(a) 0, (b) 0.1, (c) 1.0, and (d) 10 (mol/mol).

The ammonia solution plays a role to avoid the agglomeration of prepared Ga₂O₃ particles. In the heating process below 100°C, the mixed solution of Ga(NO₃)₃ and ammonia solution formed a gel containing Ga(OH)₃ and NH₄NO₃ as shown by the chemical reaction (Suda et al., 2000):



From the measurement of XRD pattern (not shown here), we found that after temperature reaching 100°C, NH₄NO₃ was formed without Ga(OH)₃ pattern on it. We considered that the nucleation growth of Ga(OH)₃ was restrained by the formation of gel during evaporation of solution. This caused formation of Ga(OH)₃ in amorphous phase or their crystal size were very small that can be detected by XRD measurement. After temperature reaching 200 °C, the solution was completely evaporated, and there is no NH₄NO₃ pattern has been detected by XRD. That means NH₄NO₃ was already decomposed within the heating process between 100°C and 200°C. From temperature 200 °C, Ga₂O₃ pattern of XRD has been detected. The chemical reaction of preparation of Ga₂O₃ from Ga(OH)₃ could be: 2Ga(OH)₃ → Ga₂O₃ + 3H₂O. Due to Ga(OH)₃ were isolated and dispersed very well in the NH₄NO₃ gel (or matrix), the produced Ga₂O₃ particles become smaller and non-agglomeration.

In the next part, we will consider only samples prepared using NH₃(aq)/Ga(NO₃)₃ = 1 (mol/mol). A TEM picture of Ga₂O₃ particles prepared at 800°C using NH₃(aq)/Ga(NO₃)₃ = 1 (mol/mol) is shown in Fig. 2.3(a), and the corresponding XRD patterns are shown in Fig. 2.3(b):(i). A particle size of about 20 nm is observed in the TEM image. The XRD peaks clearly confirm that the sample was Ga₂O₃. The size of the produced Ga₂O₃ particles is small enough to expect rapid conversion into GaN under an ammonia flow, based on the reaction Ga₂O₃ + 2NH₃ → 2GaN + 3H₂O.

To determine the optimum GaN conversion temperature, we tried three conversion temperatures (650°C, 800°C, and 900°C). All Ga₂O₃ samples were previously synthesized at 800 °C. The evolution of XRD patterns as a function of the conversion temperature is displayed in Fig. 2.3 (b):(ii)-(iv). At a conversion temperature of 650°C, the XRD patterns did not differ much from those of Ga₂O₃. The patterns changed to broad hexagonal GaN (h-GaN) patterns at 800°C, and became those of the highly crystalline h-GaN phase at 900°C. For comparison, we also treated commercially available Ga₂O₃ particles (Kanto Chemicals, Japan) with particle sizes of about 1 μm at a conversion temperature of 800°C (NH₃ flow rate 500 sccm and Ar flow rate 500 sccm). The XRD patterns obtained are shown in Fig. 2.3(c) and the corresponding SEM picture is placed in the inset of Fig. 2.3(c). In this sample, we did not obtain clear GaN peaks. Instead, we observed what were likely weak GaN peaks with a strong Ga₂O₃ pattern in the background. Since the commercial Ga₂O₃ particles are large in size, they require a longer conversion time to allow N atoms to diffuse into the inner part of the Ga₂O₃ particles and completely replace oxygen atoms.

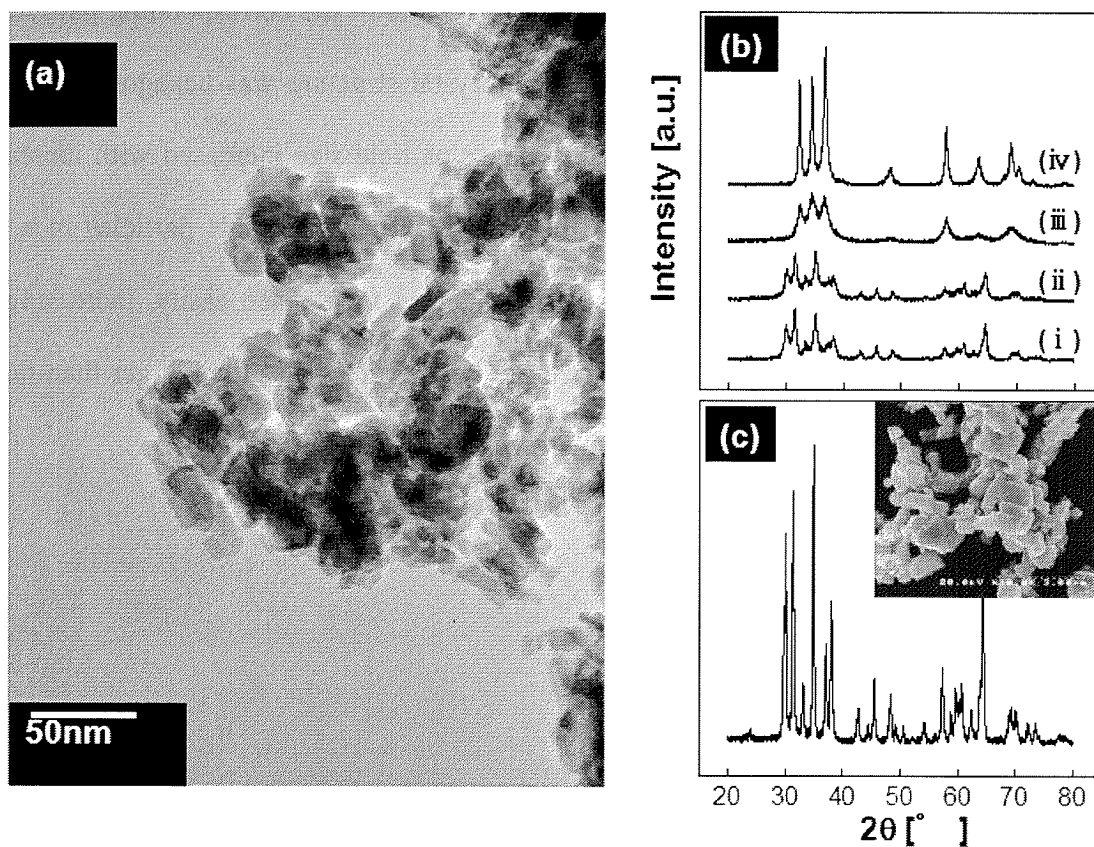


Fig.2.3 (a) TEM image of Ga_2O_3 prepared at 800°C with $\text{NH}_3(\text{aq})/\text{Ga}(\text{NO}_3)_3 = 1.0$; (b) XRD patterns of various samples: (i) Ga_2O_3 prepared at 800°C with $\text{NH}_3(\text{aq})/\text{Ga}(\text{NO}_3)_3 = 1.0$, (ii) sample in Fig. 2.3(a) after nitridation at (ii) 650°C , (iii) 800°C , and (iv) 900°C ; (c) XRD patterns of commercial GaN sample after nitridation at 800°C , the inset shows the corresponding SEM image.

TEM images of GaN samples prepared at 800°C and 900°C are shown in Fig. 2.4. The insets show high magnification HR-TEM images of the corresponding particles. A particle size below 40 nm is observed. The crystal structure was hexagonal, which is consistent with the XRD patterns. The primary particle size increased with increasing heating temperature. After Ga₂O₃ had been transformed into GaN particles in a high temperature environment, coalescence and sintering took place easily, increasing the final size of GaN particles. The final size of GaN particles was then larger than that of the Ga₂O₃ particles, which is in agreement with Fig. 2.3a and Fig. 2.4.

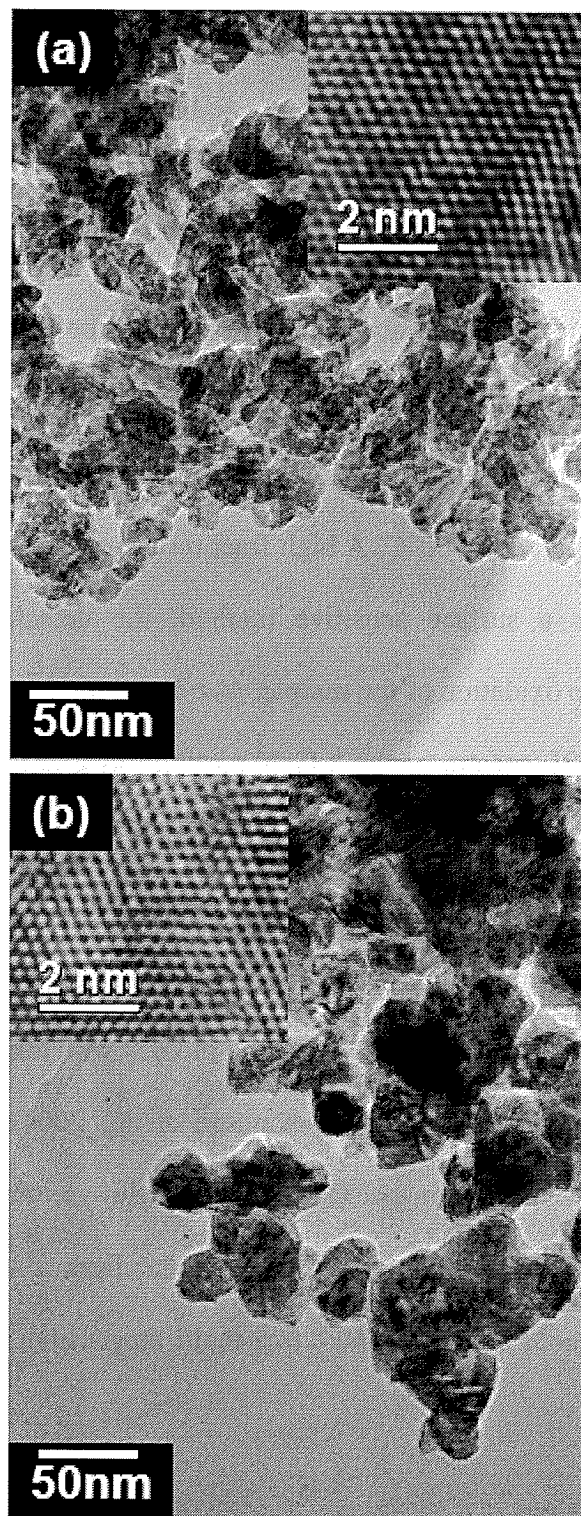


Fig.2.4 TEM images of GaN samples after nitridation at (a) 800°C and (b) 900°C. Insets give the corresponding HR-TEM images.

Chemical compositions of the GaN particles were determined using ICP-AES to determine the gallium content and a thermal conductometric method after fusion in a current of inert gas for the nitrogen content. The Ga/N ratios (atom/atom) of the GaN particles prepared at 700°C and 800°C, based on the bulk analyses, were 1.54 and 1.12, respectively. The increase in the nitrogen content should be attributed to the thermally enhanced diffusion rate of nitrogen atoms. AES results for GaN samples show an atomic ratio of Ga/N between 0.94-0.97 for samples prepared at 800 °C and between 0.96 – 1.36 for samples prepared at 900°C. A high fraction of oxygen was shown by the AES data. Since AES is a surface sensitive method, the detected oxygen should be attributable to surface oxidation of the sample. (Azuma et al., 2004)

Fig. 2.5 shows PL spectra of the h-GaN particles as a function of the conversion temperatures (a) 700 °C, (b) 800 °C, and (c) 900 °C. The peak wavelength of the sample was 364 nm at room temperature. The crystallinity of h-GaN particles increased with increasing conversion temperature, which in turn improved the PL intensity.

In previous work, it was shown that doping of GaN with alkali earth metals greatly improved the luminescence intensity (Nakamura et al., 2000). The present method described here allows easy doping of GaN particles with various metals. In this study, Mg-doped gallium oxide nanoparticles were prepared from a solution with 0.5 mol/l gallium nitrate, 0.5 mol/l ammonia and 0.025 mol/l magnesium nitrate at temperatures of 750°C and 800°C.

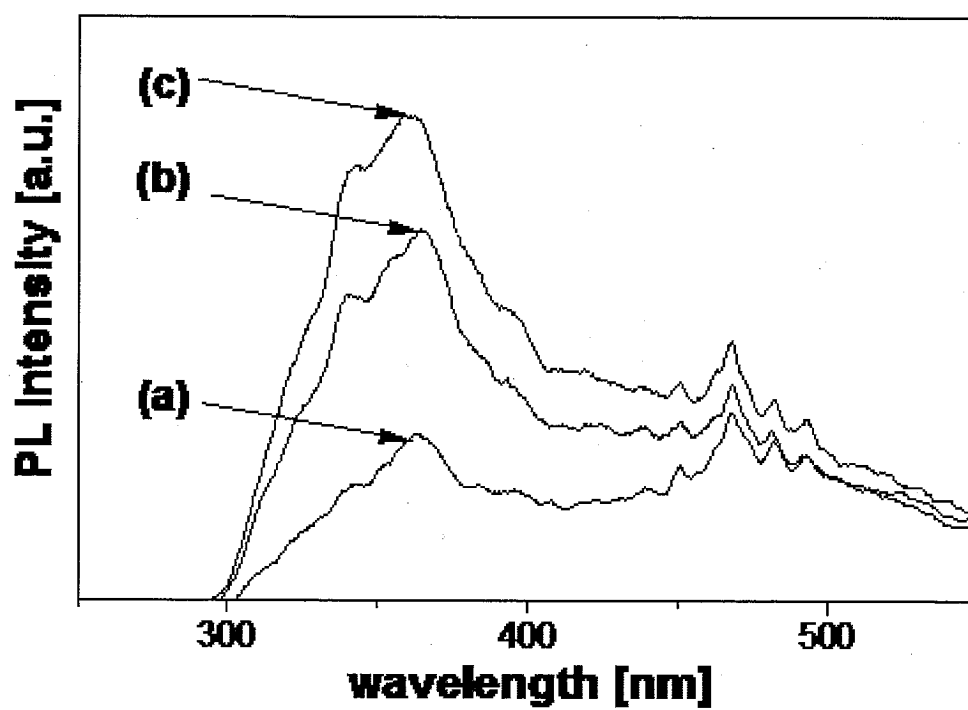


Fig.2.5 PL spectra of GaN samples after nitridation at (a) 700 °C, (b) 800 °C and (c) 900 °C.

Fig. 2.6 shows the PL intensity of GaN and Mg-doped GaN at room temperature with a fixed excitation wavelength of 254 nm. The addition of Mg as a doping material in GaN caused a shift in the peak PL to 450 nm (blue). Furthermore, the PL intensity of Mg-doped GaN was higher than the PL intensity of undoped GaN. As the conversion temperature increased to 800°C, the PL intensity of GaN:Mg also increased. However, a further increase in conversion temperature (to 900°C) resulted in a decrease in the PL intensity (not shown). This result has a similar trend to that of previous research (Nakamura et al., 2000). A possible reason for this could be that at higher temperatures GaN starts to decompose.

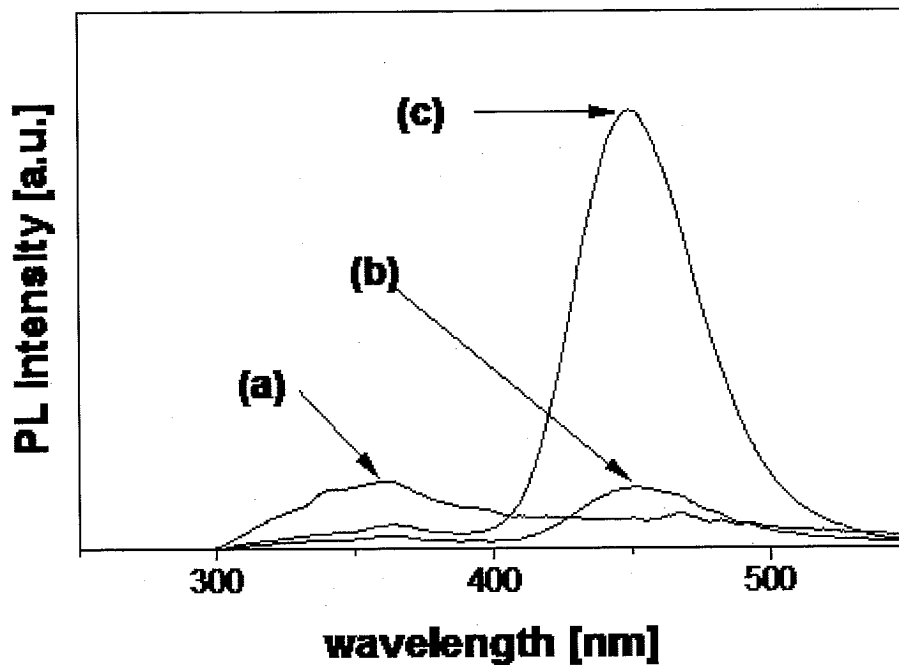


Fig.2.6 PL spectra of (a) undoped GaN prepared at 800°C, and Mg-doped GaN prepared at (b) 750°C and (c) 800°C.

2.4. Summary

Highly crystalline nano-sized GaN and GaN:Mg particles were prepared from Ga₂O₃ nanoparticles. The addition of a proportional amount of ammonia to the solution is a key factor in the production of well-dispersed nano-sized gallium nitride particles. Nitridation of gallium oxide nanoparticles under a flow of ammonia resulted in highly crystalline nano-sized GaN particles less than 40 nm in size. The GaN particles exhibited a weak PL intensity, while Mg-doped GaN particles showed a strong PL intensity peaking at 450 nm. The chemical ratio of Ga/N was almost stoichiometric. This methodology for converting oxide nanoparticles into their nitrides would be useful for achieving a high production rate for GaN particles, and should be applicable to the production of other metal nitrides as well.

References

- Azuma, Y., M. Shimada, K. Okuyama, *Chem. Vap. Deposit.* 10, 11(2004)
- Cheng, G.S., S.H. Chen, X.G. Zhu, Y.Q. Mao, L.D. Zhang, *Mater. Sci. Eng. A286*, 165. (2000)
- Cheng, G.S., L.D. Zhang, X.G. Zhu, S.H. Chen, Y. Li, Y. Zhu, G.T. Fei, *Nanostructure Mater.* 11 (1999) 421.
- Coffer, J.L., M.A. Johnson, L. Zhang, R.L. Wells, *Chem. Mater.* 9 (1997) 2671.
- Craford, M.G., S.A. Stockman, M.J. Peanasky, F.A. Kish, *Electroluminescence*, ed. G. Mueller (Academic Press, San Diego, 2000) Semiconductors and Semimetals, 64 Chap. 1.
- Janik, J.F., R.L. Wells, *Chem. Mater.* 8 (1996) 2708.

Jung, W.-S., *Mater. Lett.* 57 (2002) 110.

Kisailus, D., J.H. Choi, F.F. Lange, J. *Crystal Growth* 249 (2003) 106.

Mićić, O.I., S.P. Arhenkiel, D. Bertram, A.J. Nozik, *Appl. Phys. Lett.* 75 (1999) 478.

Nakamura, S., S. Pearton, G. Fasol, *The Blue Laser Diode*, ed. Springer 2000.

Park, Y.J., C.S. Oh, T.H. Yeom, Y.M. Yu, *J. Cryst. Growth* 264 (2004) 1.

Schlotter, P., J. Baur, Ch. Hielscher, M. Kunzer, H. Obloh, R. Schmidt, J.

Schneider, *Mater. Sci. Eng. B* 59 (1999) 390.

Suda, J., Y. Sato, F. Kataoka, H. Toki, H. Nomura, Japan patent JP 2000198978, 2000.

Yang, Y., V. J. Leppert, S. H. Risbud, B. Twamley, P.P. Power, H.W.H. Lee, *Appl. Phys. Lett.* 74 (1999) 2262.

Zolper, J.C., R.J. Shul, A.G. Baca, R.G. Wilson, S. Pearton, R.A. Stall, *Appl. Phys. Lett.* 68 (1996) 2273.

Chapter 3

Simple Synthesis of GaN Nanoparticles from Gallium Nitrate and Ammonia Aqueous Solution under a Flow of Ammonia Gas

3.1 Introduction

Due to a unique combination of properties, gallium nitride (GaN) and related compounds has become a promising material for use in applications such as advanced light emitting devices (Nakamura et al., 2000) and high power electronic devices (Zolper et al., 1996). Moreover, nanoparticles and nanostructured materials comprised of metals and semiconductors that exhibit size-dependent optical, magnetic, electronic and catalytic properties have recently been heralded as the next generation of electronic devices in the design of advanced materials. Therefore, a method for the simple, scalable and low-cost production of well-dispersed nanosized GaN particles would be desirable, especially on an industrial scale.

The synthesis of GaN nanoparticles has been reported by many authors, using techniques such as metal organic chemical vapor deposition (MOCVD) (Azuma et al., 2004), synthesis of GaN nanoparticles in a polymer or silica matrix (Yang et al., 1999,

Yang et al., 2000), pyrolysis at high temperatures (Janik et al., 1996, Coffey et al., 1997), and the formation of colloidal GaN quantum dots (Mičić et al., 1999). However, these methods entail a very high production cost together, are typically complicated and usually involve several steps thus making the overall process time consuming.

In the present work, we report on a simple method for the synthesis of nanosized GaN particles from a mixture of $\text{Ga}(\text{NO}_3)_3$ and ammonia solutions under a flow of ammonia gas. The use of an aqueous ammonia solution aids in the formation of well-dispersed GaN nanoparticles (Ogi et al., 2005). The proposed method has a number of advantages over previously used methods (Azuma et al., 2004, Yang et al., 1999, Janik et al., 1996, Coffey et al., 1997) in that it is a straightforward process with a high production rate. In addition, the fact that it is a simple process suggests that it would be amenable to low cost production. In a previous study, we used Ga_2O_3 nanoparticles produced by the pyrolysis of $\text{Ga}(\text{NO}_3)_3$, for the synthesis of GaN nanoparticles. In that report, the size of the resulting GaN nanoparticles was larger than that obtained using the present method.

3.2 Experimental procedure

The precursors used in preparing GaN nanoparticles included gallium nitrate ($\text{Ga}(\text{NO}_3)_3 \cdot n\text{H}_2\text{O}$, Mitsuwa Chemicals Co., Ltd., Japan) as the gallium source, and ammonia solutions (28 wt %, Kanto Kagaku, Japan). The number n , for $\text{Ga}(\text{NO}_3)_3 \cdot n\text{H}_2\text{O}$ was determined to be 7.64 by ICP-AES analysis. $\text{Ga}(\text{NO}_3)_3$ was dissolved in ultra pure water and the total concentration of Ga was fixed at 0.5 mol/l. Ammonia solutions, ranging from 0 to 1.8 mol/l were mixed with the precursor solution at room temperature. The resulting solution was transparent except at high NH_3

concentrations.

In the preparation process, a tubular reactor was used at a fixed temperature of either 700°C, 800°C or 900°C. The quartz boat was placed in the furnace, and carrier gas (N₂) and ammonia gas (NH₃) were introduced into the reactor. The flow rates of NH₃ and N₂ were maintained at 500 sccm and 500 sccm, respectively, using mass flow controllers (MFCs). The reaction time was varied between 1 and 8 h. After nitridation, the sample was cooled to room temperature under an N₂ atmosphere.

The prepared particles were collected under a nitrogen atmosphere and stored in a sample vessel with calcium oxide to avoid oxidation and the absorption of water vapor. The surface morphology was observed by field emission scanning electron microscopy (FE-SEM; HITACHI S-5000). The crystalline phase was determined by powder X-ray diffraction (XRD; RIGAKU RINT-2200V) with CuK α radiation ($\lambda = 1.54058 \text{ \AA}$). Photoluminescence (PL) spectra were recorded at room temperature using a spectrophotometer (SHIMADZU RF-5300PC) with a xenon lamp source.

3.3. Results and Discussion

XRD patterns of GaN nanoparticles prepared at various temperatures showed diffraction lines that were consistent with those of hexagonal GaN (JCPDS No. 74-0243) (Fig. 3.1). The diffraction peaks became sharper with increasing preparation temperature, especially when a temperature of 900°C was used, resulting in highly crystalline GaN nanoparticles. From the XRD results, no Ga₂O₃ diffraction patterns were observed even when the particles were prepared at lower temperatures (< 700°C). This indicates that the production of GaN from the precursors occurred without the

formation of intermediate Ga_2O_3 crystals. However, the possibility that amorphous Ga_2O_3 is formed prior to the production of GaN cannot be excluded. This differs from previously reported findings in other studies which showed that the conversion of GaN from gallium nitrate precursors usually proceeds through the formation of intermediate Ga_xO_y (Yang et al., 2000, Ogi et al., 2005).

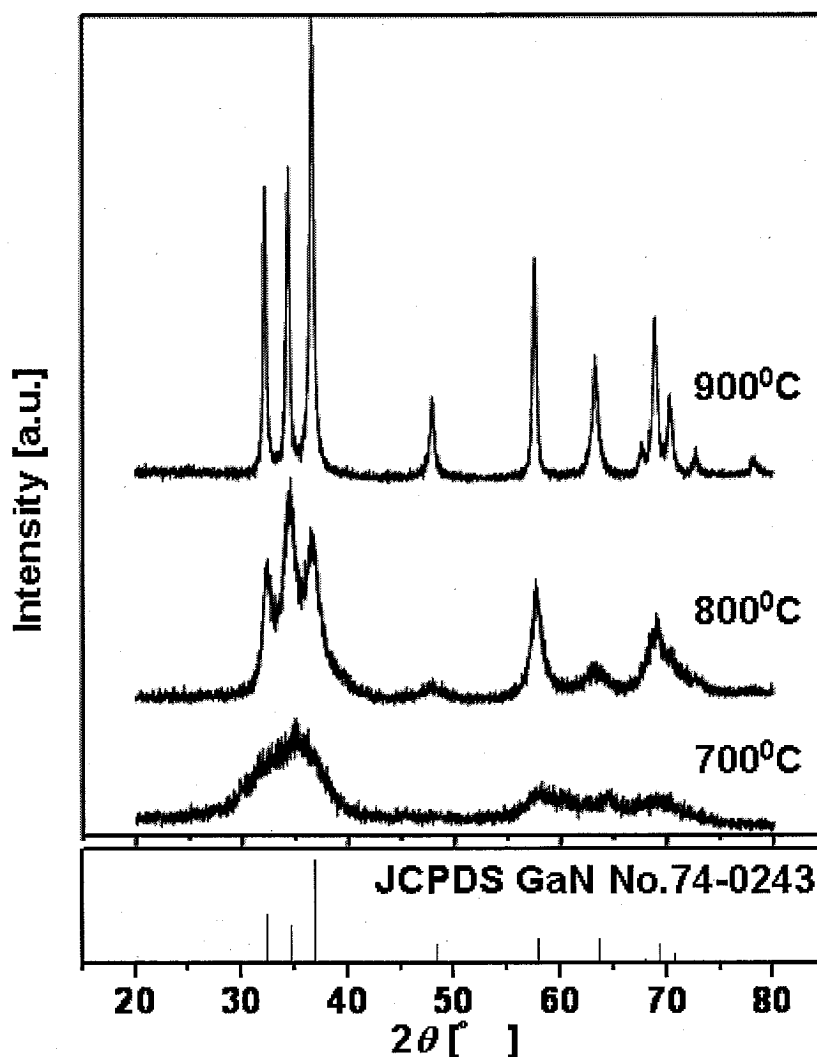


Fig. 3.1 XRD patterns of samples obtained by the pyrolysis of a mixture of $\text{Ga}(\text{NO}_3)_3$ and ammonia solutions as precursors in flowing ammonia at various temperatures: 700 °C, 800 °C and 900 °C, respectively, for 2 h.

SEM photographs of GaN nanoparticles prepared using different methods are shown in Fig. 3.2. The average particle size of GaN prepared using the present method at 800°C (Fig. 3.2b) was smaller (around 30 nm) than the average particle size obtained using our previous method (> 60 nm). In addition, no coalescence or sintering phenomena occurred on the particles when the present method was used. As shown in Fig. 3.2a, the nitridation of Ga₂O₃ at high temperatures resulted in sintered and agglomerated particles, while in the case of the direct preparation from Ga(NO₃)₃ and an aqueous NH₃ solution (the present method), since no intermediate Ga₂O₃ was formed, the resulting particles were well dispersed without agglomeration and the particle sizes were smaller.

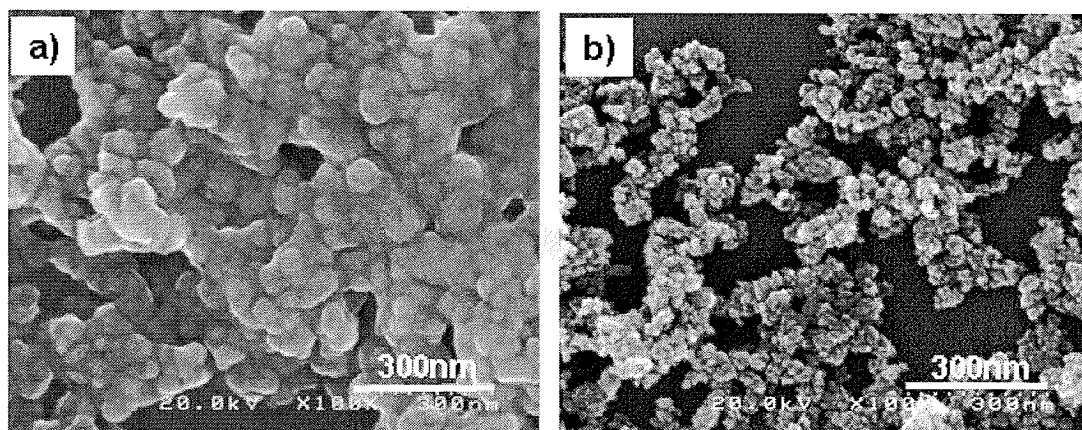


Fig. 3.2 SEM photographs of samples prepared from: a) Ga₂O₃ powder and b) a mixture of Ga(NO₃)₃ and ammonia solution; in a NH₃ atmosphere for 2 h at 800°C.

PL spectra for samples obtained at various temperatures were obtained at room temperature. As shown in Fig. 3.3, samples prepared between 700°C and 900°C showed an emission wavelength at 364 nm and an excitation wavelength at 254 nm, indicating

that the band edges of GaN had a wurtzite structure. A very high emission intensity was observed for a sample prepared at 800°C. Generally, for photoluminescence materials, a higher degree of crystallinity results in a higher PL intensity. However, in spite of the fact that the crystallinity of the sample prepared at 900°C was higher than the sample prepared at 800°C (see Fig. 3.1), the PL intensity was very low. This might be caused by the relatively small change in the crystal structure of the sample, which would not be detectable by the XRD measurements. It is known that the color of such materials is affected by their crystal structure as well as the band gap energy. In fact, GaN sample prepared at 900°C was black while GaN powders prepared at 700°C and 800°C were dark yellow in color.

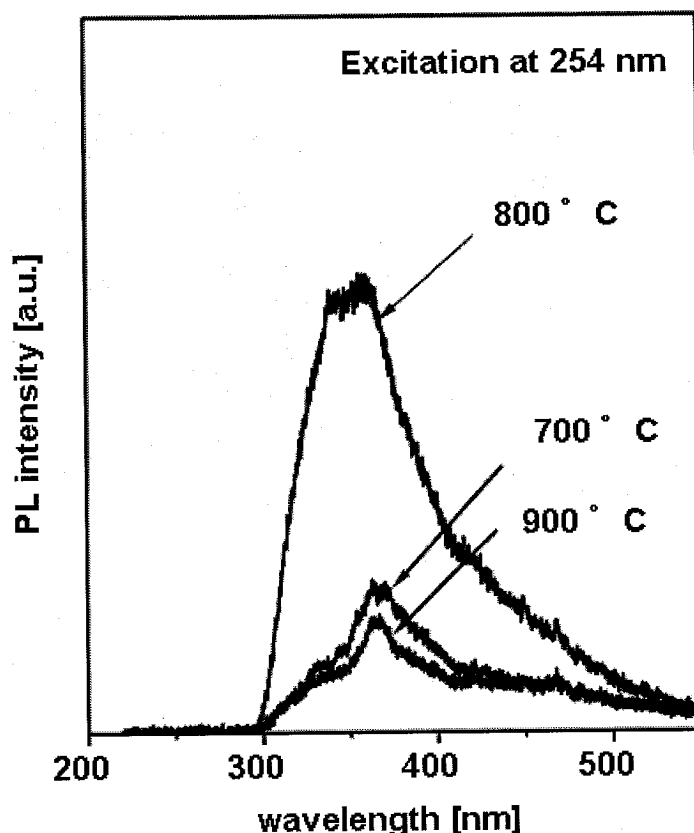


Fig.3.3 Room temperature PL spectra of samples obtained at various temperatures: 700 °C, 800 °C and 900 °C.

The crystallinity and PL intensities of the samples were also affected by the length of the heating time used. From the experimental results (data not shown), the used of a temperature of 800°C, and a heating time longer than 2 h was required to produce stable crystalline GaN nanoparticles. It was also found that when the heating time is increased in the first 4 h, the PL intensity increased with increasing heating time and then reached a maximum intensity at 4 h. This nitridation time is faster than that reported in previous reports, for instance, more than 15 h were needed for completion of the nitridation process (Yang et al., 2000). The faster nitridation time might be caused by the simple process associated with the present method, in which the $\text{Ga}(\text{NO}_3)_3$ precursor appears to be directly converted to GaN nanoparticles. The PL intensity of samples prepared for 8 h was lower than that for samples prepared for 4 h. This might also be caused by the different composition/structure of GaN nanoparticles that are prepared using 8 h; and in fact, it was also found that the sample prepared for 8 h was black in color.

Fig. 3.4 shows the effects of different concentrations of aqueous NH_3 aqueous solutions added to the precursors, on PL intensity. We found that the highest PL intensity was obtained when a 1.2 mol/l ammonia solution was used. This suggests that NH_3 molecules in the precursor affect the structure of the GaN particles that are produced. Further study will be needed to explain why NH_3 molecules in the precursor affect the structure of GaN particles.

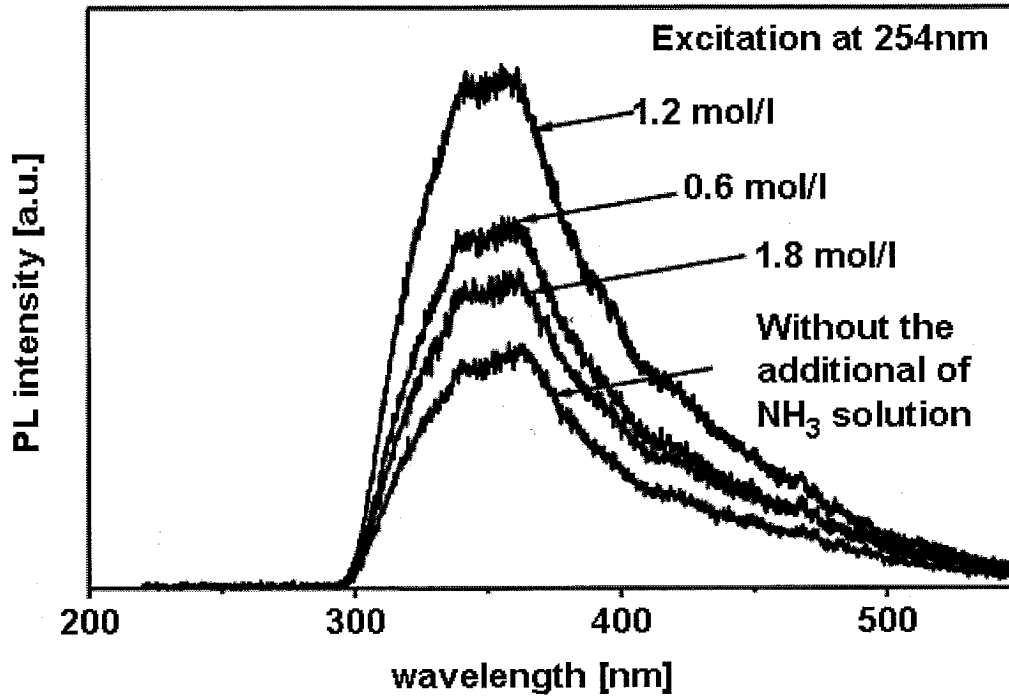


Fig. 3.4 Effects of different concentrations of ammonia solutions on PL intensity.

3.4. Summary

In summary, a simple, scalable process using gallium nitrate and ammonia solutions as precursors was developed for the synthesis of nanosized GaN particles. The method permits nanosized GaN particles, approximately 20 - 50 nm in average diameter, to be produced. We also found that the GaN nanoparticles had an intense photoluminescence at 364 nm when UV excitation at 254 nm was used.

References

- Azuma, Y., M. Shimada, K. Okuyama, *Chem. Vap. Deposit.* 10 (2004) 11.
- Coffer, J.L., M.A. Johnson, L. Zhang, R.L. Wells, *Chem. Mater.* 9 (1997) 2671.
- Janik, J.F., R.L. Wells, *Chem. Mater.* 8 (1996) 2708.
- Mićić, O.I., S.P. Arhenkiel, D. Bertram, A.J. Nozik, *Appl. Phys. Lett.* 75 (1999) 478.
- Nakamura, S., S. Pearton, G. Fasol, *The Blue Laser Diode*, ed. Springer 2000.
- Ogi, T., Y. Itoh, M. Abdullah, F. Iskandar, Y. Azuma, K. Okuyama, *J. Crystal Growth*, 281 (2005) 234.
- Yang, Y., C. Tran, V. Leppert, S. H. Risbud, *Mater. Lett.* 43 (2000) 240.
- Yang, Y., V. J. Leppert, S. H. Risbud, B. Twamley, P.P. Power, H.W.H. Lee, *Appl. Phys. Lett.* 74 (1999) 2262.
- Zolper, J.C., R.J. Shul, A.G. Baca, R.G. Wilson, S. Pearton, R.A. Stall, *Appl. Phys. Lett.* 68 (1996) 2273.

Chapter 4

Synthesis of nanocrystalline GaN from Ga₂O₃ nanoparticles derived from salt-assisted spray pyrolysis

4.1 Introduction

GaN and its related compounds have recently received considerable attention for their potential use in applications, such as blue-light-emitting and laser diodes, high-speed field-effect transistors, UV photodetectors, and high-temperature electronic devices (Gil, et al., 1998). In particular, GaN colloidal nanocrystals, also termed, “quantum dots” (QDs), are expected to have good thermal, chemical, and radiation stability, in addition to excellent optical properties (Pan, et al., 2006). For these reasons, a rational method for the dispersion of nanoparticles or colloids of free-standing nanocrystals of GaN is highly desirable.

GaN nanoparticle preparation has been investigated in many studies, which examined various methods, such as metal organic chemical vapor deposition (MOCVD) (Azuma, et al., 2004), in situ synthesis of amorphous GaN nanoparticles in a polymer (Yang, et al., 1999) and formation of colloidal GaN QD using non-aqueous solvothermal reactions (Micic, et al., 1999). However, these methods require

expensive precursors and produce GaN nanoparticles at relatively low rates. Therefore, a simple, scalable, low-cost method for the preparation of highly crystalline GaN nanoparticle powder is desirable for industrial-scale synthesis.

Our research group previously reported a simple scheme for the production of highly crystalline GaN nanoparticles based on transformation of Ga₂O₃ nanoparticles into their nitride-form under a flow of ammonia (Ogi, et al., 2005, Iskandar, et al, 2005). Although this method produced GaN nanoparticles at a high rate, the as-prepared GaN nanoparticles were agglomerated and had a broad particle size distribution. The Ga₂O₃ nanoparticles that were used as the starting material were prepared using a liquid synthesis method. It is difficult to produce non-agglomerated nanoparticles with narrow size distribution using this liquid synthesis method without a strong dispersing agent. Thus, the production of well-dispersed GaN nanoparticles is highly dependent on the particle distribution of the starting material— Ga₂O₃ nanoparticles. A salt-assisted spray pyrolysis (SASP) method has the potential to successfully produced well-dispersed Ga₂O₃ nanoparticles with homogeneous composition and a narrow size distribution. SASP is a modified spray pyrolysis (SP) process, in which salts are added to the precursor solution before atomization. The addition of flux salts to the precursor, which inhibit agglomeration of the as-prepared particles, resulted in well-dispersed, nanometer-sized oxide particles. This modified SP method is quite simple because nanometer-sized particles form at atmospheric pressure. Therefore, the present study investigated a novel method of synthesizing highly crystalline GaN nanoparticles with a narrow size distribution using Ga₂O₃ nanoparticles derived from salt-assisted spray pyrolysis as the starting material. The effects of the crystallinity of the Ga₂O₃ particles and of the nitridation time on transformation to GaN also were investigated. Elemental

mapping of GaN nanoparticles was studied via electron energy-loss spectrometry (EELS). In parallel, GaN nanoparticles were examined in detail using high transmittance electron microscopy and powder X-ray diffraction.

4.2 Experimental procedure

Fig. 4.1 illustrates the method and experimental apparatus used in nitride nanoparticle formation. This method used Ga₂O₃ and GaN preparation systems.

4.2.1. Ga₂O₃ preparation system

Gallium nitrate (Ga(NO₃)₃•nH₂O, Mitsuwa Chemicals Co., Ltd., Japan) was used as the gallium source. The number of water molecules, n, in the Ga(NO₃)₃•nH₂O was determined to be 7.64 by ICP-AES analysis. Ga(NO₃)₃ was dissolved in ultra pure water and the total concentration of Ga was fixed at 0.05 mol/l. Lithium chloride (LiCl, Kanto Chemicals Co., Ltd., Japan) was used as the flux salt at Li/Ga molar ratios ranging from 0 to 10 and was mixed with the precursor solution at room temperature. Solutions containing salts were atomized using an ultrasonic nebulizer operated at 1.7 MHz (NE-U17, Omron Co., Ltd., Tokyo, Japan). The resulting mist was carried by oxygen gas flowing at 2 l/min into a tubular alumina reactor maintained at a pre-determined temperature (700 - 1000°C), followed by heating for several seconds. The resulting particles were collected in an electrostatic precipitator that was maintained at approximately 180°C to avoid water condensation. The nanoparticles were obtained after washing the product with water to remove the flux salts. Details of the SASP method can be found elsewhere (Xia, et al., 2001, Okuyama, et al., 2006, Okuyama, et al., 2003).

4.2.2. GaN preparation system

For the preparation of the nitride nanoparticles from the oxide nanoparticles, ammonia (NH₃) gas and nitrogen gas (N₂) were used as the nitrogen source and carrier gas, respectively. First, the tubular reactor was heated at a fixed temperature of 900°C. The quartz boat was settled in the furnace and NH₃ and N₂ gases were introduced into the reactor. The flow rates of the NH₃ and N₂ gases were maintained at 0.5 l/min. After nitridation for various times, ranging from 1 to 120 min, the sample was collected under a N₂ atmosphere to avoid oxidation.

4.2.3. Characterization

The morphology and grain size of the resulting particles were observed by field emission scanning electron microscopy (FE-SEM, S-5000, Hitachi Corp., Tokyo, Japan) at 20 kV. The inner structure of the prepared particles was analyzed using a field emission transmittance electron microscope (FE-TEM; JEM - 3000F, JEOL, Tokyo, Japan) operated at 297 kV. Elemental mapping of the oxide/nitride particles was carried out using 3 windows method by a post column 90 degree energy filter system (GIF-2000 Gatan Inc., USA). The crystal phase was also characterized by powder X-ray diffraction (XRD, RINT 2200 V, Rigaku Denki, Tokyo, Japan) using nickel – filter Cu K α radiation ($\lambda= 1.54 \text{ \AA}$) at 40 kV and 30 mA with a scan step of 0.02° in 2 θ and a scan speed of 4°/min. Photoluminescence (PL) spectra of the prepared particles were recorded at room temperature using a spectrofluorophotometer (RF-5300PC, Shimadzu Corp., Kyoto, Japan) equipped with a xenon laser source excited at 254 nm.

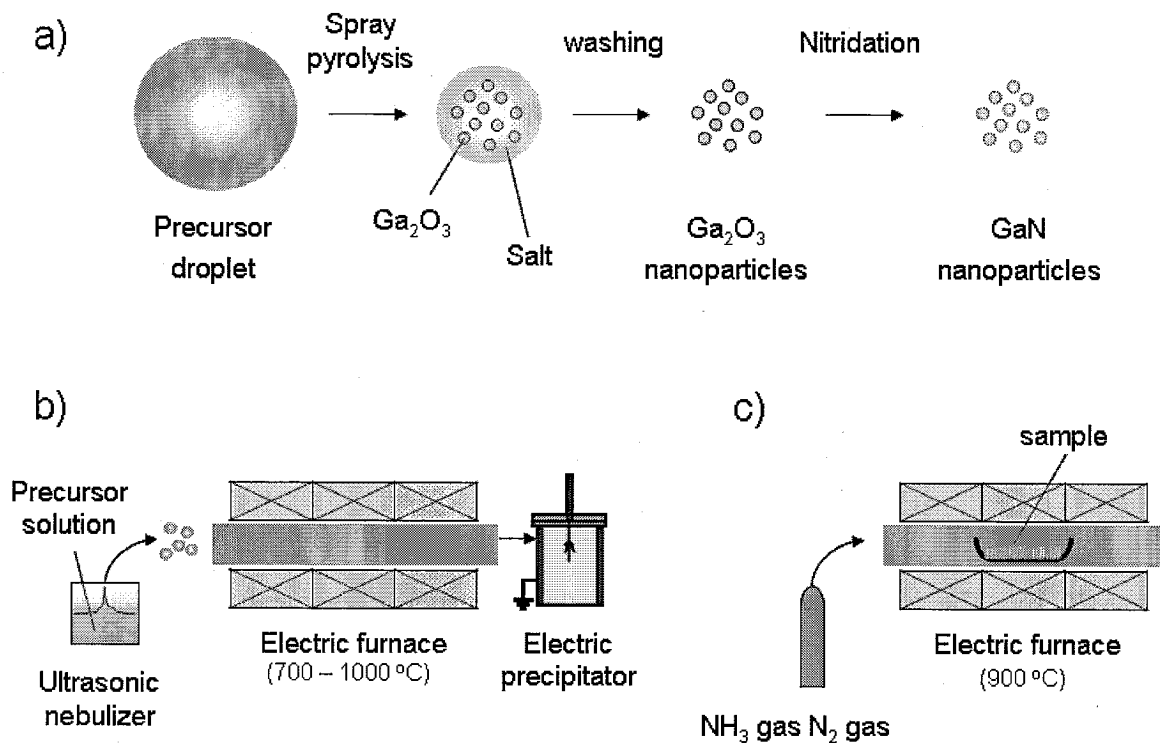


Fig. 4.1 (a) Procedure for the formation of nitride particles, (b) experimental apparatus for oxide particles, (c) experimental apparatus for nitride particles

4.3. Results and Discussion

4.3.1. Preparation of Ga₂O₃ nanoparticles

4.3.1.1. Effect of the salt concentration on particle morphology.

The effect of the salt concentration on particle morphology was investigated using FE-SEM. Fig. 4.2 shows FE-SEM images of the samples prepared at 800°C using the SASP method at Li/ Ga molar ratios of 0, 5, and 10. The geometric mean diameter and geometric standard deviation of the particles are shown in the inset of Fig. 4.2. The FE-SEM images showed that the particles synthesized without LiCl were spherical and dense submicrometer particles with a mean size, d_p , of 346 nm. In contrast, when LiCl was added to the precursor solution, the prepared particles were well-dispersed, and the particle size was reduced to the nanometer scale, as shown in Fig. 4.2(b, c). At a Li/Ga molar ratio of 5.0, nearly nonagglomerated particles with a mean size, d_p , of 9.6 nm and geometric standard deviation, σ_g , of 1.54 were obtained. An additional increase in the flux salt concentration resulted in an increase in particle size. Thus, it was assumed that a high flux salt concentration enhanced crystallization of the resulting particles and increased particle size.

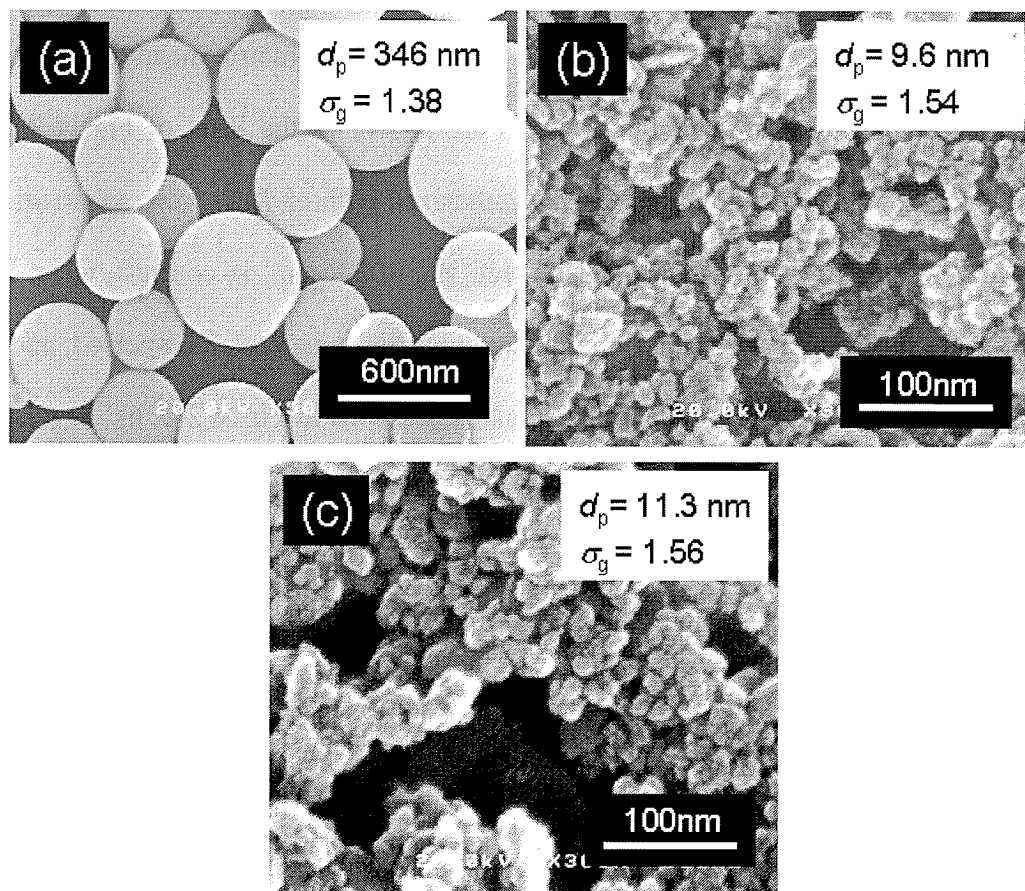


Fig. 4.2 FE-SEM images of Ga_2O_3 particles prepared at 800°C with various molar ratios of Li/Ga: (a) 0, (b) 5.0, and (c) 10.0.

4.3.1.2. Effect of operating temperature on particle morphology.

The effect of preparation temperature on Ga₂O₃ nanoparticles was also investigated. Fig. 3 shows the FE-SEM and FE-TEM images of the samples prepared at 700°C, 800°C, 900°C, and 1000°C with the Li/Ga molar ratio fixed at 5.0. As shown in Fig. 4.3(a), when the operating temperature was 700°C, nano-sized particles were not produced. Based on this result, it might be concluded that salts do not play a role in the inhibition of agglomeration of the prepared Ga₂O₃ particles because the melting point of the salt is 650°C. However, when the particles were prepared at 800°C, 900°C, and 1000°C, well-dispersed nanoparticles were obtained. The insets in Fig. 4.3 show high-magnification images of the particles. Greater crystallinity of the prepared particles was observed as the operating temperature increased. The XRD measurements indicated that the samples prepared at 800°C, 900°C and 1000°C had Ga₂O₃ phase.

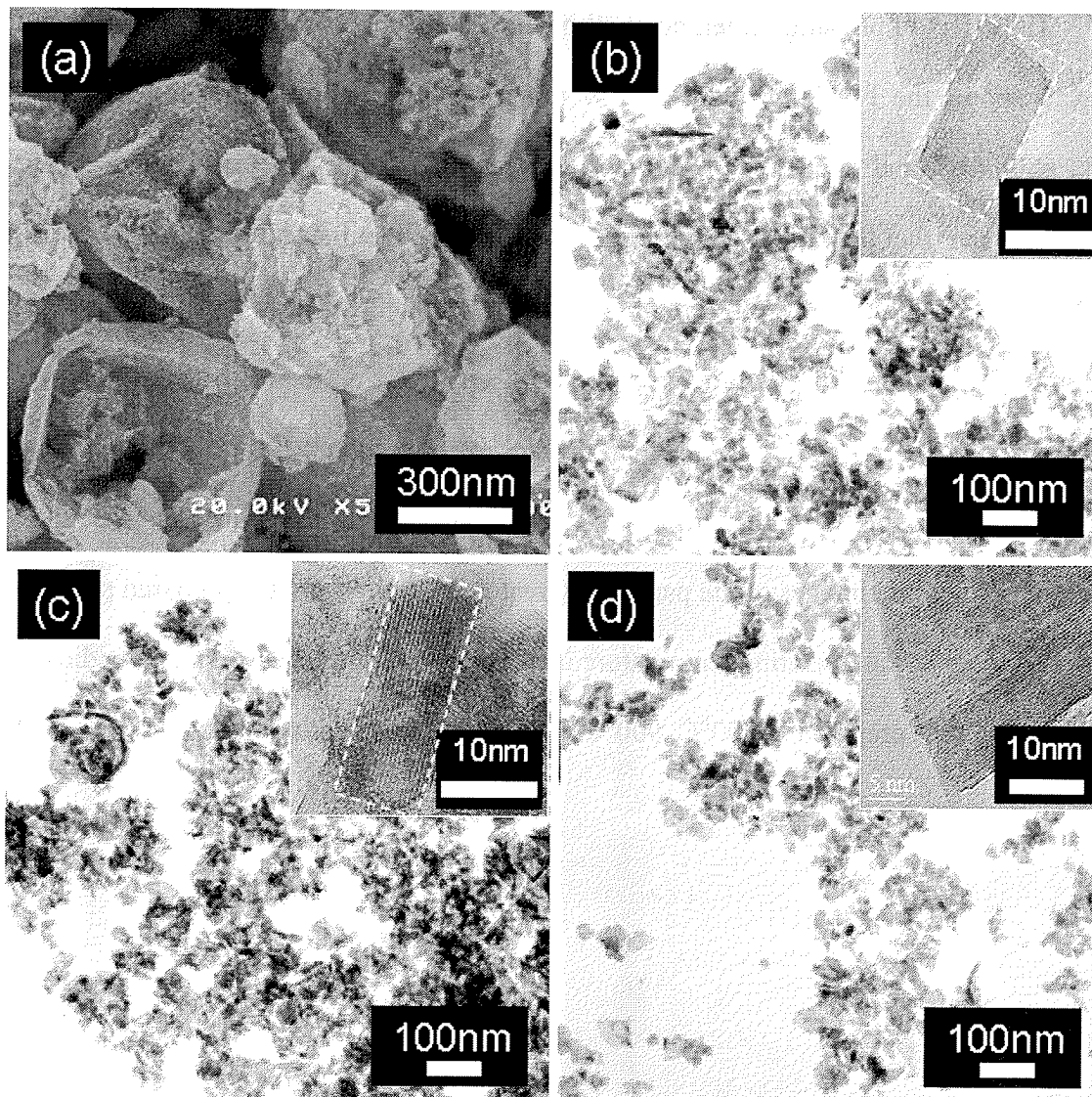


Fig.4.3 FE-SEM and FE-TEM images of Ga_2O_3 particles prepared using 0.05 mol/l of precursor and a Li/Ga molar ratio of 5.0 at different operating temperatures: (a) 700°C, (b) 800°C, (c) 900°C, and (d) 1000°C. High magnification TEM images are shown in the Figure insets.

4.3.2. Nitridation of Ga₂O₃ nanoparticles

4.3.2.1. Effect of preparation temperature of Ga₂O₃ particles on nitridation.

To investigate the effect of the crystallinity of the Ga₂O₃ particles on transformation to GaN, Ga₂O₃ particles prepared at different operating temperatures were nitridated under the same conditions. Fig. 4.4 shows the XRD patterns of particles resulting from exposure of Ga₂O₃ particles prepared at 800°C, 900°C and 1000°C to a flow of ammonia at 900°C for 120 min. As shown in Fig. 4.4, the oxygen content of the sample gradually declined with lower Ga₂O₃ particle preparation temperatures. When Ga₂O₃ nanoparticles prepared at 800°C were used, the structures of resulting particles had a single-phase of GaN (Fig. 4.4 c). In contrast, peaks assigned to Ga₂O₃ and GaN were detected in the samples synthesized from Ga₂O₃ particles prepared at 900°C and 1000°C. This result suggests that after the Ga₂O₃ structure was crystallized at high temperature, greater energy was required for the transformation of Ga₂O₃ to GaN. Similar experimental results were also obtained when amorphous nanoparticles of tantalum oxide was used as the conversion material (J. Buha, et al., 2007).

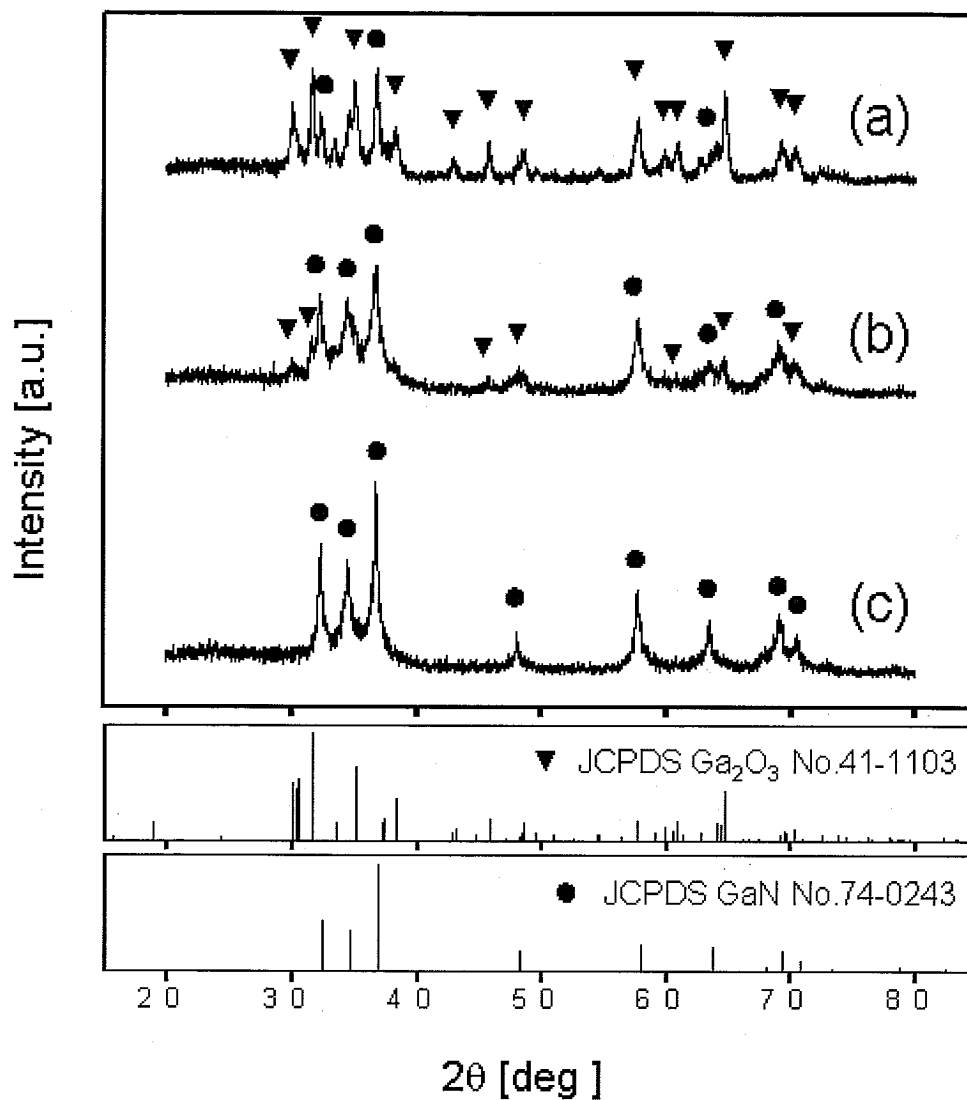


Fig.4.4 XRD patterns of the particles resulting from nitridation at 900°C for 120 min using Ga₂O₃ particles prepared at various operating temperatures: (a) 1000°C, (b) 900°C, and (c) 800°C.

4.3.2.2. Effect of nitridation time

To confirm the minimum time required to nitridate Ga₂O₃ nanoparticles, the effect of nitridation time on the crystal structure of the samples was investigated. Ga₂O₃ nanoparticles prepared at 800°C were used in this nitridation experiment. Fig. 4.5 shows XRD patterns of the samples nitridated at 900°C with nitridation times of 1, 5, 30, 60, and 90 min. The XRD patterns indicated that the crystallinity of the particles was altered by the nitridation time. In the case of the 1-min nitridation, the pattern was different from that of the Ga₂O₃ reference. A 30-min nitridation resulted in a broad h-GaN phase and a nitridation time of 60 min produced a highly crystalline h-GaN phase.

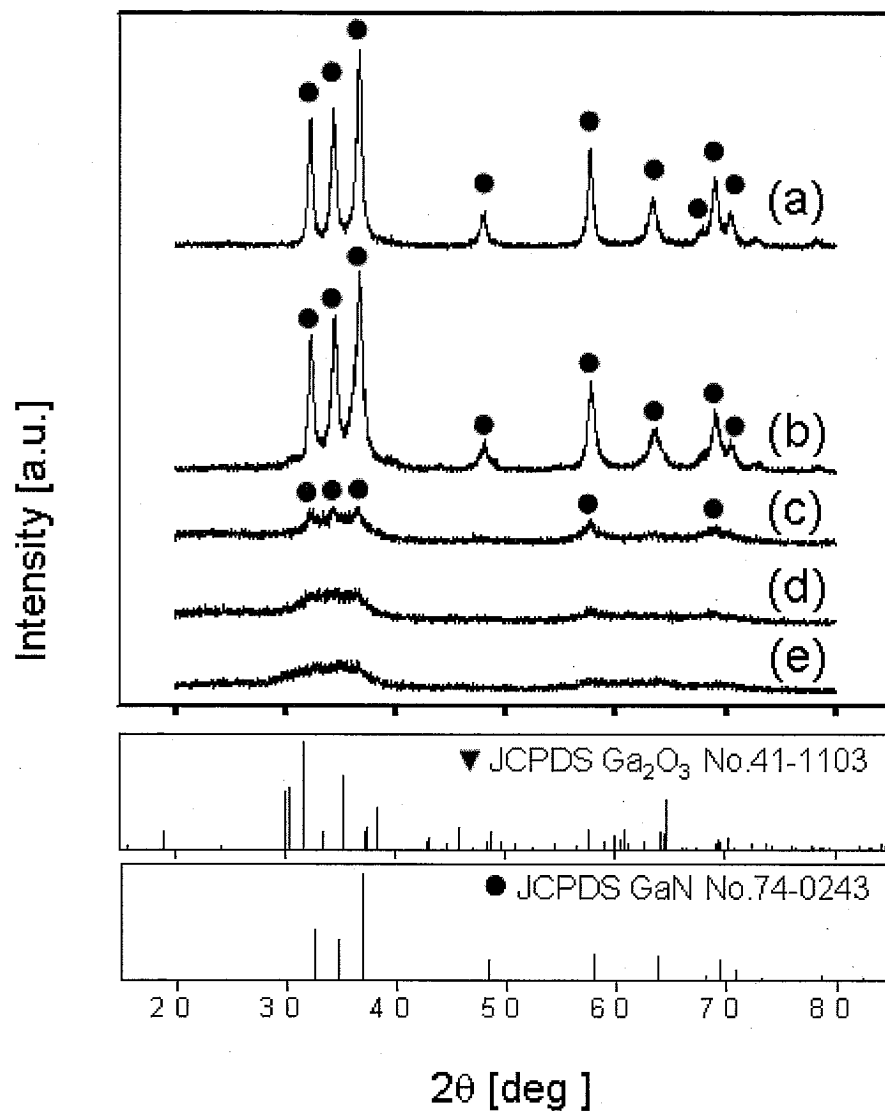


Fig. 4.5 XRD patterns of particles resulting from nitridation at 900°C with a various nitridation times: (a) 90 min, (b) 60 min, (c) 30 min, (d) 5 min, and (e) 1 min.

A SEM image of the GaN sample corresponding to Fig. 4.5(b) is shown in Fig. 4.6. The inset shows a high magnification TEM image of the particle. GaN nanoparticles with a mean size, d_p , of 23.4 nm and geometric standard deviation, σ_g , of 1.68 were obtained. Despite the high temperature of the transformation reaction, the resulting nanoparticles were softly agglomerated and had a narrow size distribution.

To verify the internal chemical composition of the particles, elemental mapping was conducted using the 3-windows method, which is an effective tool for the analysis of elemental distribution (L. W. Yin, et al., 2005). Two samples were selected for elemental mapping analysis: Ga₂O₃ particles nitridated for 5 min and 60 min. The morphologies of the two samples in the zero-loss images are shown in Fig. 4.7a (T1), b(T2). The corresponding maps for nitrogen (N) and oxygen (O) are shown in Fig. 4.7. Based on these results, N atoms diffuse from the particle surface and the area of N atoms increases with reaction time. The particles with a nitridation time of 60 min had N atoms that were well distributed inside the particles. In contrast, the particles that were nitridated for 5 min had N atoms distributed only on the surface of the particles.

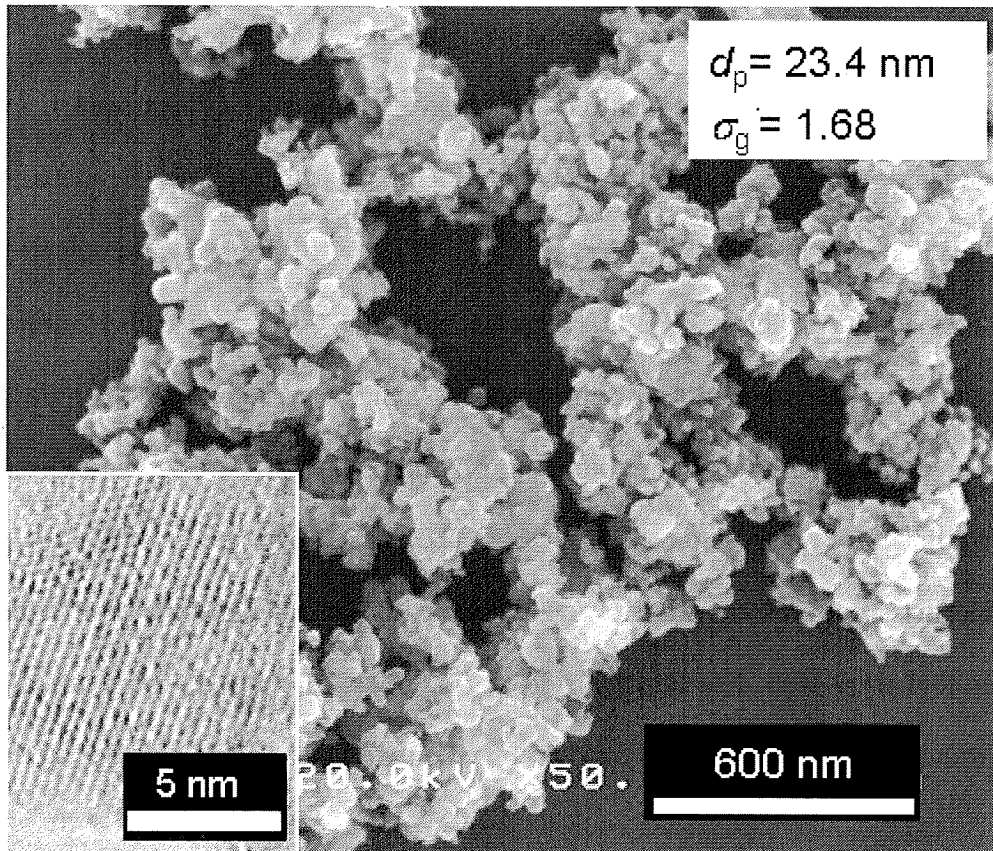


Fig. 4.6 SEM image of GaN sample after nitridation at 900°C for 60 min using Ga₂O₃ particles prepared at 800°C. The corresponding high magnification TEM image is shown in the figure inset.

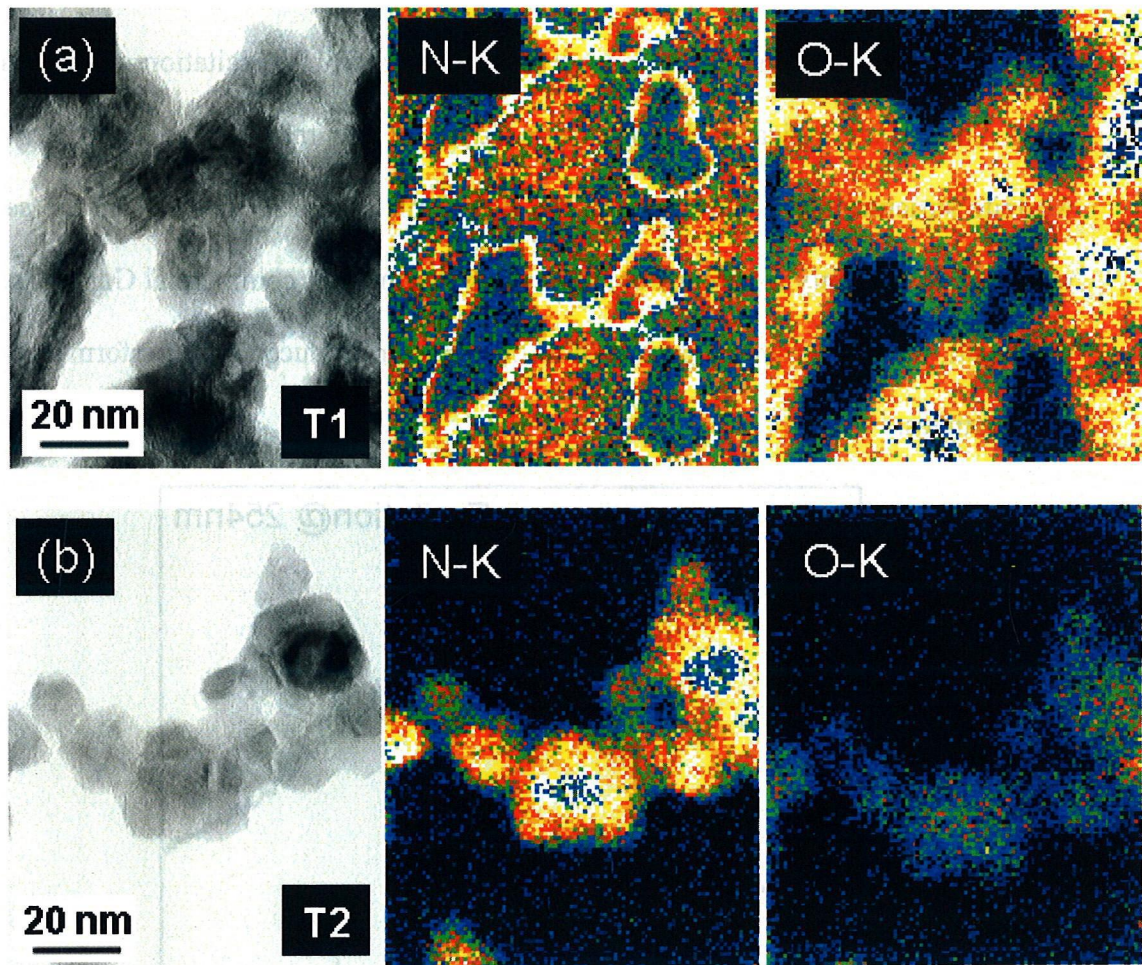


Fig. 4.7 Elemental EELS maps of the particles resulting from nitridation at 900°C with a various nitridation time: (a) 5 min, and (b) 60 min. T1 and T2 indicate the corresponding zero-loss images.

The PL spectra of GaN samples prepared at 900°C for 60 min are shown in Fig. 4.8. For comparison, commercial GaN powder (High Purity Chemicals, Japan) with a mean particle size of approximately 4 μm was also measured. The peak wavelength of the prepared sample was 364 nm at room temperature when UV excitation at 254 nm was used. This result indicates that the band edges of the resulting nanoparticles were wurtzite structure GaN. Furthermore, the waveform and peak intensity of the sample were not significantly different from the values obtained for commercial GaN. Based on this result, the novel method described in this chapter produced high performance GaN nanoparticles.

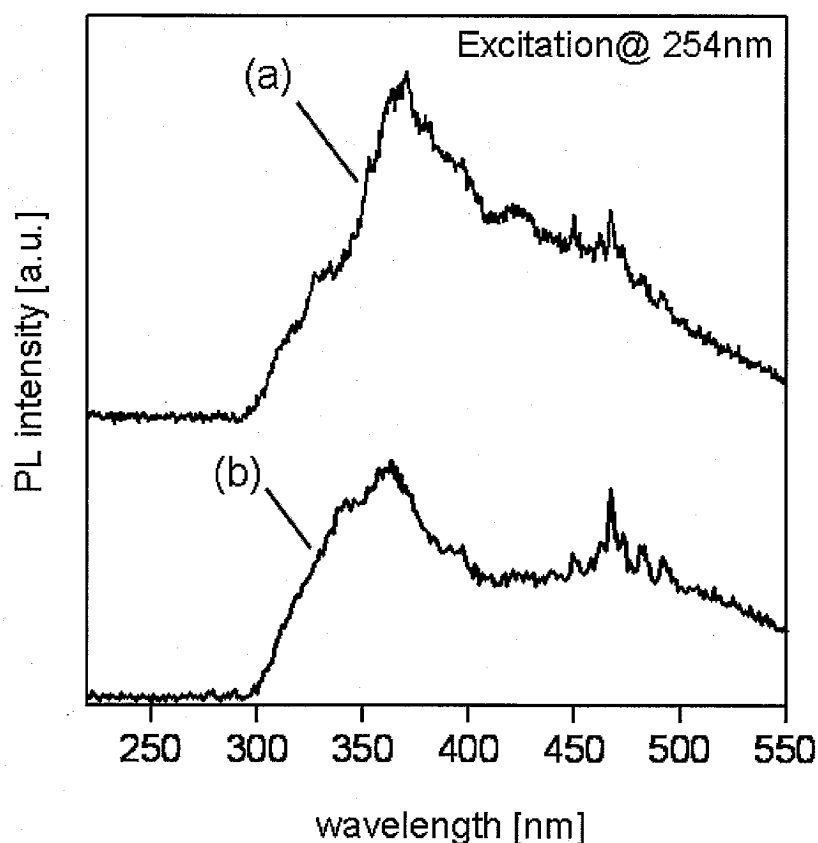


Fig. 4.8 PL emission spectra of the GaN sample after nitridation at 900°C for 60 min (a) and that of the commercial product (b).

4.4. Summary

In summary, highly crystalline GaN nanoparticles were synthesized using a new preparation method that involves nitridation of Ga₂O₃ nanoparticles obtained from salt-assisted spray pyrolysis. Addition of a proportional amount of flux salt (LiCl) to the solution is a key factor in the production of nano-sized Ga₂O₃ particles with a narrow size distribution. Nitridation of Ga₂O₃ nanoparticles under a flow of ammonia resulted in highly crystalline GaN nanoparticles with a mean size, d_p , of 23.4 nm and geometric standard deviation, σ_g , of 1.68. This study revealed that Ga₂O₃ particles prepared at low temperatures were more easily converted into GaN particles than those prepared at high temperatures. According to the elemental mapping analysis, nitrogen atoms were homogeneously distributed in the resulting GaN nanoparticles. Furthermore, it was determined that the GaN nanoparticles exhibited photoluminescence at 364 nm when UV excitation at 254 nm was used. The method developed in the present study may provide a simple and potentially economical way to form other high performance nitride materials.

References

- B. Gil, Group (III) Nitride Semiconductors: Physics and Applications, Oxford Univ. Press, 1998.
- B. Xia, K. Okuyama, and I. W. Lenggoro, Novel route to nanoparticle synthesis by salt-assisted aerosol decomposition (vol 13, pg 1579, 2001), Adv. Mater. 13, 1744-1744 (2001).
- F. Iskandar, T. Ogi, and K. Okuyama, Simple synthesis of GaN nanoparticles from

- gallium nitrate and ammonia aqueous solution under a flow of ammonia gas, *Mater. Lett.* 60, 73-76 (2006).
- G. Pan, M. E. Kordesch, and P. G. V. Patten, New pyrolysis route to GaN quantum dots, *Chem. Mater.* 18, 3915-3917 (2006).
- J. Buha, I. Djerdj, M. Antonietti, and M. Niederberger, Thermal transformation of metal oxide nanoparticles into nanocrystalline metal nitrides using cyanamide and urea as nitrogen source, *Chem. Mater.* 19, 3499-3505 (2007).
- K. Okuyama, and I. W. Lenggoro, Preparation of nanoparticles via spray route, *Chem. Eng. Sci.* 58, 537-547 (2003).
- K. Okuyama, M. Abdullah, I.W. Lenggoro, and F. Iskandar, Preparation of functional nanostructured particles by spray drying, *Adv. Powder Technol.* 17, 587-611 (2006).
- L. W. Yin, Y. Bando, D. Golberg, A. Gloter, M. S. Li, X. Yuan, and T. Sekiguchi, Porous BCN nanotubular fiber : Growth and spatially resolved cathodoluminescence, *J. Am. Chem. Soc.* 127, 40, 16354-16355 (2005).
- O. I. Micic, S. P. Ahrenkiel, D. Bertram, and A. J. Nozik, Synthesis, structure, and optical properties of colloidal GaN quantum dots, *Appl. Phys. Lett.* 75, 478-480 (1999).
- S. Nakamura, S. Pearton, G. Fasol, *The Blue Laser Diode*, Springer-Verlag, 1997.
- T. Ogi, Y. Itoh, M. Abdullah, F. Iskandar, Y. Azuma, and K. Okuyama, Fabrication and photoluminescence of highly crystalline GaN and GaN : Mg nanoparticles, *J. Cryst. Growth* 281, 234-241 (2005).
- Y. Azuma, M. Shimada, and K. Okuyama, The synthesis of monodisperse ultrapure gallium nitride nanoparticles by MOCVD, *Chem. Vap. Deposition* 10, 11-13

(2004).

Y. Yang, V. J. Leppert, S. H. Risbud, B. Twamley, P. P. Power, and H. W. H. Lee, Blue luminescence from amorphous GaN nanoparticles synthesized in situ in a polymer, *Appl. Phys. Lett.* 74, 2262-2264 (1999).

Chapter 5

Facile Synthesis of New Full-Color-Emitting BCNO Phosphors with High Quantum Efficiency

5.1 Introduction

In recent years, oxynitride and nitride compounds have attracted much attention as host lattices for phosphors, due to their excellent properties, such as nontoxicity, outstanding thermal and chemical stability, a broad range of excitation and emission wavelengths, and high luminescence efficiency when activated by rare-earth ions, etc (Hirosaki, et al., 2005, Xie, et al., 2006, Li, et al., 2005). For example, a bright yellow phosphor of $\text{Ca-}\alpha\text{-SiAlON:Eu}^{2+}$ and the green-emitting $\beta\text{-SiAlON:Eu}^{2+}$ were synthesized and used in white-light-emitting diode (LED) lamps featuring high luminous efficacy (Sakuma, et al., 2004). However, production of these materials generally requires high temperature and high pressure (Hirosaki, et al., 2005, Xie, et al., 2006, Li, et al., 2005). In addition, rare-earth ions, such as Eu^{2+} , Ce^{3+} , Yb^{2+} , and Tb^{3+} , which are required for use as luminescence centers, are very expensive. Therefore, finding a feasible method for the production of oxynitride and nitride phosphor particles without using rare-earth ions, at relatively low temperatures under ambient atmospheric

pressure is desirable for white LED applications. On the other hand, much effort has been devoted to the preparation of carbon-based boron nitride (BCN) semiconductors for use as phosphors (Kawaguchi, et al., 1991, Watanabe, et al., 1996, Watanabe, et al., 1997, Wu, et al., 2004, Bai, et al., 2000). Theoretical studies suggest that it should be possible to use BCN materials to tune the emitted light wavelength across the spectrum of visible light by varying the composition of the BCN compounds. BCN compounds are expected to behave as semiconductors with band gap energies that can be controlled by atomic composition, since these compounds are thought to be intermediates between graphite and hexagonal-BN (Watanabe, et al., 1996). In previous studies, however, BCN compounds were reported to produce only single emission peaks in the photoluminescence (PL) spectra (Watanabe, et al., 1996, Bai, et al., 2000, Yin, et al., 2005). In addition, the PL intensity and quantum efficiency (QE) remained very low (Watanabe, et al., 1996). To the best of our knowledge, full-color-emitting BCN materials are yet to be reported.

In this chapter, we report for the first time a new oxynitride phosphor, which is composed of BCNO atoms, produced by a one-step liquid process at low temperature (below 900°C) under ambient atmospheric conditions. The color emission of the BCNO phosphor can be easily tailored from violet to near red by varying the carbon content. In addition, high external quantum efficiency and a broad range of excitation wavelengths were obtained using the BCNO phosphor particles. Available, inexpensive chemicals, i.e., boric acid (H_3BO_3) and urea ($(\text{NH}_2)_2\text{CO}$) were used as the raw materials in this process. Various weight-fractions of polyethylene glycol (PEG) were added to the solution to vary the carbon component. The effects of the PEG fraction and heat treatment on the photoluminescence properties of the resulting powder were

investigated.

5.2 Experimental procedure

The BCNO phosphors were synthesized from the following precursors: boron acid (H_3BO_3 , Wako Chemicals Co., Ltd., Japan), as the boron source; urea ($(\text{NH}_2)_2\text{CO}$, Wako Chemicals Co., Ltd., Japan), as the nitrogen source; and, polyethylene glycol, ($\text{H}(\text{EG})_n\text{OH}$, with $M_w = 20,000$ and $\text{EG} = \text{OCH}_2\text{CH}_2$, Wako Pure Chemicals), as the carbon source. The precursors were mixed and the resulting solution was heated at 700-900°C for 30-60 min to obtain BCNO particles. The prepared products were characterized by field emission scanning electron microscopy (FE-SEM, S-5000, Hitachi Corp., Tokyo, Japan) at 20 kV and high-resolution transmission electron microscopy (HR-TEM, JEM-3000F, JEOL, Tokyo, Japan) at 300 kV. The chemical composition of the BCNO phosphors was analyzed using an electron energy-loss spectrometer (EELS) attached to the transmission electron microscope and inductively coupled plasma (ICP). The PL spectra of prepared BCNO phosphors were recorded at room temperature by means of a spectrofluorophotometer (RF-5300PC, Shimadzu Corp., Kyoto, Japan) equipped with a xenon laser source. The external quantum efficiency (EQE) of the prepared particles also was analyzed at an excitation wavelength of 365 nm produced by a 150 W Xe lamp using an absolute PL quantum yield measurement system (C9920-02, Hamamatsu Photonics, Shizuoka, Japan) with an A-10095-01 powder sample holder.

5.3. Results and Discussion

Fig. 5.1 (a) shows a transmission electron microscopic (TEM) image of the particles prepared at 800°C. Polyethylene glycol (PEG), $\text{H}(\text{CH}_2\text{CH}_2\text{O})_n\text{OH}$, with $\text{MW}=20,000$ and polyethylene glycol/Boron ($\text{PEG/B} = 2.0 \times 10^{-3}$ (mol/mol)) were added to the precursor solution. The prepared particle size was approximately 2.5 μm . A typical electron diffraction (ED) pattern and high resolution TEM (HR-TEM) image taken from the prepared sample are shown in Fig. 5.1 (b) and (c), respectively. The diffraction rings in the ED pattern were indexed as (002), (100), (004), and (110) peaks, consistent with the corresponding hexagonal boron nitride (h-BN) X-ray diffraction (XRD) pattern (JCPDS reference No 73-2095). As shown in the HR-TEM image (Fig. 5.1c), the sample was polycrystalline, composed of numerous nanocrystals; each crystal was approximately 5 nm in size. The lattice spacing of primary crystals, as measured in the HR-TEM image, was 0.34 nm, which was larger than the value at (002) (0.33nm) of h-BN, indicating that the prepared phosphor powder had crystals of turbostratic boron nitride (t-BN) (Guo, et al., 2005). Electron energy loss spectroscopy (EELS) of the resulting powder is shown in Fig. 5.1 (d). Four ionization edges at ca. 188eV, 284eV, 400eV, and 532eV, corresponding to the characteristic K-edges of B, C, N, and O, respectively, were observed. The results described above indicate that the synthesized particles were comprised of boron, carbon, nitrogen, and oxygen atoms, and contained partially crystallized t-BN.

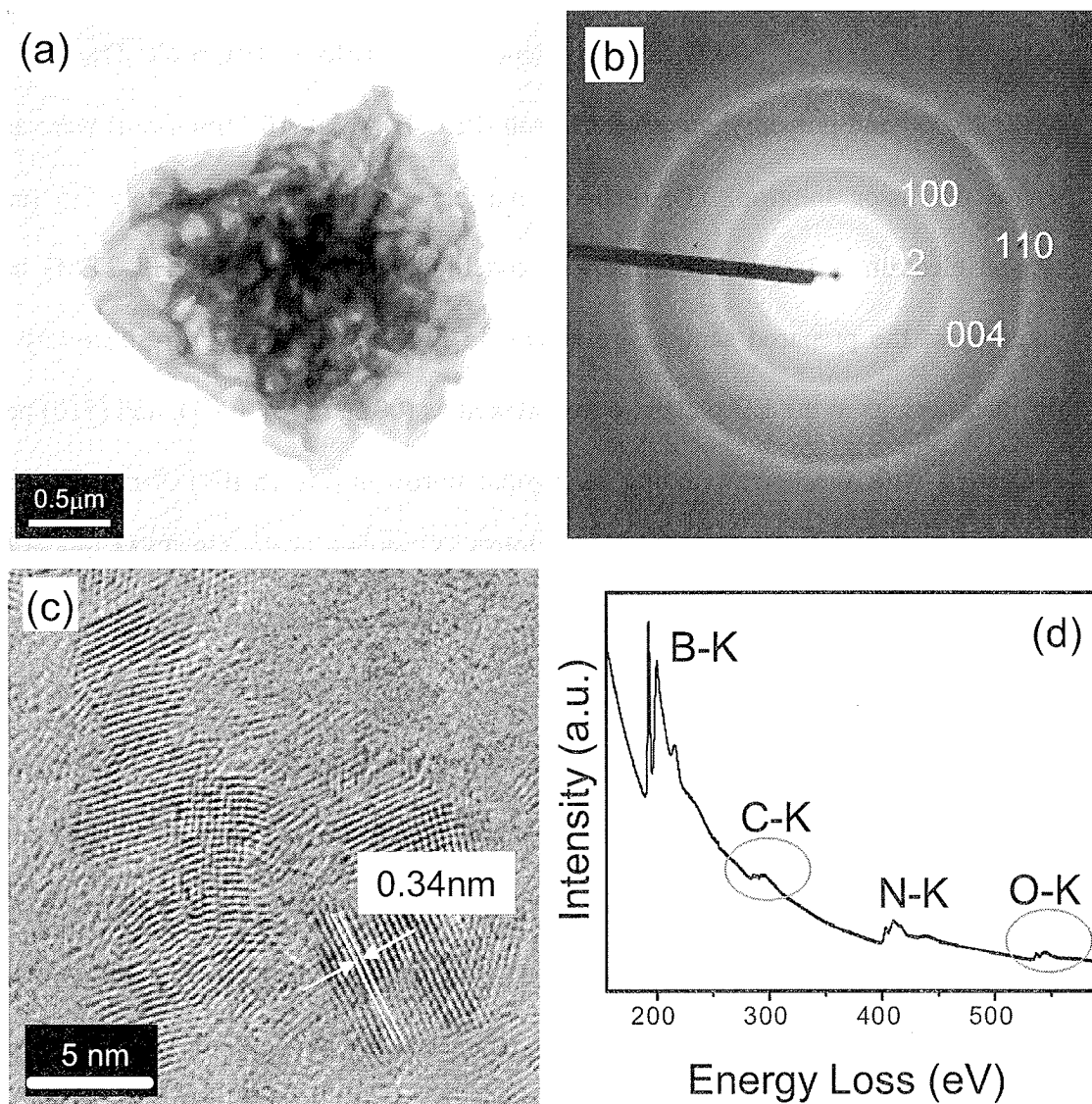


Fig. 5.1 (a) Low-magnification TEM image of a BCNO particle. (b) ED pattern. (c) High-resolution TEM image. (d) Electron energy loss spectroscopy of a sample.

Fig. 5.2 shows an example excitation and emission spectrum of the BCNO phosphor particles measured at room temperature. The sample shown in Fig. 5.2 was prepared at 800°C using $\text{PEG/B} = 2.0 \times 10^{-3}$. The excitation spectrum was broad, covering the spectral region from the UV to the visible range. The emission spectrum showed a single, intense, broad emission band at 475 nm under excitation at 365 nm, which is generally used as the standard excitation wavelength in the long UV range.

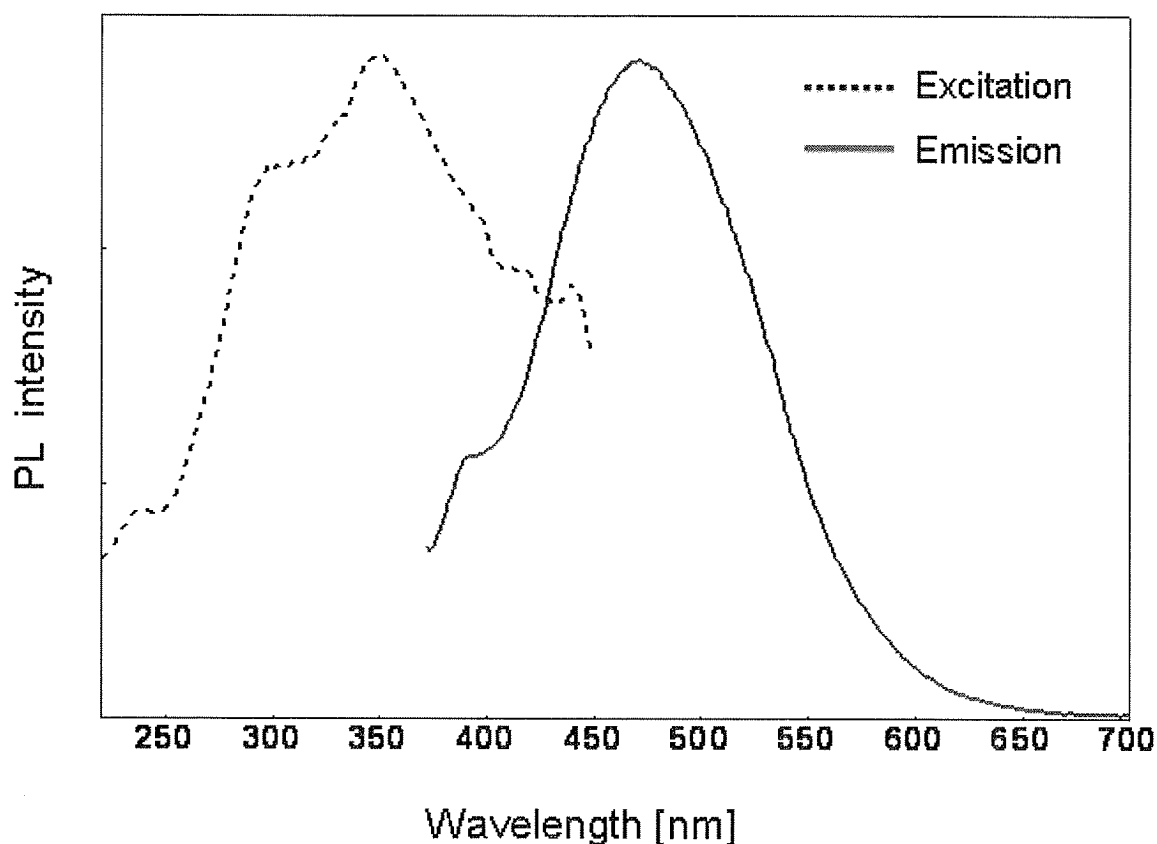


Fig. 5.2 Excitation and emission spectra for BCNO phosphor prepared at 800°C using $\text{PEG/B} = 2.0 \times 10^{-3}$ (mol/mol).

The effect of preparation temperature on the photoluminescence (PL) properties of BCNO phosphor particles was investigated. Fig. 5.3 shows the PL spectra of the

samples prepared at 700°C, 800°C, and 900°C using $\text{PEG/B} = 2.0 \times 10^{-3}$. Similar PL spectra were obtained for the samples prepared at 700°C and 800°C, with corresponding emission peaks located at 460 nm and 475 nm, respectively. An emission peak with higher intensity was observed for the sample prepared at 800°C compared with the sample prepared at 700°C. This result was expected because for photoluminescence materials a higher operation temperature generally results in a higher PL intensity due to higher crystallinity (Wang, et al., 2005, Ogi, et al., 2005, Iskandar, et al., 2006). However, the PL intensity of the sample prepared at 900°C was the lowest intensity observed, and the wave pattern was very different from those of the samples prepared at 700 and 800°C. A possible explanation for this phenomenon is that the carbon in the sample evaporated at 900°C, changing the composition of the sample.

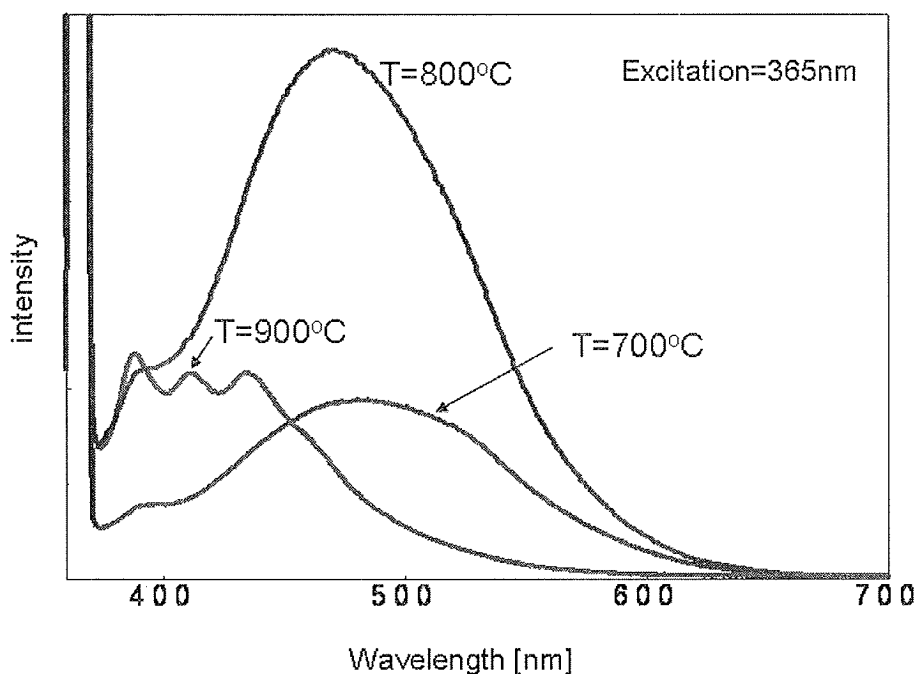


Fig. 5.3 PL spectra of BCNO samples prepared at 700°C, 800°C and 900°C

using $\text{PEG/B} = 2.0 \times 10^{-3}$ (mol/mol)

To further investigate the effect of carbon content on the PL properties of the sample, BCNO phosphors with various PEG fractions were prepared at 800°C. PL spectra for the BCNO phosphor particles prepared using various PEG fractions were measured at room temperature (Fig. 5.4). The excitation wavelength was fixed at 365 nm. As shown in Fig. 5.4, the emission intensities observed for samples prepared using PEG were very high. When the PEG/B ratio in the precursor solution was increased from 2.0×10^{-3} to 6.0×10^{-3} , the emission spectra red-shifted from 475 nm to 500 nm. To identify the cause of the PL spectra shift, the chemical composition (B, C, N, and O) of the prepared samples were measured. The carbon content of the samples prepared using PEG/B = 2.0×10^{-3} and 6.0×10^{-3} were 0.079% and 0.1415%, respectively, based on bulk analysis. This result shows that the carbon concentration of the prepared sample increased when additional PEG was added to the samples. Based on this analysis, the PL spectra shift was attributed to the variation in the chemical composition of the BCNO phosphor particles. With an increase in the PEG concentration, impure carbon atoms primarily substituted for boron or nitrogen atoms in the t-BN crystal, and the electron transition between the band in the t-BN-type matrix and the levels generated by carbon was changed (M. Kawaguchi, et al., 1991). Thus, the shift in the PL peaks was due to variations in the BCNO band gap, corresponding to the chemical composition of the BCNO particles. Previous studies reported that the band gap of BCN compounds is highly dependent on the atomic arrangement of the compounds (A. Y. Liu, et al., 1989, H. Nozaki, et al., 1996, Y. Miyamoto, et al., 1995).

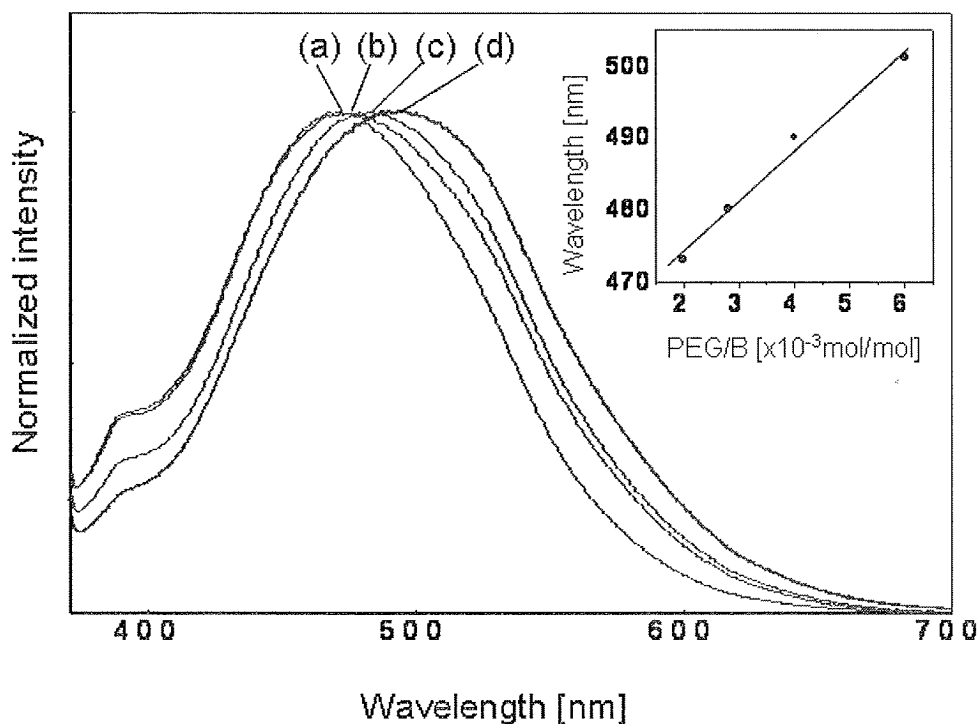


Fig. 5.4 PL spectra of BCNO prepared at 800°C using PEG/B= (a) 2.0×10^{-3} (b) 2.8×10^{-3} , (c) 4.0×10^{-3} , (d) 6.0×10^{-3} (mol/mol).

As mentioned above, effects of operating temperature and PEG fraction on PL properties were investigated and the emission peak of the BCNO phosphors was changed over the blue region. In addition, the possibility of full-color emitting was explored by changing various parameters, such as the synthesis temperature, PEG fraction, and heating time, etc. Fig. 5.5 shows the PL spectra of multi-color-emitting BCNO samples prepared under various conditions. The position of the measured PL peak shifted from 387 nm (violet emission) to 571 nm (near red emission), as shown in the inset images of the corresponding BCNO samples in Fig. 5.5. The peak positions tended to shift to longer wavelengths as the PEG fraction increased, possibly due to increased carbon content inside the BCNO particles. The results described above

revealed that a low synthesis temperature and a high PEG fraction increased the red shift of the BCNO phosphors.

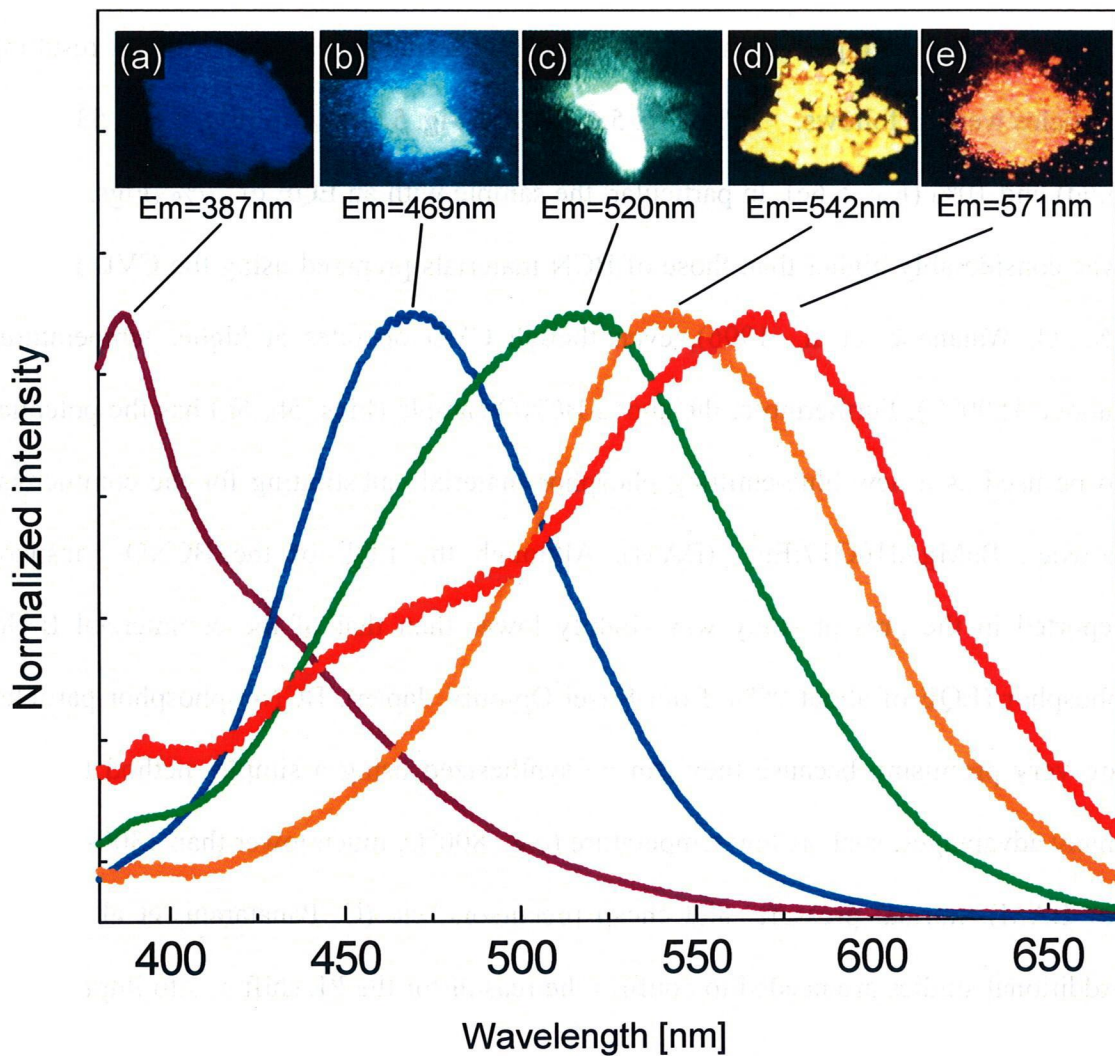


Fig. 5.5 PL spectra and digital photograph of BCNO samples prepared under various conditions: PEG/B, operating temperature, heating time = (a) 2.0×10^{-3} , 900°C , 30 min, (b) 2.0×10^{-3} , 800°C , 30 min, (c) 2.8×10^{-3} , 800°C , 60 min, (d) 4.0×10^{-3} , 700°C , 60 min, and (e) 4.4×10^{-3} , 700°C , 30 min.

Fig. 5.6 shows the CIE diagram of the BCNO phosphor particles prepared under the conditions described in Fig. 5.5. The CIE X-Y coordinates of the particles were (0.174, 0.107), (0.181, 0.137), (0.259, 0.36), (0.318, 0.476) and, (0.455, 0.398), indicating the phosphor color changed from dark blue, to white, green, yellow, and near red. As shown in Fig. 5.6, the external quantum efficiencies (EQE) of the resulting particles were as follows: 34% (Fig. 5.6a), 79% (Fig. 5.6b), 76% (Fig. 5.6c), 53% (Fig. 5.6d) and 10% (Fig. 5.6e). In particular, the sample with an EQE of 79% (Figs. 5b, 6b) was considerably higher than those of BCN materials prepared using the CVD method (M. O. Watanabe, et al., 1996), even though CVD operates at higher temperatures (above 1500°C). Furthermore, the above BCNO sample (Figs. 5b, 6b) has the potential to be used as a new blue-emitting phosphor material, substituting for the commercial powder, BaMgAl₁₀O₁₇:Eu²⁺ (BAM). Although the EQE of the BCNO phosphor reported in the present study was slightly lower than that of the commercial BAM phosphor (EQE of about 95%, from Kasei Optonix, Japan), BCNO phosphor particles are very promising because they can be synthesized using a simple method that has many advantages, such as low temperature (e.g., 800°C, much lower than 1300-1500°C for BAM), normal pressure, and cheap precursors, etc (C. Panatarani, et al., 2005). Additional studies are needed to confirm the reason for the PL shift and to improve the EQE of BCNO phosphors.

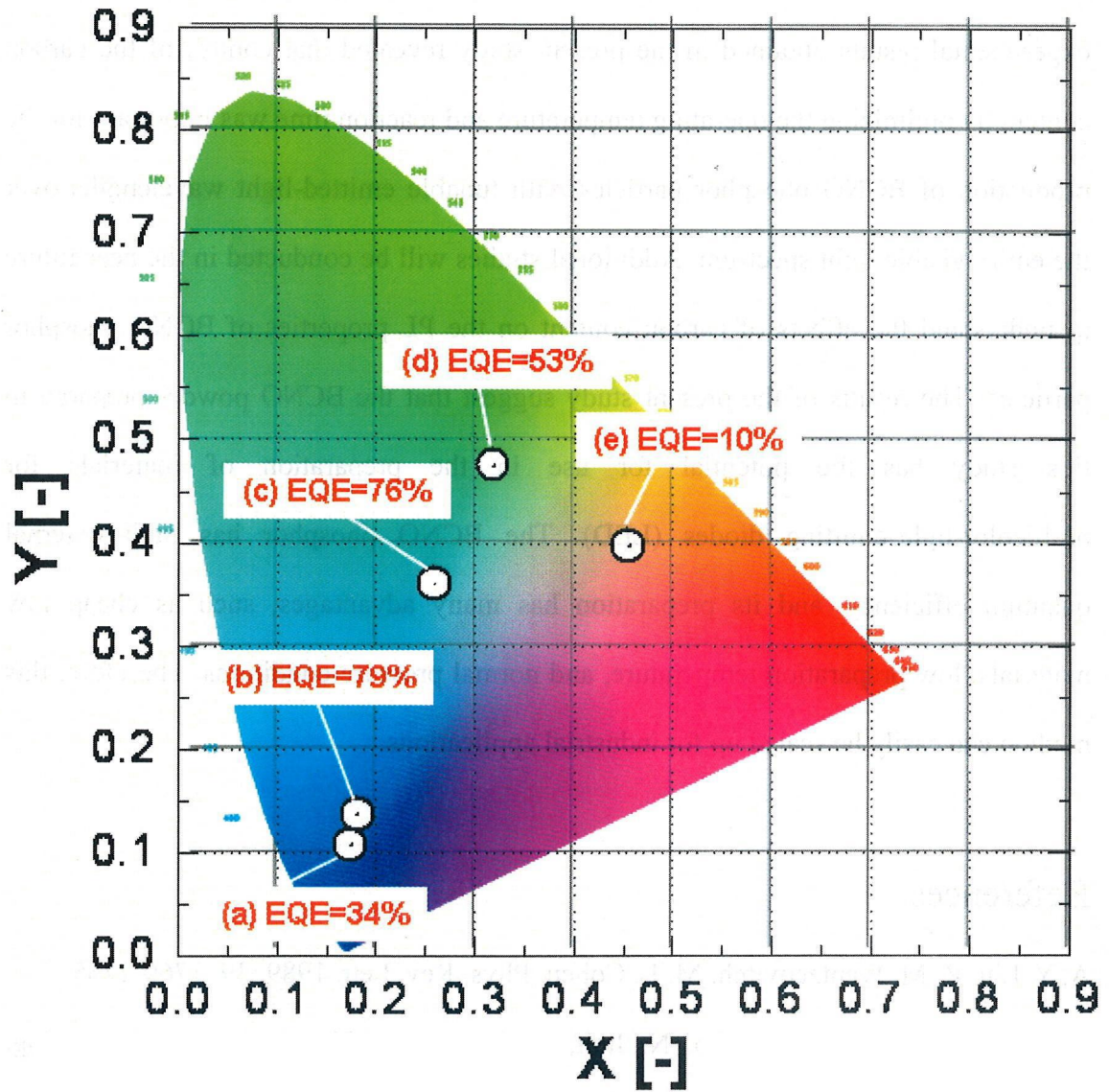


Fig. 5.6 CIE diagram and external quantum efficiency of BCNO powders prepared under various conditions: PEG/B, operating temperature, heating time = (a) 2.0×10^{-3} , 900°C , 30 min, (b) 2.0×10^{-3} , 800°C , 30 min, (c) 2.8×10^{-3} , 800°C , 60 min, (d) 4.0×10^{-3} , 700°C , 60 min, and (e) 4.4×10^{-3} , 700°C , 30 min.

5.4. Summary

BCNO phosphor particles with a tunable emitted-light wavelength from 380 nm to 571 nm were prepared using a facile liquid process at relatively low temperatures. The experimental results obtained in the present study revealed that control of the carbon content by optimizing the operating temperature and reaction time was important for the production of BCNO phosphor particles with tunable emitted-light wavelengths over the entire visible light spectrum. Additional studies will be conducted in the near future to understand the effects of carbon content on the PL properties of BCNO phosphor particles. The results of the present study suggest that the BCNO powder prepared in this study has the potential for use in the preparation of materials for multicolor-light-emitting diodes (LED). The BCNO phosphor has high external quantum efficiency, and its preparation has many advantages, such as cheap raw materials, low preparation temperature, and normal pressure conditions. Therefore, this method can easily be scaled up for industrial applications.

References

- A. Y. Liu, R. M. Wentzcovitch, M. L. Cohen, *Phys. Rev. Lett.* 1989, 39, 1760-1765.
- C. Panatarani, I. W. Lenggoro, N. Itoh, H. Yoden, K. Okuyama, *Mater. Sci. Eng. B-Solid State Mater. Adv. Technol.* 2005, 122, 188-195.
- F. Iskandar, T. Ogi, K. Okuyama, *Mater. Lett.* 2006, 60, 73-76.
- H. Nozaki, S. Itoh, *Phys. B* 1996, 220, 487-489.
- J. Wu, W. Q. Han, W. Walukiewicz, J. W. Ager, W. Shan, E. E. Haller, A. Zettl, *Nano Lett.* 2004, 4, 647-650.

- K. Sakuma, K. Omichi, N. Kimura, M. Ohashi, D. Tanaka, N. Hirosaki, Y. Yamamoto, R. J. Xie, T. Suehiro, *Opt. Lett.* 2004, 29, 2001-2003.
- L. W. Yin, Y. Bando, D. Golberg, A. Gloter, M. S. Li, X. L. Yuan, T. Sekiguchi, *J. Am. Chem. Soc.* 2005, 127, 16354-16355.
- M. Kawaguchi, *Adv. Mater.* 1997, 9, 615-625.
- M. Kawaguchi, K. Nozaki, Y. Kita, M. Doi, *J. Mater. Sci.* 1991, 26, 3926-3930.
- M. O. Watanabe, S. Itoh, T. Sasaki, K. Mizushima, *Phys. Rev. Lett.* 1996, 77, 187-189.
- N. Hirosaki, R. J. Xie, K. Kimoto, T. Sekiguchi, Y. Yamamoto, T. Suehiro, M. Mitomo, *Appl. Phys. Lett.* 2005, 86, 1-3.
- Q. X. Guo, Y. Xie, C. Q. Yi, L. Zhu, P. Gao, *J. Solid State Chem.* 2005, 178, 1925-1928.
- R. J. Xie, N. Hirosaki, T. Suehiro, F. F. Xu, M. Mitomo, *Chem. Mater.* 2006, 18, 5578-5583.
- T. Ogi, Y. Itoh, M. Abdullah, F. Iskandar, Y. Azuma, K. Okuyama, *J. Cryst. Growth* 2005, 281, 234-241.
- W. N. Wang, W. Widiyastuti, T. Ogi, I. W. Lenggoro, K. Okuyama, *Chem. Mater.* 2007, 19, 1723-1730.
- X. D. Bai, E. G. Wang, J. Yu, H. Yang, *Appl. Phys. Lett.* 2000, 77, 67-69.
- Y. Miyamoto, M. L. Cohen, S. G. Louie, *Phys. Rev. B* 1995, 52, 14971-14975.
- Y. Q. Li, A. C. A. Delsing, G. de With, H. T. Hintzen, *Chem. Mater.* 2005, 17, 3242-3248.

Chapter 6

Direct synthesis of barium magnesium aluminate blue phosphor particles via a flame route

6.1 Introduction

It is well known that $\text{BaMgAl}_{10}\text{O}_{17}:\text{Eu}^{2+}$ (BAM: Eu) is one of the most important blue phosphors for the next generation of displays and lighting devices (Blasse et al., 1994). The BAM phosphor has been applied to Plasma Display Panels (PDPs) because it has a good efficiency under vacuum ultraviolet excitation. Its $4f^65d \rightarrow 4f^7$ emission has its maximum at about 450 nm. It is important to develop a process that can produce phosphor, including BAM:Eu, particles of controlled size, morphology, and composition. Using the solid state reaction method (Ravichandran et al., 1997, Oshio et al., 1999) by which almost all phosphors are synthesized, some processes in the operation such as firing and milling must be repeated to obtain particles with uniform properties. The incorporation of impurities that accumulate during these operations decreases the luminescent intensity. Some reports concerning alternative methods for the preparation of BAM: Eu phosphors such as sol-gel (Ravichandran et al., 1997, Zhang et al., 2002) or combustion methods (Ekambaram et al., 1995, Park et al., 2003) have been published.

The combustion reaction method leads to severe agglomeration of the particles, causing an irregular shape and a broad particle size distribution (Park et al., 2003). Particle synthesis by spray pyrolysis involves the atomization of a precursor solution into discrete droplets. These droplets are subsequently transported through a heating zone (e.g. electrical furnace) where the solvent is evaporated and the dissolved species react to form the particulate product. Each droplet has an identical composition; thus, multi-component particles can be easily synthesized (Messing et al., 1993). A number of research groups have prepared BAM: Eu particles using a variety of starting solutions and spray pyrolysis with an electrical furnace (Kang et al., 1999, Saitoh et al., 2002, Kang et al., 2000, Jeon et al., 2001, Jung et al., 2003). However, in most of these studies, a post-annealing process at a higher temperature (than the preparation temperature) is required for the formation and further crystallization of the BAM phase. We have demonstrated that even without a post-annealing process, BAM: Eu²⁺ particles can be obtained at a preparation temperature of around 1700°C (Kang et al., 1999). This letter reports on the design of a flame spray pyrolysis method that demonstrates the direct synthesis of BaMgAl₁₀O₁₇:Eu²⁺ phosphors. Flame was used as the heating source rather than an electrical furnace. The relationship between synthesis conditions and crystallinity, morphology, and photoluminescence (PL) of the phosphor particles was investigated.

6.2 Experimental procedure

A schematic diagram of the experimental setup, which basically consists of an ultrasonic atomizer (1.7 MHz), a flame and a precipitator, is shown in Fig. 6.1. Generated droplets were carried into the diffusion flame burner, which consists of three

concentric pipes with a central pipe 12 mm in diameter, by nitrogen gas with a flow rate of 2.0 l/min. Methane and oxygen gases were used for the diffusion flame as a fuel and an oxidizer, respectively. The feeding rates of methane and oxygen, the equivalence ratio, and the estimated adiabatic flame temperature are summarized in Table 6.1. The equivalence ratio, ϕ , is defined as the fuel to air ratio normalized with respect to the stoichiometry fuel to air ratio. The adiabatic flame temperature was predicted using software (Reynolds et al., 1986). The estimated adiabatic flame temperatures ranged from 2804 K to 2887 K when no precursor solution was fed into the flame and the calculation was conducted using 1 atm and 298 K for the reactant gases. Starting precursor solutions were prepared by dissolving known amounts of nitrate precursors of barium ($\text{Ba}(\text{NO}_3)_2$), aluminum ($\text{Al}(\text{NO}_3)_3 \cdot 9\text{H}_2\text{O}$), magnesium ($\text{Mg}(\text{NO}_3)_2 \cdot 6\text{H}_2\text{O}$), and europium ($\text{Eu}(\text{NO}_3)_3 \cdot 6\text{H}_2\text{O}$) in distilled water. All chemicals had purities between 98.0 and 99.95%, were purchased from Kanto Chemical, and were used without further purification. The concentration of the overall precursor solution was fixed at 0.3 M for all experiments. To investigate the quenching concentration in the dopant, the concentration of europium was varied from 3 to 14 at.% with respect to barium. The crystallinity of the particles was studied at room temperature using an X-ray diffractometer (XRD, RINT 1000, Rigaku-Denki) operated at 40 kV. The morphology was observed with a field-emission scanning electron microscope (FE-SEM, S5000, Hitachi) operated at 20 kV. PL properties were measured at room temperature using a spectrophotometer (Shimadzu RF-5300PC). The phosphors were placed on a cylindrical aluminum holder with a diameter of 4.5 mm and a height of 1.5 mm. A xenon lamp was used for excitation of the phosphor in the UV region (254 nm). For comparison, a commercial BAM: Eu^{2+} phosphor (Kasei Optonix, Ltd.) was used.

Table 6.1 The experimental conditions used for the study on effect of gases feeding rates on photoluminescence intensity of as-prepared particles

Feeding gas flow rate [l/min]			Equivalent ratio, ϕ	Estimated adiabatic flame temperature [K]
CH ₄	O ₂	N ₂		
1.25	3.57	2.00	0.7	2804
1.25	3.13	2.00	0.8	2835
1.25	2.78	2.00	0.9	2853
1.25	2.63	2.00	0.95	2857
1.25	2.55	2.00	0.98	2859
1.00	2.11	2.00	0.95	2813
1.50	3.16	2.00	0.95	2887

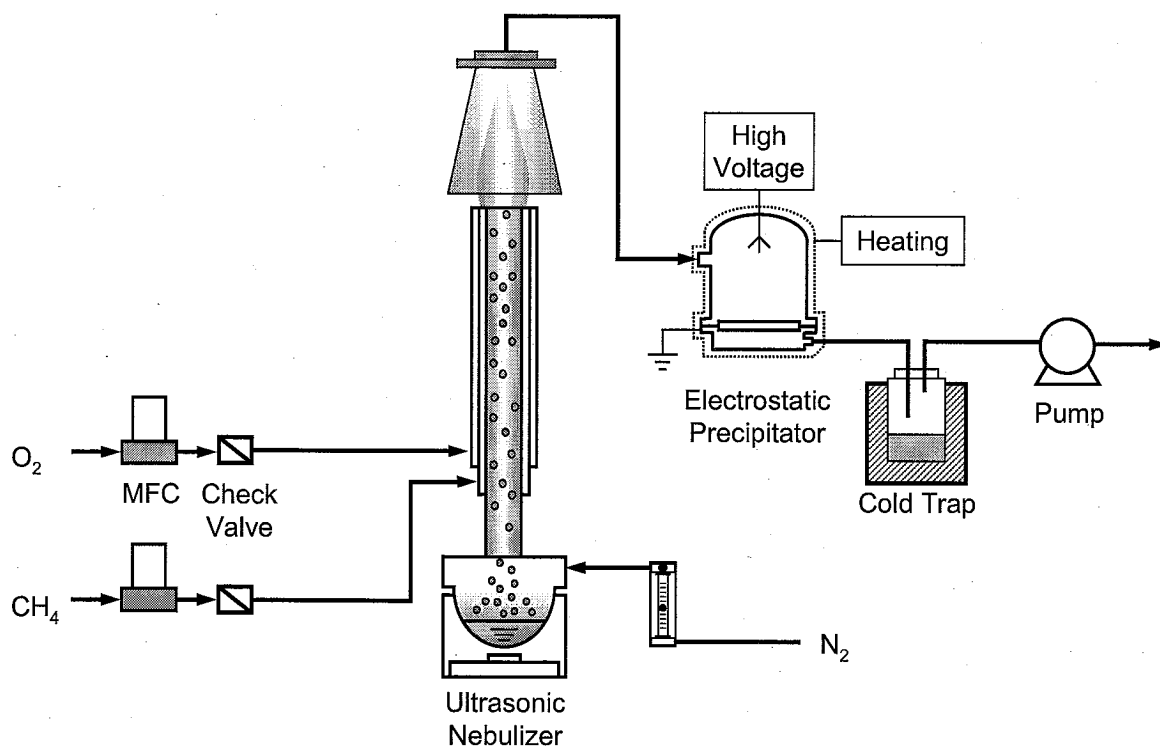


Fig. 6.1 Experimental setup

6.3. Results and Discussion

In order to find the optimal flame conditions, the flow rate of methane was changed from 1.0 l/min to 1.5 l/min at a fixed equivalence ratio of feeding gases ($\phi=0.95$), and then ϕ was changed from 0.7 to 0.98 by adjusting the flow rate of oxygen gas from 3.57 to 2.55 l/min at a fixed methane flow rate. Fig. 6.2 shows the PL spectra of as-prepared phosphor as a function of (a) the equivalence ratio at a fixed methane flow rate (1.25 l/min) and (b) the methane flow rate at fixed $\phi=0.95$, with an excitation wavelength of 254 nm and a fixed Eu doping concentration of 10 at.%. The highest PL intensity was obtained at a methane flow rate of 1.25 l/min and $\phi=0.95$. The as-prepared phosphors exhibit blue emission. This indicates that the matrix already has the BAM phase and that the Eu ion is divalent (Eu^{2+} , blue emission) rather than trivalent (Eu^{3+} , red emission). Emission spectra consist of a wide band with a peak at about 450 nm, which corresponds to the 4f–5d transition of the Eu^{2+} ion (Blasse et al., 1994, Zhang et al., 2002). The excitation spectra of as-prepared particles also indicate the existence of Eu^{2+} ions (Fig. 6.4), in which two wide bands with peaks at about 255 and 330 nm correspond to the crystal field splitting of the Eu^{2+} d-orbital (Blasse et al., 1994, Zhang et al., 2002). The phosphor particles produced at a short heating time (order of seconds) are well crystallized because all phenomena such as precipitation and thermal decomposition occur inside the micron-sized droplet in the gas phase. This operation time is remarkably shorter than that of other methods and demonstrates the advantage of the flame spray route.

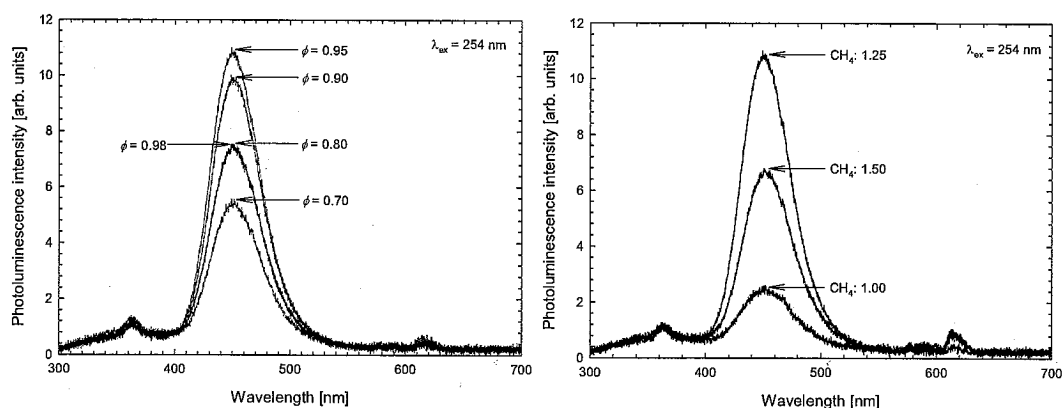


Fig. 6.2 PL emission of as-prepared BAM:Eu (Eu: 10%) phosphor, with an excitation of 254 nm, as a function of (a) Equivalence ratio (ϕ) and (b) flow rate of methane in l/min.

The commercial phosphor prepared by solid state reaction has micron-sized (about 3 μ m) particles with an irregular morphology. Fig. 6.3 (a)~(c) show images of our phosphors obtained at different methane flow rates. The particles prepared by flame spray pyrolysis are smaller (below 1 μ m) and more spherical than the commercial particles. Although there was no considerable difference between the morphologies of the particles prepared with different methane flow rates, some aggregates are present in the samples prepared at a high methane flow rate. It is well known that a high methane flow rate, at constant ϕ , causes a high flame temperature. The nanoparticles (a few tens of nanometers) on the submicron particle surface probably originated from the deposition of vapor evaporated from the surface of the precursor droplet in the high temperature flame. The optimal flame condition for high PL intensity and non-aggregated particle morphology was found to occur at a methane flow rate of 1.25 l/min with $\phi = 0.95$. The flame condition was fixed at this condition unless otherwise stated.

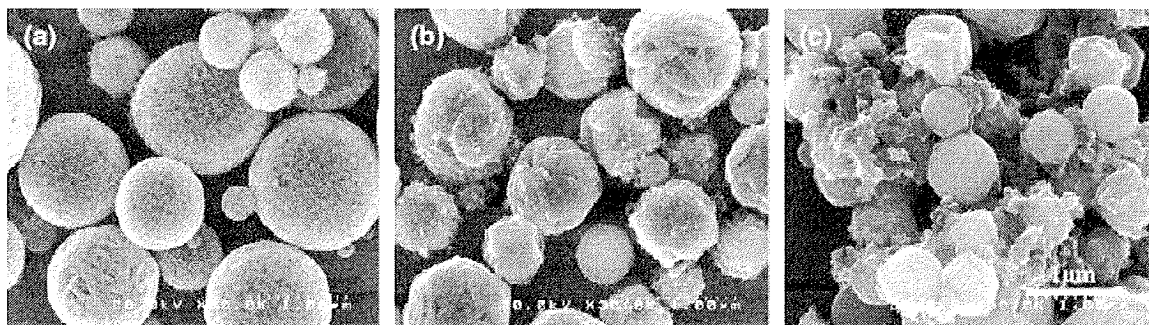


Fig. 6.3 FE-SEM images of particles prepared with different flow rates of methane (l/min): (a) 1.0, (b) 1.25, and (c) 1.5, at equivalence ratio of 0.95.

The excitation and emission spectra of as-prepared phosphor as a function of Eu doping concentration are shown in Fig. 6.4. The quenching concentration of Eu was found to be 12 at.% of Eu. This value is comparable to those obtained in previous studies (Kang et al., 1999, Saitoh et al., 2002, Kang et al., 2000, Jeon et al., 2001, Jung et al., 2003) and indicates that there is no loss (e.g. due to evaporation) of Eu ions during the spray-flame process.

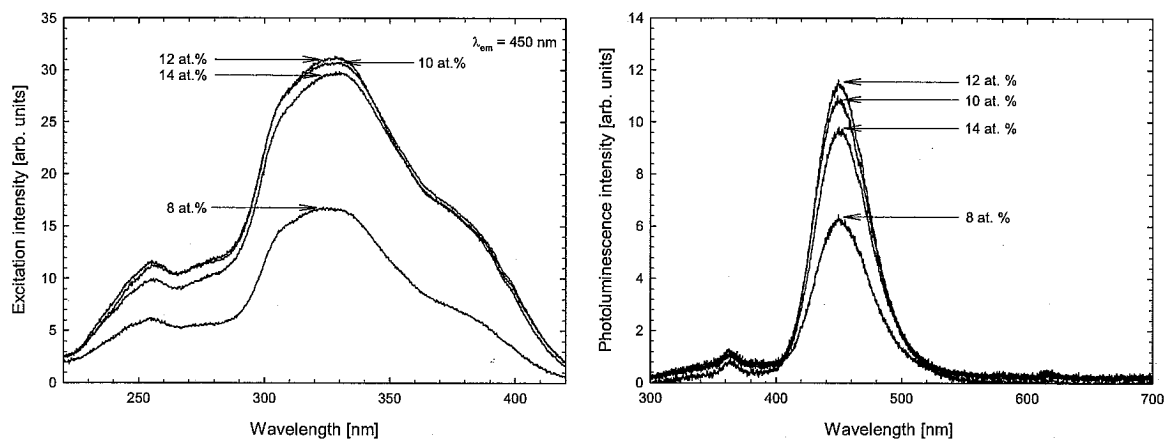


Fig. 6.4 (a) Excitation spectra with an emission of 450 nm, and (b) Emission spectra with an excitation of 254 nm, of as-prepared particles with different Eu concentrations

Overall concentration of precursor solutions was fixed at 0.3 M.

Examples of XRD spectra of the as-prepared phosphor at different flame conditions with reference to those of the commercial ones, $\text{BaMgAl}_{10}\text{O}_{17}$ and BaAl_2O_4 , are shown in Fig. 6.5. Although the BAM phase appears under all conditions, a few BaAl_2O_4 peaks did not disappear completely at low equivalence ratios of 0.8 and 0.9. Therefore, for acquiring the pure BAM crystal, an equivalence ratio (ϕ) above 0.95 is required. The as-prepared BAM:Eu phosphors were also post annealed at temperatures between 1200°C and 1400°C, for 3 h under a reducing atmosphere (30% H_2/Ar mixture gas). No changes in the crystalline phase of the XRD peaks (position) were observed when the as-prepared BAM:Eu particles were post-annealed. From Fig. 6.6, it is clear that by annealing above 1200°C, nanoparticles on the surface of submicron phosphors disappeared completely (compared to Fig. 6.3). However, increasing the annealing temperature causes the particles to start sintering with each other.

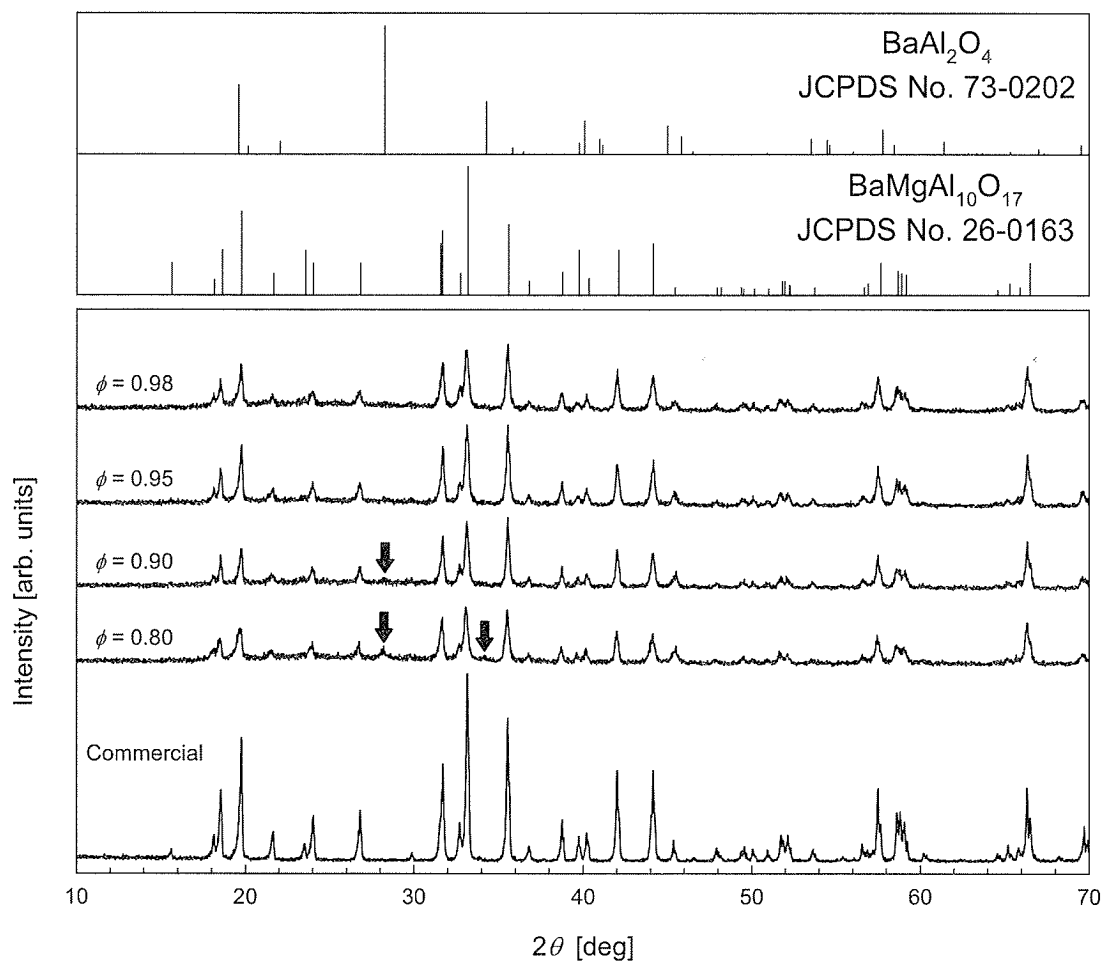


Fig. 6.5 Examples of XRD spectra of particles prepared at different equivalence ratio with references to those of the commercial one, $\text{BaMgAl}_{10}\text{O}_{17}$ and BaAl_2O_4 .

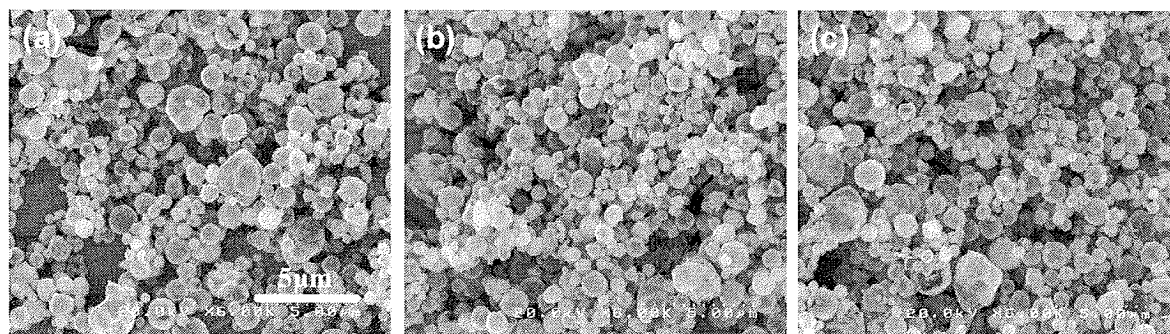


Fig. 6.6 FE-SEM images of particles obtained after post-annealing at difference furnace temperature: (a) 1200 °C, (b) 1300 °C, and (c) 1400 °C.

Fig. 6.7 shows the PL emission spectra of phosphors prepared with different post-annealing temperatures. The intensity of phosphor post-annealed at 1400 °C is four times higher than that of the as-prepared phosphor, and as high as 85% of that of the commercial phosphor.

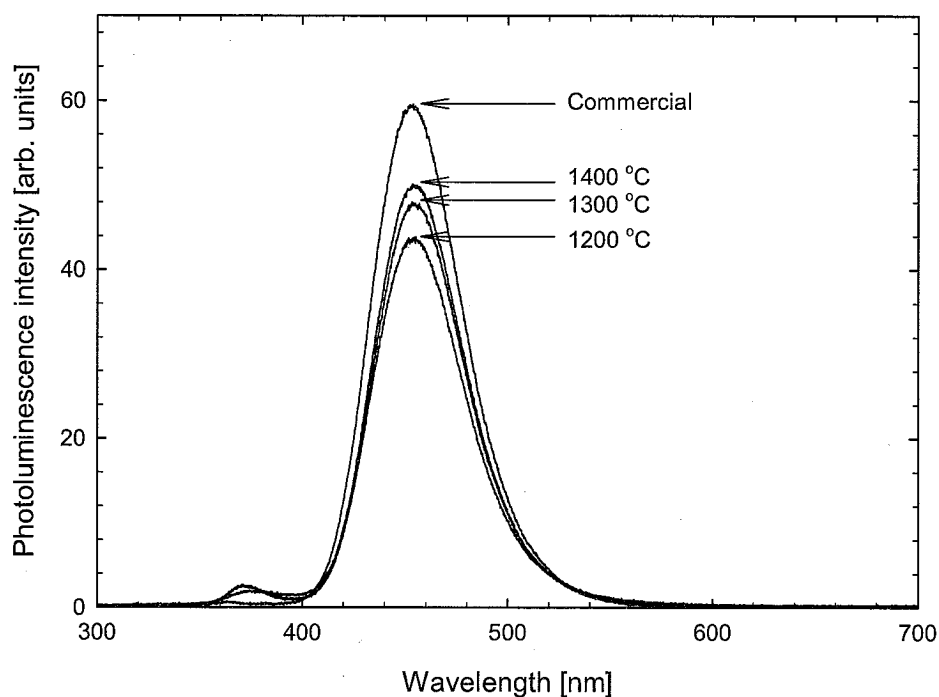


Fig.

6.7 PL emission spectra of particles after post-annealing at difference temperatures and that of the commercial product.

6.4. Summary

A flame spray pyrolysis method was designed and used to directly prepare $\text{BaMgAl}_{10}\text{O}_{17}:\text{Eu}^{2+}$ blue phosphors. The phosphors were submicron-sized particles with spherical morphology. Without post-annealing, the as-prepared particles showed blue emission at 450 nm. With post annealing, the PL emission intensity was increased, to four times that of the as-prepared phosphors.

References

Blasse, G., B.C. Grabmaier, Luminescent materials, Springer-Verlag, 1994.

Ekambaram, S., K.C. Patil, Bull. Mater. Sci. 18 (1995) 921.

Jeon, B.S., G.Y. Hong, Y.K. Yoo, J.S. Yoo, J. Electrochem. Soc. 148 (2001) H128.

Jung, K.Y., D.Y. Lee, Y.C. Kang, H.D. Park, J. Lumin. 105 (2003) 127.

Kang, Y.C., S.B. Park, I.W. Lenggoro, K. Okuyama, J. Electrochem. Soc. 146 (1999) 2744.

Kang, Y.C., S.B. Park, J. Electrochem. Soc. 147 (2000) 799.

Messing, G.L., S. Zhang, G.V. Jayanthi, J. Am. Ceram. Soc. 76 (1993) 2707.

Oshio, S., K. Kitamura, T. Shigeta, S. Horii, T. Matsuoka, S. Tanaka, H. Kobayashi, J. Electrochem. Soc. 146 (1999) 392.

Park, S., S.H. Kang, J. Mater. Sci., Mater. Electron. 14 (2003) 223.

Ravichandran, D., R. Roy, W.B. White, S. Erdei, J. Mater. Res. 12

(1997) 819.

Reynolds, W.C., The element potential method for chemical equilibrium analysis: Stanjan, Stanford University, 1986.

Saitoh, H., K. Kawahara, S. Ohshio, A. Nakamura, N. Nambu, J. Ceram. Soc. Jpn. 110 (2002) 874.

Zhang, J.Y., Z.T. Zhang, Z.L. Tang, Z.S. Zheng, Y.H. Lin, Powder Technol. 126 (2002) 161.

Chapter 7

Summary

7.1 Conclusions of All Chapters

Various kinds of functional fine particles, such as nitride oxynitride oxide phosphor materials were successfully synthesized by means of liquid phase process including sol-gel method and spray method. Furthermore, preparation of porous or hollow particles using spray drying and fabrication and characterization of ITO film using its nanoparticles prepared by LPSP were also investigated.

The major conclusions of this thesis are as follows:

- 1) GaN nanoparticles have been prepared using nitridation of Ga₂O₃ particles under flow of ammonia. In order to convert from Ga₂O₃ to GaN with a short reaction time, nano-sized Ga₂O₃ particles were used as starting materials. Ga₂O₃ nanoparticles were synthesized by two types of liquid phase processes, i.e., sol gel process with addition of aqueous ammonia to precursor solution and salt assisted spray pyrolysis. Changing of precursor parameters, such as concentration, additives, and precursor molar ratios were investigated. It was found that these parameters are of importance for nanoparticle synthesis. In the case of using sol gel process for producing Ga₂O₃ particles, the addition of a proportional amount of ammonia to the solution is a key factor in the production of well-dispersed nano-sized Ga₂O₃ particles. Meanwhile,

addition of a proportional amount of flux salt (LiCl) to the solution and operating temperature were important factors in the preparation of nano-sized Ga₂O₃ particles with a narrow size distribution. Furthermore, in this gas solid reaction, the effects of particle size and crystallinity of Ga₂O₃, nitridation time, and operating temperature on transformation to GaN, the optical characteristics were investigated as well. According to powder X-ray diffraction, nano-sized Ga₂O₃ particles were more easily converted into GaN than large-sized Ga₂O₃ particles. Ga₂O₃ particles prepared at low temperatures were more easily converted into GaN particles than those prepared at high temperatures. Generally, the crystallinity of GaN particles increased with increasing conversion temperature, which in turn improved the PL intensity.

2) In this thesis a new oxynitride phosphor, which is composed of BCNO atoms was produced by a one-step liquid process at low temperature under ambient atmospheric condition. BCNO phosphor particles with a tunable emitted-light wavelength from 380 nm to 571 nm were prepared using a facile liquid process at relatively low temperatures. The experimental results obtained in the present study revealed that control of the carbon content by optimizing the operating temperature and reaction time was important for the production of BCNO phosphor particles with tunable emitted-light wavelengths over the entire visible light spectrum.

Additional studies will be conducted in the near future to understand the effects of carbon content on the PL properties of BCNO phosphor particles. The results of the present study suggest that the BCNO powder prepared in this study has the potential for use in the preparation of materials for multicolor-light-emitting diodes (LED). The BCNO phosphor has high external quantum efficiency, and its

preparation has many advantages, such as cheap raw materials, low preparation temperature, and normal pressure conditions. Therefore, this method can easily be scaled up for industrial applications.

- 3) A flame spray pyrolysis method to directly prepare submicron $\text{BaMgAl}_{10}\text{O}_{17}:\text{Eu}^{2+}$ (BAM:Eu) phosphor particles was designed. Characteristics such as photoluminescence, crystallinity and particle morphology were investigated for products prepared under various conditions and they were compared with those of the commercial product. Without post-annealing, the as-prepared particles showed blue emission at 450 nm. With post annealing, the PL emission intensity was increased, to four times that of the as-prepared phosphors.

Appendix I: List of Figures

Figures Caption

- Fig. 1.1 Schematic diagram of white LEDs system
- Fig. 1.2 Schematic diagram of FEDs system
- Fig. 1.3 Modification of sol gel process
- Fig. 1.4 Organization and structure of chapters of present thesis
- Fig. 1.5 Shrinkage core model illustration without changing particle size
- Fig. 1.6 Preparation methods of GaN nanoparticles in this thesis
- Fig. 2.1 Powder preparation procedure.
- Fig. 2.2 SEM images of Ga_2O_3 prepared at 800°C with various ratios of $\text{NH}_3(\text{aq})/\text{Ga}(\text{NO}_3)_3$: (a) 0, (b) 0.1, (c) 1.0, and (d) 10 (mol/mol).
- Fig. 2.3 (a) TEM image of Ga_2O_3 prepared at 800°C with $\text{NH}_3(\text{aq})/\text{Ga}(\text{NO}_3)_3 = 1.0$; (b) XRD patterns of various samples: (i) Ga_2O_3 prepared at 800°C with $\text{NH}_3(\text{aq})/\text{Ga}(\text{NO}_3)_3 = 1.0$, (ii) sample in Fig. 3(a) after nitridation at (ii) 650°C , (iii) 800°C , and (iv) 900°C ; (c) XRD patterns of commercial GaN sample after nitridation at 800°C , the inset shows the corresponding SEM image.
- Fig. 2.4 TEM images of GaN samples after nitridation at (a) 800°C and (b) 900°C . Insets give the corresponding HR-TEM images.
- Fig. 2.5 PL spectra of GaN samples after nitridation at (a) 700°C , (b) 800°C and (c) 900°C .
- Fig. 2.6 PL spectra of (a) undoped GaN prepared at 800°C , and Mg-doped GaN prepared at (b) 750°C and (c) 800°C .

-
- Fig. 3.1 XRD patterns of samples obtained by the pyrolysis of a mixture of $\text{Ga}(\text{NO}_3)_3$ and ammonia solutions as precursors in flowing ammonia at various temperatures: 700°C, 800°C and 900°C, respectively, for 2 h.
- Fig. 3.2 SEM photographs of samples prepared from: a) Ga_2O_3 powder and b) a mixture of $\text{Ga}(\text{NO}_3)_3$ and ammonia solution; in a NH_3 atmosphere for 2 h at 800°C.
- Fig. 3.3 Room temperature PL spectra of samples obtained at various temperatures: 700°C, 800°C and 900°C.
- Fig. 3.4 Effects of different concentrations of ammonia solutions on PL intensity.
- Fig. 4.1 (a) Procedure for the formation of nitride particles, (b) experimental apparatus for oxide particles, (c) experimental apparatus for nitride particles.
- Fig. 4.2 FE-SEM images of Ga_2O_3 particles prepared at 800°C with various molar ratios of Li/Ga: (a) 0, (b) 5.0, and (c) 10.0.
- Fig. 4.3 FE-SEM and FE-TEM images of Ga_2O_3 particles prepared using 0.05 mol/l of precursor and a Li/Ga molar ratio of 5.0 at different operating temperatures: (a) 700°C, (b) 800°C, (c) 900°C, and (d) 1000°C. High magnification TEM images are shown in the figure insets.
- Fig. 4.4 XRD patterns of the particles resulting from nitridation at 900°C for 120 min using Ga_2O_3 particles prepared at various operating temperatures: (a) 1000°C, (b) 900°C, and (c) 800°C.
- Fig. 4.5 XRD patterns of particles resulting from nitridation at 900°C with a various nitridation times: (a) 90 min, (b) 60 min, (c) 30 min, (d) 5 min, and (e) 1 min.
- Fig. 4.6 SEM image of GaN sample after nitridation at 900°C for 60 min using Ga_2O_3 particles prepared at 800°C. The corresponding high magnification TEM image is shown in the figure inset.
- Fig. 4.7 Elemental EELS maps of the particles resulting from nitridation at 900°C with a various nitridation time: (a) 5 min, and (b) 60 min. T1 and T2 indicate the

corresponding zero-loss images.

- Fig. 4.8 PL emission spectra of the GaN sample after nitridation at 900°C for 60 min (a) and that of the commercial product (b).
- Fig. 5.1 (a) Low-magnification TEM image of a BCNO particle. (b) ED pattern. (c) High-resolution TEM image. (d) Electron energy loss spectroscopy of a sample.
- Fig. 5.2 Excitation and emission spectra for BCNO phosphor prepared at 800°C using PEG/B= 2.0×10^{-3} (mol/mol).
- Fig. 5.3 PL spectra of BCNO samples prepared at 700°C, 800°C and 900°C using PEG/B= 2.0×10^{-3} (mol/mol).
- Fig. 5.4 PL spectra of BCNO prepared at 800°C using PEG/B= (a) 2.0×10^{-3} (b) 2.8×10^{-3} , (c) 4.0×10^{-3} , (d) 6.0×10^{-3} (mol/mol).
- Fig. 5.5 PL spectra and digital photograph of BCNO samples prepared under various conditions: PEG/B, operating temperature, heating time = (a) 2.0×10^{-3} , 900°C, 30 min, (b) 2.0×10^{-3} , 800°C, 30 min, (c) 2.8×10^{-3} , 800°C, 60 min, (d) 4.0×10^{-3} , 700°C, 60 min, and (e) 4.4×10^{-3} , 700°C, 30 min.
- Fig. 5.6 CIE diagram and external quantum efficiency of BCNO powders prepared under various conditions: PEG/B, operating temperature, heating time = (a) 2.0×10^{-3} , 900°C, 30 min, (b) 2.0×10^{-3} , 800°C, 30 min, (c) 2.8×10^{-3} , 800°C, 60 min, (d) 4.0×10^{-3} , 700°C, 60 min, and (e) 4.4×10^{-3} , 700°C, 30 min.
- Fig. 6.1 Experimental setup.
- Fig. 6.2 PL emission of as-prepared BAM:Eu (Eu: 10%) phosphor, with an excitation of 254 nm, as a function of (a) Equivalence ratio (ϕ) and (b) flow rate of methane in l/min.
- Fig. 6.3 FE-SEM images of particles prepared with different flow rates of methane (l/min): (a) 1.0, (b) 1.25, and (c) 1.5, at equivalence ratio of 0.95.
- Fig. 6.4 (a) Excitation spectra with an emission of 450 nm, and (b) Emission spectra with an excitation of 254 nm, of as-prepared particles with different Eu concentrations.

Overall concentration of precursor solutions was fixed at 0.3 M.

Fig. 6.5 Examples of XRD spectra of particles prepared at different equivalence ratio with references to those of the commercial one, $\text{BaMgAl}_{10}\text{O}_{17}$ and BaAl_2O_4 .

Fig. 6.6 FE-SEM images of particles obtained after post-annealing at difference furnace temperature: (a) 1200°C , (b) 1300°C C, and (c) 1400°C .

Fig. 6.7 PL emission spectra of particles after post-annealing at difference temperatures and that of the commercial product.

Appendix II: List of Tables

Tables Caption

Tables 1.1 GaN phosphors materials prepared by various methods.

Tables 1.2 B/C/N phosphors materials prepared by various methods

Tables 6.1 The experimental conditions used for the study on effect of gases feeding rates on photoluminescence intensity of as-prepared particles

Acknowledgements

The studies presented in this dissertation have been carried out at the Thermal Fluids and Materials Engineering Laboratory (Okuyama Laboratory), Department of Chemical Engineering, Graduate School of Engineering, Hiroshima University during the years 2006 and 2008, where I enjoyed my research in a friendly atmosphere. There are a number of people, who have helped or motivated me in one way or another along the way, which certainly are gratefully acknowledged.

First of all, I would like to express my deepest gratitude to my supervisor, Professor Kikuo Okuyama, Department of Chemical Engineering, Graduate School of Engineering, Hiroshima University, for his continuing guidance, kind support and great consideration both in research and life during these years. His unprecedented enthusiasm and perspicacity on science has motivated and encouraged me significantly.

I also want to thank Associate Professor Akihiro Yabuki at the same laboratory, for his encouragements, kindness and useful advices. Special thanks are sent to Assistant Professor Ferry Iskandar, Department of Chemical Engineering, Hiroshima University, for his intensive discussions, and insightful suggestions in research, great help and friendly consideration in daily life.

I'd like to thank Professor Shigeki Takishima, and Professor Kazuo Takimiya at Chemistry and Chemical Engineering, Graduate School of Engineering, Hiroshima University, for their careful review and valuable comments to this dissertation. I also want to thank Professor Hiroshi Fukuoka for his kindness and useful advices.

I also would like to thank Dr Yoshifumi Itoh, Seiko Epson; Wei-Ning Wang at Department of Chemical Engineering, Dr Hye Moon Lee at Korea Institute of Machinery & Materials Nano

Powder Materials Group for their supports and advices;

Dr. Eishi Tanabe in Hiroshima Prefectural Institute of Industrial Science and Technology is grateful for helping in HR-TEM, EDS analysis and discussion. Assitant Professore Toshinori Tsumura at the workshop of the department and the staff at the glass work shop, for their useful cooperation on manufacturing the experimental apparatuses.

Mr. Agus Purwanto, Ms. Hendri Widiyandari, Ms. Widiyastuti, Mr. Yun kimyoungyun, Mr. Hiroshi Sumi, Mr. Jun Nakamura, Mr. Yutaka Kaihatsu, Mr. Takuya Nishiwaki, Mr. Nandiyanto Asep Bayu Dani, Mr. Hideyuki Kaneda, Ms Yui Kawano, and members in Okuyama Laboratory are thanked for their kind help in experiments and daily life as well, which makes my life in colorful and memorable.

Ministry of Education, Culture, Sports, Science and Technology of Japan (MEXT) and the Japan Society for the Promotion of Science (JSPS) are acknowledged for the financial support of my research in Hiroshima University and my life.

I would express my appreciation to my father, Yasuo Ogi and my mother, Ms. Keiko Ogi, and my grand mother Yoshiko Ogi and Mitsu Yuasa, and all other family members, for their patience, support and love, without which it would have been very difficult to persevere through many years of school. This dissertation is also in memory of my grandfather, Hachiro Ogi and Katsumi Yuasa, who passed away on 2004.

Last, and certainly not the least, I wish to thank Reiko Koushita, for her love, care, sacrifice and encouragement throughout all these years, and with these I can finish my study smoothly in Hiroshima University.

Takashi Ogi

Higashi-Hiroshima, Japan

February, 2008